Intelligent heat flow control of double skin facade systems.

Eškinja, Zdravko

Doctoral thesis / Disertacija

2019

Degree Grantor / Ustanova koja je dodijelila akademski / stručni stupanj: **University of Zagreb, Faculty of Electrical Engineering and Computing / Sveučilište u Zagrebu, Fakultet elektrotehnike i računarstva**

Permanent link / Trajna poveznica: https://urn.nsk.hr/urn:nbn:hr:168:974869

Rights / Prava: In copyright / Zaštićeno autorskim pravom.

Download date / Datum preuzimanja: **2024-10-04**

Repository / Repozitorij:

FER Repository - University of Zagreb Faculty of Electrical Engineering and Computing repozitory

University of Zagreb

FACULTY OF ELECTRICAL ENGINEERING AND COMPUTING

Zdravko Eškinja

INTELLIGENT HEAT FLOW CONTROL OF DOUBLE SKIN FAÇADE SYSTEMS

DOCTORAL THESIS

Zagreb, 2019

University of Zagreb

FACULTY OF ELECTRICAL ENGINEERING AND COMPUTING

Zdravko Eškinja

INTELLIGENT HEAT FLOW CONTROL OF DOUBLE SKIN FAÇADE SYSTEMS

DOCTORAL THESIS

Supervisor: Professor Zoran Vukić, PhD

Zagreb, 2019

Sveučilište u Zagrebu

FAKULTET ELEKTROTEHNIKE I RAČUNARSTVA

Zdravko Eškinja

INTELIGENTNO UPRAVLJANJE TOPLINSKIM TOKOM U SUSTAVIMA DVOSLOJNIH FASADA

DOKTORSKI RAD

Mentor: Prof. dr. sc. Zoran Vukić

Zagreb, 2019.

DOCTORAL THESIS is written at the University of Zagreb, Faculty of Electrical Engineering and Computing, Department of Control and Computer Engineering.

Supervisor: professor Zoran Vukić, PhD

DOCTORAL THESIS has: 130 pages

Dissertation No.: _____

About the Supervisor

Zoran Vukić is a Full Professor at the University of Zagreb, with 40 years of experience in education and research. He was Department Chair between 1992 and 1996 and is at present Head of the Laboratory for Underwater Systems and Technologies (http://labust.fer.hr). He was a member of the University of Zagreb Council (2011-2015) and is a member of Croatian Registry of Shipping. Obtained M.Sc (1972) and PhD. (1989) from the University of Zagreb. He was a Fulbright Fellow (non-degree programme, 1985) at Vanderbilt University (Nashville, USA) and specialized in control at Royal Institute of Technology (KTH) in Stockholm, Sweden (1984). He was a visiting professor at Vanderbilt University in 1986/87, and University of Maribor (Slovenia) in 1994. He published four books, two book chapters and more than 200 papers(in journals and at conferences) as author or co-author. His research interest is in the application of control theory for marine vessels (surface and underwater), especially the area of cooperative navigation guidance and control, robust and adaptive control, nonlinear control, intelligent control, fault tolerant and reconfigurable control. He has led a number of research projects (domestic and international).

O mentoru

Zoran Vukić je redoviti profesor na Sveučilištu u Zagrebu, s 40 godina iskustva u obrazovanju i istraživanju. Bio je predstojnik Zavoda za automatiku i procesno računarstvo između 1992. i 1996., a trenutno je voditelj Laboratorija za podvodne sustave i tehnologije (http://labust.fer.hr). Bio je član Vijeća Sveučilišta u Zagrebu (2011.-2015.) Član je Hrvatskog registra brodara. 1972 stjeće akademski stupanj magistra znanosti, a 1989. doktora znanosti na Sveučilišta u Zagrebu. Bio je "Fulbright Fellow" (nediplomski program, 1985.) na Sveučilištu Vanderbilt (Nashville, SAD), a specijalizaciju pohađa na području upravljanja na Kraljevskom institutu za tehnologiju (KTH) u Stockholmu, Švedska (1984). Bio je gostujući profesor na Sveučilištu Vanderbilt 1986/87. i na Sveučilištu u Mariboru (Slovenija) 1994. Objavio je četiri knjige, dva poglavlja knjiga i više od 200 radova (u časopisima i na konferencijama) kao autor ili koautor. Njegov istraživački interes je u primjeni teorije upravljanja za morska plovila (površinska i podvodna), posebno za područje kooperativo vođenje i upravljanja, robusno i adaptivno upravljanje, nelinearno upravljanje, inteligentno upravljanje, upravljanje optorno na kvarove i upravljanje s promjenjivom strukturom. Vodio je niz istraživačkih projekata (domaćih i međunarodnih)

“The trick is to regard everything as an image on a screen . . . the objects become weak and powerless, under my full control. Symbolic of a world I have created and can banish immediately by closing my eyes."

Ranko Marinković

Acknowledgements

Foremost, I would like to express my deepest thanks to my supervisor Professor Zoran Vukić and Dr Ognjen Kuljača who provided me the possibility to obtain my PhD research on a multidisciplinary field. Theirs patience, motivation, immense knowledge and over all, their cooperation was a key of a success to complete the thesis.

My sincere thanks also go to my colleges from Brodarski Institue: Ilija Beatović, Stanislav Ružić, Hrvoje Sušilović and Nikica Kokir who made numerical and experimental simulation possible. Beside engineering, I am deeply appreciative of all the help given to me by assistant Ljiljana Martić.

I would also like to take this opportunity to thank associate professor Professor Mario Vašak and his team for good advises generous access to their resources.

A special thanks to my family. Words cannot express how grateful I am to my mother-in law, father-in-law, my mother, and father for all of the duties that you've fulfilled on my behalf. At the end, I would like to express appreciation to my beloved wife Anita who was always my support in the moments when there was no one to answer my queries.

Abstract

Double skin façades are frequently used in modern civil engineering, especially in high buildings with the glass envelope. The main reasons for the popularity of such design are easier maintenance properties, less weight load and more natural illumination in relation to conventional façade systems. Until recently, automatic process control of the double skin façade was designed only to maintain interior comfortable temperature or ventilation. With the development of technology, new possibilities have occurred to override multiple control barriers as thermal and airflow behaviours have become more observable in both technical and economic sense. One solution is to upgrade Double Skin Façades into an intelligent system. This dissertation presents such a novel design for a double skin façade system and appropriate control method. Therefore, the system analysis has been performed from the perspective of desired temperature homogeneity, with a goal to achieve equal comfort in the interior. Furthermore, the applied neural network control method is proved to be the best choice for the heat flow control as an immeasurable state variable. Estimation methods have been analysed as a part of a novel control algorithm. Computer simulations on a mathematical model and experimental tests on the scaled model have shown that it is possible to achieve better thermal conditions in interiors with Double Skin Façades. Since, the used control algorithm has significant adaptive property, the method is not constrained with dimensions, but the only structure, what justifies performing tests on a scaled model.

Keywords: double skin façade, adaptive neural control, simulations, experiments, scaled modelling

Inteligentno upravljanje toplinskim tokom u sustavima dvoslojnih fasada

Dvostruke dvoslojne fasade su uobičajene u suvremenim građevinama, osobito u visokim zgradama sa staklenom ovojnicom. Glavni razlozi popularnosti ove fasade su zasigurno svojstva jednostavnijeg održavanja, manje težinsko opterećenje te više prirodnog osvjetljenja od klasičnih fasada. Zračni međuprostor između stijenki donekle umanjuje problem loše izolacije staklenih stijenki. Ipak, ovo je još uvijek kritična točka u energetskoj učinkovitosti ovakve ovojnice. Sve do nedavno, automatsko upravljanje toplinskim procesima u zgradarstvu se svodio na regulaciju unutarnje temperature i ventilacije. Razvojem tehnologije omogućena je primjena novih metoda za premošćenje višestrukih barijera u upravljanju zahvaljujući pristupačnijoj informaciji o toplinskim i zračnim strujanjima, u tehničkom i financijskom smislu. Jedno od rješenja je unaprjeđenje dvoslojne fasade u inteligentni sustav. Ova disertacija pod naslovom „Inteligentno upravljanje toplinskim tokom u sustavima dvoslojnih fasada“, predstavlja modifikaciju u dizajnu dvoslojne fasade i odgovarajuću upravljačku metodu. Sustav je analiziran iz perspektive izjednačenja toplinskih tokova kroz ovojnicu s ciljem povećanja komfora i korisnog prostora. Konvencionalni temperaturni regulatori ne mogu na zadovoljavajući način regulirati temperaturne tokove u dvoslojnoj fasadi jer ne postoji matematički model koji bi mogao objasniti sve moguće radne uvjete. Zbog toga se autor opredijelio za temperaturne regulatore koji ne trebaju matematičke modele, a zbog imanentne vremenske promjenjivosti termalnih procesa u dvoslojnoj fasadi, adaptivna neuronska mreža je odabrana. Adaptivnost regulatora toplinskog toka je bitna, jer bez svojstva prilagodbe, željene performanse ne bi se mogle postići. Primijenjeni neuronski regulator je dokazan kao najbolji izbor pri upravljanju toplinskim tokovima gdje su stanja nemjerljiva. Estimacijske metode su analizirane kao dio upravljačkog algoritma. Računalne simulacije fizikalnog modela i eksperimentalni testovi na skaliranom modelu, su pokazale poboljšanje termalnih uvjeta u prostorima s dvoslojnom fasadom. S obzirom na to da je korišteni algoritam upravljanja izrazito adaptivnog karaktera, metoda nije ograničena na promjenu dimenzija, već samo na promjenu strukture što opravdava testiranje na skaliranom modelu.

Prvo poglavlje (“Uvod”) daje pozadinu i motivaciju za istraživanje, te postavlja glavne hipoteze i očekivane znanstvene doprinose. Kratak povijesni pregled dvoslojnih fasada u zgradama je dan, te su kratko opisane suvremene dvoslojne fasade. Trendovi modernog zgradarstva usmjereni su u povećanje energetske efikasnosti i maksimalno iskorištavanje prostora. Dvoslojna fasada je vrlo pogodna za istraživanje i primjenu novih

tehnologija zbog svoje specifične konstrukcije.

U drugom poglavlju ("Opis sustava") opisan je koncept dvoslojnih fasada te sve njene komponente. Dvoslojni fasadni sustav se analizira, te se izvode odgovarajući matematički modeli. Nelinearnosti u ovim sustavima se često mijenjaju s vremenom, što otežava problem rješavanja regulacije temperature. Matematički model je lineariziran i sveden na standardnu formu omogućivši proračun toplinskog toka u dvoslojnim fasadama. Pokazano je da linearizirani matematički model ne može opisati dinamiku procesa u svim radnim režimima i u svim uvjetima (unutarnjim i vanjskim), ali se može iskoristiti da se dobiju približni kvalitativni odzivi temperature zgrade na vanjske temperaturne poremećaje. Iz razlike temperaturnih odziva, ponašanje toplinskog toka moguće je estimirati. Toplinski tok predstavlja glavnu informaciju o kvaliteti dvoslojne fasade pa je on u fokusu interesa. Obavljene su simulacije s dva različita numerička postupka kako bi se vidjelo na što treba obratiti pozornost kod ocjene kvalitete. Analiza je provedene primjenom programskog paketa za numeričku analizu dinamike fluida (Computational Fluid Dynamics - CFD) te naprednim postupkom analize utroška energije. Rezultati CFD analize pokazali su da oblik koridora dvoslojne fasade i iznos protoka zraka imaju glavnu ulogu u definiranju matematičkog modela. Simulacije su provjerene eksperimentom s termalnom kamerom u umanjenom modelu zgrade. Matematički model, koji se koristio u disertaciji, koristi jednadžbe simulatora (HAMBASE) koji se u građevinarstvu koristi za analizu energije u zgradama. Uočena su određena ograničenja HAMBASE simulatora, te su za potrebe disertacije prilagođene samo jednadžbe za proračun termičkih prijelaza. Eksperimenti su se provodili na umanjenom modelu zgrade kako bi se pokazala kvaliteta termičkog modela. Rezultati su pokazali da ovaj prilagođeni linearni model zadovoljavajuće estimira odziv na testiranu pobudu samo u užem radnom području, i to oko onih radnih uvjeta u kojima su parametri modela identificirani. Promjena područja zahtijeva promjenu parametara, iz čega proizlazi zaključak da linearni model ne može dovoljno dobro opisati dinamički odziv temperatura u unutrašnjosti skaliranog modela kada raspon vanjskih temperatura prekorači iznos korišten pri identifikaciji prilagođenog modela. Ipak, svi testirani linearni modeli imaju zajedničku karakteristiku jer je red prijenosne funkcije koji opisuje model uvijek jednak. Eksperimenti su se provodili pri različitim uvjetima promjenom karakteristike umanjenog modela. Promjene su uključivale izmjenu materijala i dimenzija svih ključnih elemenata: kako kod dvoslojnih fasada tako i kod zidova. Rezultati su potvrdili pretpostavke koje su primijenjene pri modeliranju. Odabir odgovarajućih senzora i njihovo pozicioniranje zahtijevalo je dodatnu analizu. Pokazalo se da senzori za toplinski tok i tlak nisu

preporučljivi za dobivanje informacije za povratnu vezu. Međutim, temperaturni senzori daju dovoljno informacija za estimaciju ponašanja. Primjenom principa pasivnosti pokazana je stabilnost otvorenog kruga.

Treće poglavlje ("Projektiranje zatvorenog sustava upravljanja toplinom u dvoslojnom fasadnom sustavu") bavi se strategijama upravljanja za regulaciju toplinskim tokom u dvoslojnim fasadnim sustavima. Analizira se specijalan slučaj dvoslojne fasade bez prirodne ventilacije budući da tu postoji statički zračni pojas koji se može iskoristiti za svrhu upravljanja. Mogućnost upravljanja toplinskim tokom postiže se dodavanjem dodatnog toplinskog izvora u koridor. Glavni izazov kod upravljanja leži u tome da se postigne jednak toplinski tok u dvoslojnoj fasadi i svim zidovima. Kao što je opisano u poglavlju 2., moguće je, no nije praktično mjeriti stanja u umanjenom modelu zgrade, pa se stoga koristi estimacija stanja. Nova strategija i adaptivni neuronski regulator predlažu se za upravljanje toplinskih procesa kod dvoslojnih fasadnih sustava. Cilj je izjednačiti gubitke topline u zgradi (umanjenom modelu zgrade) kod koje postoji samo jedan kritičan element – dvoslojna fasada. Istražen je problem globalne stabilizacije sustava. Pasivna stabilnost otvorenog kruga, pokazana u poglavlju 2, osigurava da će zatvoreni krug također naslijediti svojstva pasivnosti. Nadalje, pasivnost omogućuje da se temeljem funkcije Ljapunova odredi jednostavan postupak za ugađanje adaptivnog neuronskog regulatora. Pri određivanju početnih uvjeta, korištene su pojednostavljene diferencijalne jednadžbe kojima je opisano ponašanje upravljanog procesa. Zahvaljujući karakteristikama adaptivnog regulatora i poznatim ograničenjima, ovo je bilo dovoljno da se garantira konvergencija zatvorenog kruga iako zadovoljavajući matematički model procesa nije poznat. Ovakvo ugađanje osigurava željene performanse kod umanjenog modela zgrade te se može preporučiti za prave zgrade s dvoslojnim fasadama, pri čemu valja na odgovarajući način prilagoditi adaptivni neuronski regulator. Poglavlje završava dajući teoretski dokaz stabilnosti i učinkovitosti predložene adaptivne neuronske mreže.

Uobičajena je praksa u građevinarstvu i u automatici da se nove metode simuliraju, pa tek onda primijene u praksi. Četvrto poglavlje ("Analiza termalnog sustava upravljanja uz pomoć simulacija") bavi se simulacijama s primjenom adaptivne neuronske mreže kao termalnog regulatora, kako bi se provjerile dobivene performanse sustava. Temeljem eksperimenata obavljenih na umanjenom modelu zgrade (opisan u poglavlju 2), toplinski tok se ne može dobro estimirati korištenjem lineariziranog matematičkog modela i samo izmjerenih podataka o temperaturi. Simulacije su stoga korištene kako bi se vidjelo da li je opravdano iskoristiti pojednostavljene jednadžbe za svrhu ugađanja adaptivne neuronske mreže, te za dokaz stabilnosti opisan u poglavlju 3. Simulacije

s lineariziranim matematičkim modelom nisu bile u stanju dati precizne odgovore, no dale su kvalitativne odgovore kakve prijelazne procese se može očekivati. Umanjeni model zgrade s dvoslojnom fasadom se razmatrao pri različitim simulacijskim uvjetima. Simulacijski alat HAMBASE korišten je u preliminarnim testovima. Testovi su ponovno pokazali ograničenost ovakvog modela. Za proučavanje razlika između regulirane i neregulirane dvoslojne fasade korišten je prilagođeni model lineariziran oko užeg radnog područja. Ovakva usporedna analiza je korisna jer daje odgovor o učinkovitosti regulirane dvoslojne fasade u odnosu na nereguliranu. Adaptivna neuronska mreža u stanju je učiti i adaptirati se, te se uz dobro ugođene parametre može primijeniti za upravljanje bilo kojim stabilnim procesom. Stoga ne iznenađuje da su različiti testovi u kojima su se koristile različite upravljačke topologije pokazali da je preporučljivo koristiti adaptivnu neuronsku mrežu. Pri tome nije potrebno poznavati dinamiku zgrade niti treba naći regresijsku matricu kako bi se projektiralo adaptivni neuronski regulator.

Peto poglavlje ("Analiza termalnog sustava upravljanja iz eksperimenata") daje rezultate dobivene eksperimentima obavljenima na umanjenom modelu zgrade u termalnoj komori. Upravljačka petlja sastoji se od temperaturnog regulatora, senzora, aktuatora te umanjenog modela zgrade s jednom dvoslojnom fasadom na jednoj strani zgrade. Dva regulatora su testirana: PI regulator i adaptivni neuronski regulator. Parametri PI regulatora definirani su Cohen-Coon metodom što je zahtijevalo dodatni eksperiment koji uključuje odziv pri maksimalnim zadanim snagama grijaćih elemenata. Za razliku od PI-a, postavljanje adaptivnog neuronskog regulatora ne zahtijeva složene predradnje, inicijalizaciju težina ili treniranje. Jedini zahtjev je ispravno definiranje parametara odnosno ponašanje mehanizma za ugađanje težina adaptivnog neuronskog regulatora (opisano u poglavlju 3). Performance su se ocjenjivale primjenom kriterija integrala apsolutne pogreške (Integral Absolute Error - IAE) te integrala kvadrata pogreške (Integral of Squared Error - ISE). Opisane su sve pripreme koje su bile nužne za provedbu eksperimenata. Eksperimenti su uspješno izvedeni iako nije bio poznat matematički model umanjenog modela zgrade, postojala su kašnjenja u signalima, neizvjesnost parametara je bila velika, te su postojali poremećaji. S obzirom na to da nema prethodnog treniranja neuronske mreže, neuronski regulator nije funkcionalan u prvih nekoliko ciklusa temperaturnih oscilacija. Adaptivna neuronska mreža je bila u stanju učiti u stvarnom vremenu te osigurati tražene performanse zatvorenog sustava. Pokazano je da adaptivna neuronska mreža daje bolje rezultate od PI regulatora. Težinski koeficijenti skrivenog sloja neuronske mreže kao i pogreške bili su ograničeni tijekom eksperimenata, a neuronski regulator dobro je odradio poremećaje.

Šesto poglavlje ("Zaključak i budući rad") daje kratak osvrt na obavljena istraživanja,

daje smjernice za eventualni rad na ovom području u budućnosti, te završava s znanstvenim doprinosima. Predložena su odgovarajuća rješenja iz domene inteligentnog upravljanja koja će poboljšati regulaciju toplinskog toka u zgradama s dvoslojnim fasadama. Postojeći sustavi ne mogu postići jednoliku raspodjelu temperature u istoj toplinskoj zoni. Autor je pokazao da je to moguće postići, ako se koriste odgovarajuće upravljačke metode. Sljedeći korak je vrlo financijski i vremenski zahtijevan jer obuhvaća eksperimente u realnim uvjetima gdje nije moguće izolirati pojedine poremećaje kao što su zračna strujanja i solarna radijacija. U takvim okolnostima, nužno je uključiti i utjecaj HVAC sustava koji bi morao biti takav da ne narušava postojeće uvjete i definirane zahtjeve. Dio ovog rada publiciran je u časopisu koji je indeksiran u bazi Web of Science (SCI-E časopis), a dio predstavljen na međunarodnoj znanstvenoj konferenciji. Postignuti su originalni znanstveni doprinosi koji se mogu sažeti u sljedeće:

- Nova metoda za automatsko upravljanje toplinskim tokom u koridoru dvoslojnih fasadnih sustava je predložena i testirana. Ovom metodom moguće je ujednačiti unutarnju temperature prostora kako bi se postigao veći komfor korisnika a koja je toliko jednostavna da je mogu koristiti i oni koji nisu eksperti.
- Pokazano je da se adaptivna neuronska mreža ponaša bolje od PI regulatora u regulaciji toplinskog toka u koridoru dvoslojne fasade. Komparativna analiza pokazala je da je povoljnije koristiti regulirani od nereguliranog toplinskog toka u koridorima dvoslojnih fasada.

Ključne riječi: dvoslojna fasada, neuronski adaptivni regulator, simulacije, ekperimenti, skalirano modeliranje

Contents

Chapter 1

Introduction

My professional experience during energy audits on office buildings led me to the recognition of improvement potential by implementing automatic control. The work of Laboratory for Renewable Energy Systems (LARES - FER) [1], [2], [3], [4], [5], helped me to explore their knowledge and also to find the new domain of interests. At that time, I had more scientific experience in marine system due to a strong connection with the work of Laboratory for Underwater Systems and Technologies (LABUST - FER) [6], [7], [8], but former Control Engineering Department of Brodarski Institute encouraged me to extend our expertise [9], [10], [11] to new field. Glazed surface of the building's façade is the weakest link in a heat flow insulation. Double Skin Façade (DSF) system is well-known solution used commonly for high office buildings. The main principle of the system is to enable natural ventilation through the inner space between skins.[1] The gain of cheaper ventilation and improvement in thermal properties of the façade justifies doubling the initial expenses of investment. In the last decade, a lot of effort has been made to increase the efficiency of this system by introducing automatic control. However, due to complex requirements, these systems are not yet in the standard offer of architectural agencies. My research was focused on equalizing temperatures in interiors, what is different from the popular approach where effort has been given to save energy by increasing Heat Ventilation Air Conditioning (HVAC) efficiency. If the only financial criterion is considered, such a system is the practically worse case in terms of energy efficiency, as it spends additional energy while regulating the temperature of the corridor. However, increased user comfort and increased usable area is more often a very valuable benefit. After analysis, we concluded: We cannot collect all information about processes and its parameters, required by conventional methods. Then,

[1] In further text this space will be called corridor.

usable methods are those who don't require a model, and also those who are capable of adapting to certain variations. In the dissertation, the neural network method is used in a way to find demanded dynamics of the system and finally to modify it by defined criterion. The method was validated through different numerical simulations. Besides, a series of experimental measurements were conducted with a built scaled model of the building's segment (see Figure 2.6) that was built in the Brodarski Institute for experimental testing. The thesis covers the theory and practice of a system control developed to improve Doubles Skin Facade system. Although, developed concept has not yet been implemented in a full-scale, high building, methods are tested and ready to use. There is sufficient evidence to doubt as to whether the method can control conditions in DSF corridor without mentioned validation. However, the research goal was to prove the guaranteed ability of the adaptive neural network to handle the challenge even that building is not existing yet. This arises from basics neural network properties.

Starting with a theoretical overview and finishing with experimental tests, the thesis provides a detailed analysis of the control system used in DSF to improve energy conditions.

1.1 Hypothesis and Expected Scientific Contribution

An objective of the research is the development of new control methods for double skin façade systems with the purpose of improving the building's properties. Hypotheses are:

- Current regulation systems for heat conditioning in civil engineering cannot reach the equal distribution of temperatures in the same thermal zone. This problem appears more intensive when the difference between desired and external temperatures is large. It is possible to reach one air temperature in the same closed space with Double Skin Facade, if the integration of automation control theory is applied.
- The use of knowledge of automation control theory can provide equal thermal conditions in interiors of buildings with Double Skin Facade systems without impairing user comfort. The approach to solving the problems of thermal insulation in the system of two-layer façade, by using the procedures in the field of automatic control, can provide favourable solutions.

Expected scientific contributions of the research are described here:

- A novel method for automatic control of corridor double skin façade systems is proposed and tested. This method can equalize the interior temperature, with the purpose of increasing user comfort and is simple enough to be used by non-experts.
- AANN is proven to perform better than conventional PI regulator for heat control in DSF corridor. Comparative analysis of non-controlled corridor double skin façade systems and automatically controlled double skin façade systems is performed. Controlled versus non-controlled heat flow in DSF shows advantages of the controlled solution.

1.2 History of Double Skin Façades in Buildings

First appearances of DSF systems where found in ancient Roman bath facilities called *Thermae* (from Greek thermos, "hot"). Such buildings were designed to maximize fuel efficiency. The design of baths was discussed by Roman architect Vitruvius who wrote De Architectura [12] as a guide for building projects. DSF systems were part of central heating and were constructed as massive stone walls with ducts inside. One version of such walls is shown in Figure 1.1.

FIGURE 1.1. Antic double skin façade

The photo was taken at Pompeii's Forum Baths. These baths were built in 80 B.C. [13]. Except for ducts, there was inner space under the floor. The floor was supported by short brick pillars. The warm air, produced by the furnaces, circulated under the floor, flowed through the wall ducts and then through several chimneys. Also, there was a manual regulator to control the heat in the hot room (Latin: caldarium), a bronze disc set into the roof under a circular aperture which could be raised or lowered by a pulley to adjust the ventilation.

1.2.1 New Age DSF and Similar Envelope Structures

In the last few centuries building enclosure are very often constructed from three different building elements: bearing walls, insulation sheathing and cladding (see Figure 1.2). In this case, the sheathing is made of moisture-sensitive materials placed directly behind the cladding, separated by only a thin sheathing membrane and air gap. The use of ventilated air spaces behind claddings has been shown to protect the sheathing from moisture and accidental leaks [14]. The air in the corridor eliminates capillary flow between the cladding and sheathing, provides drainage of incidental moisture. In some designs, an air pressure difference is big enough to provide some venting or ventilation to remove evaporated/desorbed moisture. This building system, illustrated in Figure 1.2 is also known as rain-screen. In rainy climates such as coastal British Columbia (USA), this control strategy is found to be very beneficial and nowadays is required by code for most new buildings. However, occasional minor drawbacks are possible due to dirt

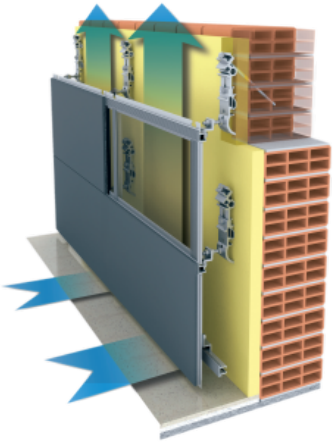

FIGURE 1.2. Wall cladding with ventilation corridor, L[14]

and moisture in the corridor brought by ventilation [15]. Another common use of double skin principle is not in façade but in airflow windows. Airflow windows integrate

windows and ventilation system by drawing the fresh air through the corridor between the panes before it enters the room [16]. Although windows are part of façade, airflow windows belong to the different research field. In some engineering manuals, such as in [17], the façade system is used as an HVAC actuator. Basically, this system functions as a fan coil. Here, the exchange media is air that is forced to flow through thermal exchanger by a fan. Input and output shafts should be placed just near the device, usually under window opening or floor. This HVAC solution can be an alternative for Air Handling Unit (AHU) without expenses for duct distribution, but with lower exchange efficiency. Beside thermal and ventilation functions, author of the paper [18] proposes to use DSF also as a mass damper by enabling movements in it. The main advantage would be reduction of structural vibrations and damage during earthquake or wind storms. A mass damper is a secondary mass attached to the primary structure that is designed to reduce structural motions. To design the functional dumping DSF multiple dumpers are needed to connect the façades system throughout the building. The motion of these dumpers are also coupled because they are connected to the same DSF system. The main challenge is to tune and optimize all the dumpers. DSF system has one weakness from the point of the fire safety view. Opening paths are existing throughout the whole buildings, so when a fire happens, the opening paths for ventilation also become paths for the smoke to spread to other non-fire spaces [19]. It is also possible to deal with the smoke problem using the same principle as natural ventilation: stack effect. The control method is yet not revealed due to the huge model identification problem: numerous parameters will affect the natural ventilation and smoke control performance of the double skin space, such as the height of the solar chimney, the wind effect and so on.

If DSF is used for ventilation of offices or other interiors, it is closely related to health conditions [20]. To preserve health quality, ventilation should be designed by verified instructions [21], [22] what is also regulated by the legislation [23], [24] and standards [25]. So, the automation possibilities and energy cuttings in this type of DSF are quite limited and will not be the subject of the presented research.

DSF systems are well-spread in cities, and there are many examples of different shapes and characteristics [26]. But overall, the DSF system is just a façade what implies that it can be added to the existing building. This is presented in [27] as an affordable option which pays out in several years.

Chapter 2

System Description

This chapter is dedicated to gather specific information about the performance of the double skin façade. Both, numerical simulation and experimental approach are used. An innovative design made it difficult to measure, and later to implement prototype on the real existing building. The lack of enthusiastic investors remains a laboratory test facility as the only option. Even-though, used simulation model gave more flexibility, the main limitation is always lack of reliability. The common practice in such cases is a comparison to other already validated simulation models, what is a practically one of the first planned steps. Existing mathematical relations are analysed with a focus on processes related to double skin façade, and it's the possibility of control. The experimental analysis should justify all approximations.

Expected modelling result is behavioural characteristic. However, my research is not looking for parameters of the model that can perfectly mimic the given process. The targeted objectives are values that may be used for synthesis of the adequate regulation method. Having that in mind, even scaled mock-up is considered.

The building is presented here as a thermodynamic system. The smallest entity of the building is a zone. The zone is a room or several adjacent rooms with the same conditions: temperature, relative humidity and climate control. Zones are bounded by different building components. Each building component has a different influence on thermodynamic processes. The reason lies in different materials, that building components are built of.

Series of tests were performed in the simulation and experimental environment to show how the simulator can be used in evaluating the performance of given policies.

2.1 Components of the DSF System

Building's components form the zone's envelope. Components consist of construction elements. Elements are usually multilayered skins that divide two thermal zones. Structural properties and strength of these elements are not the topic of the research and will not be considered in this work. The function of building components is being the border between zones or between zone and exterior. Based on thermal and hygric properties building components are categorized and will be analysed separately in next subsections.

2.1.1 Walls

Wall is the most common construction element in the modern building. Zone with quadratic shape has at least two horizontal and four vertical walls. Common construction component of the wall has a few different layers, as in Figure 2.1, where cutaways of two different walls are shown.

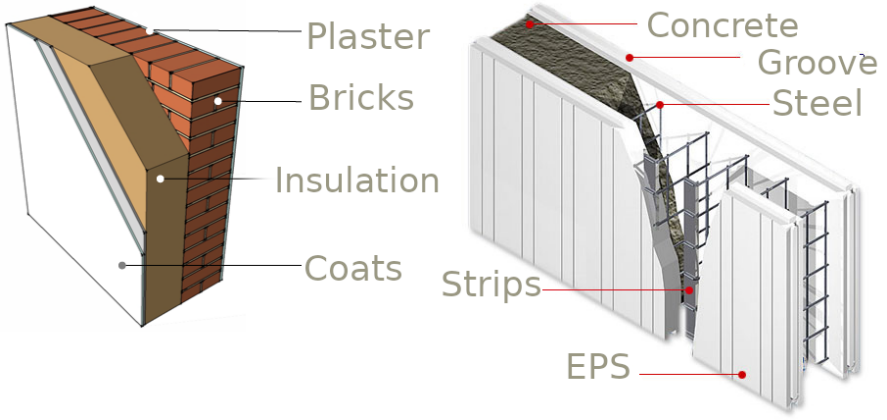

FIGURE 2.1. Exterior wall cutaways a) brick wall L[28] b) concrete wall L[29]

Wall is a basic zone's envelope, but it can be filled with other building components like windows, doors, ventilation openings, steel beams and so on. The main difference between wall and other building components is significant value of admittance property of conductivity through the construction component. Conductivity and its properties will be described more in Section 2.3.2. It is important to mention that insulation characteristic of the wall is one of the important parameters in thermal process. However, in special cases, insulation can cause the opposite effect. This is a common in pipes with moving fluids. As described in [30], in such insulation there are two processes during

fluid flow: resistance of the layer of insulation itself and the effect of the convection at its surface. While increasing thickness of insulation, the resistance is decreasing due to the thermal boundary layer. The cause is increased surface area.

2.1.2 Double Skin Façade System

According to reference [31], there are four basic types of double skin façade systems:

- Buffer Façade
- Extract-Air Façade
- Twin-Face Façade
- Hybrid Façade

FIGURE 2.2. Examples of corridor double skin façade system a) Occidental Chemical, Niagara Falls L[32], b) Business Tower, Nuremberg L[33], c) Cutaway L[34]]

Another source [35] notes DSF as Glass double façade's. Here, the types of DSF are distinguished by way of subdividing the façade corridor. There are three different variations:

- Corridor Façade - Façade is divided horizontally by every storey (see Figure 2.2)
- Shaft Façade - Façade is divided vertically and have shafts to allow natural ventilation thanks to the big temperature difference: stack effect.

- Double Window Façade - corridor is divided horizontally and vertically. The most important advantage is the elimination of fire spreading and sound insulation problem. In return, there is no possibility of exploiting the stack effect, and there is additional effort to prevent mixing the supply air and exhaust air of each separated façade section.

Double skin façade systems are two layered windows with large corridor area where natural ventilation appears due to vertical air temperature differences. The space between two glazed surfaces is called a corridor. Cavities are built in different dimensions and shapes. Their primary purpose is storage for the air, but sometimes, they are used as a pre-entrance area like lobbies. Airflow concepts of double-skin facades [36] are shown in Figure 2.3.

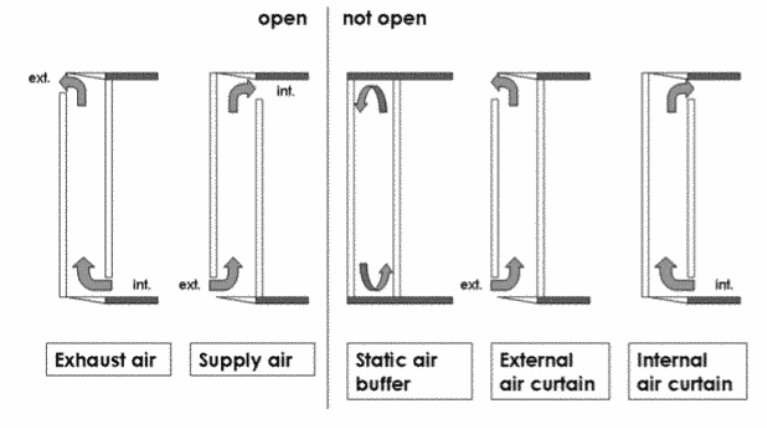

FIGURE 2.3. Airflow concepts of double-skin façades, L[36]

A thermal boundary layer develops over a flat plate when the plate's surface temperature T_s differs from the free stream temperature T_∞. The corridor airflows over the glazed surface inside the façade. This flow belongs to a group of external flows. In the thesis, it is considered the flow is simple and treated as boundary-layer flow. Simple flows are required to make just very mild turns. A boundary-layer flow is a flow in which the effects of viscosity and or/thermal effects are concentrated on a thin region near a surface of interest what is shown in Figure 2.4. When air flows over the flat plate by mechanical ventilation, then the problem is called forced laminar flow. Thermal process of the flow is caused by the dynamics of the air mass. To obtain useful mathematical relationships, we need to apply the fundamental mass, momentum and energy conservation principles.

The thermal process is very similar to the hydrodynamic process. In the corridor, at the inner side of façade, there is an assumption of a situation where the plate surface temperature T_S is greater than the free-stream temperature T_∞. Heat is thus transferred

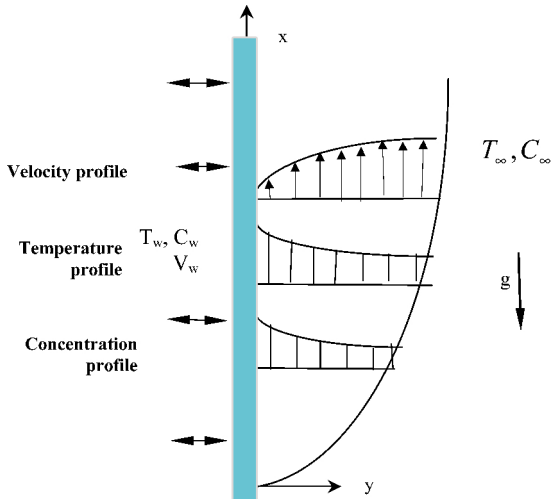

FIGURE 2.4. Thermal boundary layer due to flow on vertical flat plate L[37]

from the plate to the fluid. At the plate leading edge, the thermal boundary layer is developed.

2.1.3 Ducts

Energy loss in ducts is a well-known problem. Research from 1944 [38] yields two major facts about losses in ducts. In general, the rate of temperature drop increased as the temperature of the air in the duct increased, and as the velocity of the air decreased. The study indicated that air, commonly used in forced warm-air heating systems, has temperature drops between 0.66 $^{\circ}C$. and 3 $^{\circ}C$ per meter of the duct.

2.1.4 Thermal Energy Storage

Thermal energy can be stored as sensible heat in a material by raising its temperature [39]. The heat or energy storage can be roughly calculated as

$$\Phi_{storage} = V_{st}\rho C_p \Delta T = mC_p \Delta T \tag{2.1}$$

where:

$\Phi_{storage}$	sensible heat stored in the material	J
V_{st}	Volume of storage substance	$\frac{m^3}{s}$
C_p	Specific heat capacity of substance	$\frac{J}{kgK}$
ΔT	Temperature difference	$^{\circ}C$
ρ	Density of air	$\frac{kg}{m^3}$
m	mass of a substance	kg

Sensible storage capacity is limited by the specific heat of the storage medium. Nowadays, new materials are introduced in civil engineering. Phase change materials (PCMs) can offer a higher storage capacity that is associated with the latent heat of the phase change. Thermo-chemical storage (TCS) can offer even higher storage capacities. Thermo-chemical reactions (e.g. absorption or the adhesion of a substance to the surface of another solid or liquid) can be used to accumulate and discharge heat and cold on demand (also regulating humidity) in a variety of applications using different chemical reactants. An energy storage system can be described in terms of the following properties:

- **Capacity**: defines the energy stored in the system and depends on the storage process, the medium and the size of the system;
- **Power**: defines how fast the energy stored in the system can be discharged (and charged);
- **Efficiency**: is the ratio of the energy provided to the user to the energy needed to charge the storage system. It accounts for the energy loss during the storage period and the charging/discharging cycle;
- **Storage period**: defines how long the energy is stored and lasts hours to months (i.e. hours, days, weeks and months for seasonal storage);
- **Charge and discharge time**: defines how much time is needed to charge/discharge the system; and
- **Cost**: refers to either capacity ($\frac{€}{kWh}$) or power ($\frac{€}{kW}$) of the storage system and depends on the capital and operation costs of the storage equipment and its lifetime (i.e. the number of cycles).

Most used storage media are water, soil, rocks, concrete or molten salts. These materials are usually relatively cheap. However, the container of the storage material requires

effective thermal insulation, which may be an important element of the TES cost. Examples of TES systems usually consist of a 5,000-10,000 m^3 water container with energy content between 70-90 $\frac{kWh}{m^3}$ and investment costs between 50-200 $\frac{€}{m^3}$ of water equivalent, thus translating into a specific investment cost from 0.5-3.0 $\frac{€}{kWh}$. In the case of UTES systems, boreholes and heat exchangers to activate the underground storage are the most important cost elements. Specific costs range from 0.1-10 $\frac{€}{kWh}$ and depend heavily on local conditions.

2.2 Disturbances and Input in Control System

Disturbances are all interruptions to the system that affects the dynamic response of the controlled variable. The focus of research was one type of disturbance which refers to all process caused by the thermal difference between internal and external air temperature. All output disturbances (the difference between dry-bulb temperature and measured temperature, the difference between averaged airflow and real airflow, etc.) are neglected in this phase due to the low ratio of an impact to resulted value in defined conditions. Only two output disturbances will be mentioned in this phase.

2.2.1 Thermal differences

The air temperature of the interior is affected by the ambient air temperature that causes heat transfer through the zone's envelope. Beside transmittance, there is all admittance process, which is more significant for walls and less for glazed surfaces due to its construction materials and thickness. More details of these processes will be given in the following sections.

2.2.2 Solar Radiation

Solar radiation has the heaviest environmental influence on HVAC. The solar radiation passes inward through the glazed surfaces and acts as additional heat gain in the specific zone of the building. In winter regime it has beneficial character and in summer it is detrimental. Practically all alternative energy systems have a root somewhere in solar energy [40], even the DSF system. The research [41] shows the impact of solar radiation on the airflow and temperature of the corridor in the DSF system. One of the tested

building was exposed under direct sunlight, and it resulted with airflow of $0.05\ \frac{m^3}{s}$ (1 m width of the corridor)and temperature of blinds higher by $30\ ^\circ C$ above outside air. However,in laboratory testing, solar radiation may be isolated so it will not be analysed as it is not the subject of the research.

2.2.3 Mechanically driven airflow

Conventional HVAC systems usually generate airflow mechanically by active actuators. HVAC handbooks, [17] and [42], propose different types depending on purpose, characteristics and efficiency. The choice of the fan was not relevant for research, so the selection was made on the availability of elements. The selected fan is a centrifugal, forward curved fan (see Figure 2.5). Forward curved blades are known for a low

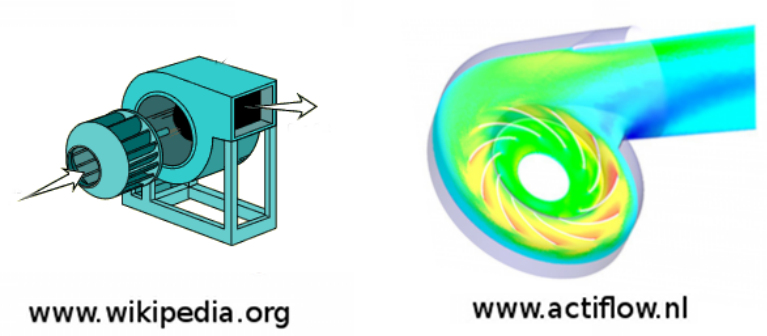

FIGURE 2.5. Forward curved centrifugal fan a) example with indication of flow direction b) result of computational fluid dynamics (CFD) pressure analysis

noise level and relatively small airflow, but a high increase in static pressure. A detailed description of the ventilator system is found in [43] but we are looking for a simple solution [44]. The airflow power may be calculated by the equation:

$$Q_{hc} = V_{hc}\rho C_p \Delta T \tag{2.2}$$

where:

Q_{hc}	Load power for heating/cooling	$\frac{m^3}{s}$
V_{hc}	Volume of air for heating/cooling	$\frac{m^3}{s}$
C_p	Specific heat capacity of air	$\frac{J}{kgK}$
ΔT	Temperature difference	$^\circ C$
ρ	Density of air	$\frac{kg}{m^3}$

Still, to directly control the airflow we need a relation between airflow speed and volume. Very simplified method is used:

$$V_{hc} = v_{hc}\rho A_{input} \tag{2.3}$$

where the measured air velocity v_{hc} is multiplied by the area of the fan face A_{input} and air density ρ.

2.3 Description of Mathematical Model of the Building with DSF

The model consists of two correlated sub-models: one represents thermal behaviour and another represents hygric behaviour. The connection is in processes where temperature variations effect the saturation vapour pressure. Here, the simplified segment of the building will be analysed (such as in Figure 2.6). The basic components of the scaled model are explained in 2.7, and listed below:

1. one glazed side represents doubles skin glass façade,
2. three other sides are vertical walls made of concrete and insulation elements, and
3. last two components are horizontal surfaces: ceiling and floor.

Constraints of used mathematical model:

- Temperature dissipation inside the zone is not neglected, but simplified to several areas were temperatures differs only during larger disturbances. In the steady state, it is assumed that the air is a perfect thermal mixer.
- The scaled segment of the building is modelled without trees around, no people in the interior, no wind and without solar radiation. Solar radiation is not neglected, but it's excluded from this research as it is not in focus.
- Influence of the moisture variations is not analysed due to isolated conditions, the absence of furniture and shorter testing periods.

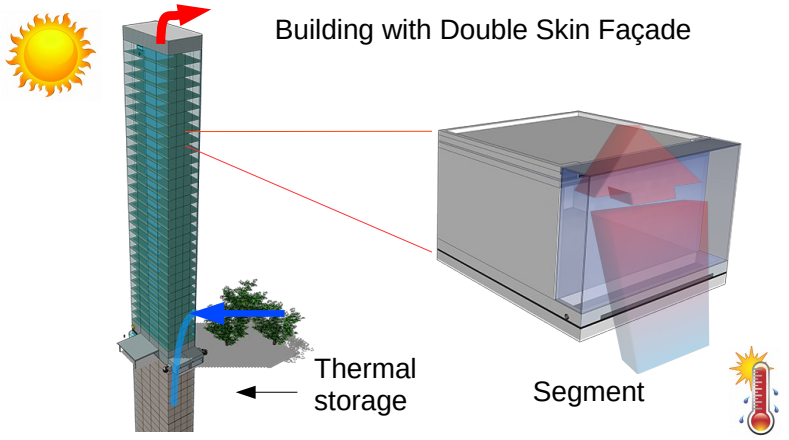

FIGURE 2.6. Segment of building with DSF

2.3.1 Thermal Model

The basic step in the synthesis of any control method is choosing the appropriate model to describe the observed thermal process. One of the most accurate ways is to find all parameters for three-dimensional parabolic Partial Differential Equation (PDE) [45]. Usually, such equation is calculated numerically what implies taking some approximations, especially while defining initial conditions and boundary values. Even more radical approach is used in engineering standards and handbooks which are implemented in 99 % of any commercial construction. For example, the heat equation is a one-dimensional linear function [46]. Also, it is usually neglected that thermo-hygric processes directly affect fluid dynamics and vice versa. Especially hard to describe are dynamics with no mechanical sources, i.e. when airflow is buoyancy driven. Such complex processes may be described mathematically but all of the methods are complex and time-consuming and as such not appropriate to use in control theory . One research [47] proposes to use basic continuum model and the Boussinesq equations for modelling in well known simulation tools *Matlab* and *CFD Comsol*. Model of the building, described here, refers only to indoor and its envelope. The starting point of describing the thermal model is the heat balance of the zone:

$$HEATLOSS + HEATSTORED = HEATGAINS + AUXILIARYHEAT \tag{2.4}$$

A thermal model of a zone is built as a thermal network of heat flow (heat rate) with only two thermal nodes: an air temperature node T_a and a resultant temperature node

T_x. A thermal network of the single zone is shown in Figure 2.7. Except for the main approximation, the HAMBASE models have few others:

- The indoor climate is described with one air temperature only and several radiant temperatures
- Radiation exchange between walls is small
- The zone air is perfectly mixed
- The surface coefficient for convection and radiation are constant
- All surfaces except windows absorb the same amount of radiant heat input per unit of surface area.

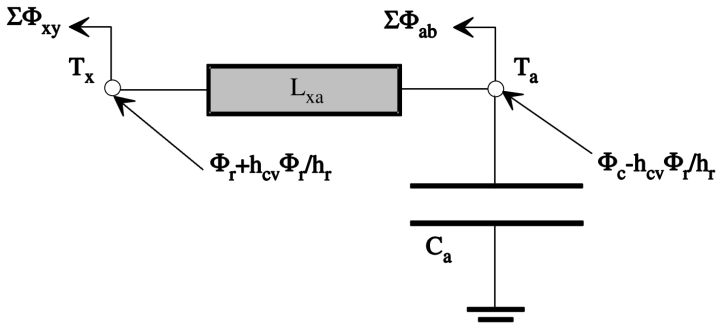

FIGURE 2.7. Thermal network for the air and resulting temperature node

Relations for different nodes are described below.
Node T_x:

$$\sum \Phi_{xy} = L_{xa}(T_a - T_x) + \left(1 + \frac{h_{cv}}{h_r}\right) \Phi_r \tag{2.5}$$

Node T_a:

$$\sum \Phi_{ab} = -C_a \frac{dT_a}{dt} + L_{xa}(T_x - T_a) + \Phi_{d2c} + \Phi_c - \frac{h_{cv}}{h_r} \Phi_r \tag{2.6}$$

Heat sum:

$$\Phi_{rez} = \sum_b \Phi_{xy} + \sum_{0<i<n} \Phi_{ab} + \sum \Phi_{cav} + \sum \Phi_{fout} \tag{2.7}$$

where components of equations (2.5), (2.6) and (2.7) are

C_a	heat storage coefficient (capacitance) of indoor air ($C_a = \rho_a c_p Vol$	$\frac{J}{K}$)
L_{xa}	coupling coefficient $L_{xa} = C_a ach/3600$)	W/K
T_a	indoor air temperature	$^\circ C$
T_x	'resultant' indoor wall temperature	$^\circ C$
h_r	surface heat transfer coefficient for radiation	$\frac{W}{m^2 K}$
h_{cv}	surface heat transfer coefficient for convection	$\frac{W}{m^2 K}$
Φ_r	heat transfer rate of the radiant input	W
Φ_{xy}	heat transfer rate from T_x node to T_y node	W
Φ_{ab}	heat transfer rate from Ta node to Tb node	W
Φ_{out}	output heat loss	W
Φ_{rez}	'resultant' heat rate of the system	W
Φ_{d2c}	heat transfer rate of the air mass that enters the corridor directly	W

Heat rate is calculated separately for each building element. Building element is a building component with specific property value (i.e. wall of the specific zone with specific orientation). So, total heat rate is the sum of heat rates of all building elements that are part of the same building component.

As seen in Figure 2.7, heat transfer can be categorized depending on building components. In the next subsections, the most important types of heat transfers will be described. The heat flow through building element is hard to measure, so the relation between the heat flow and temperatures are established. The further analysis will be done in the frequency domain.

2.3.2 Mathematical Model of the Heat Transfer through Walls

The wall of the building is given with a quite simplified mathematical model. Namely, it is of no particular interest to attempt to measure the thermal properties of each wall's element while there is no equal reproduction. The degree of reproducibility, however, is difficult to estimate and varies greatly with the type of the wall, character of workmanship, and many other properties. In practice, it is necessary to choose some reasonable approximations that would not significantly affect the observed behaviour[48].

The basic law of the heat flow equilibrium is:

$$\Phi_{LOSS} + \Phi_{STORAGE} = \Phi_{GAIN} + \Phi_{AUX} \,. \tag{2.8}$$

The extended equation to calculate T_x and T_a follows as:

$$\begin{array}{rcl} \sum_b \Phi_{ab} & = & L_{xa}(T_x - T_a) - \Phi_c + \frac{h_{cv}}{h_r}\Phi_r - C_a\frac{dT_a}{dt} \\ \sum_b \Phi_{xy} & = & L_{xa}(T_a - T_x) + \Phi_r + \frac{h_{cv}}{h_r}\Phi_r\,. \end{array} \tag{2.9}$$

The heat flow Φ_{xy} from relation (2.9) may be divided into admittance part Φ_x and transmittance part Φ_{xy}. Φ_{xy} and Φ_x are described in the next section by using differential equations.

2.3.2.1 Mathematical Model of the Heat Flow - Transmittance

The transmittance component of the heat flow (see Figure 2.7) is modelled in [49] according to the experimental data that can be seen in Figure 2.8. It is easy to notice that

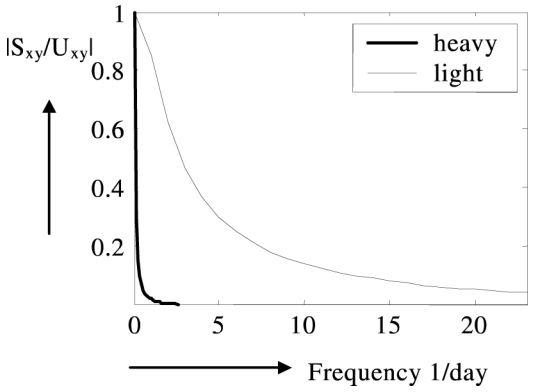

FIGURE 2.8. Cyclic transmittance for different walls, L[49]

the heat flow through the multi-layered wall may be approximated by the second order equation with a time delay:

$$kt_1\frac{d^2\Phi_{xy}}{dt^2} + kt_2\frac{d\Phi_{xy}}{dt} + \Phi_{xy} - U_{xy}\delta T_{xy}(t - t_d) = 0 \tag{2.10}$$

where:

δT_{xy}	the temperature difference	$^\circ C$
U_{xy}	total thermal transmittance through the surface A_{xy}	$\frac{W}{m^2K}$
kt_1, kt_2	coefficients	
t_d	time lag coefficients	

If we choose for coefficients to be $kt_1 = \tau_1\tau_2$ and $kt_2 = \tau_1 + \tau_2$ the equation (2.10) can

also be written as:

$$\begin{aligned} \phi_{txy1} + \tau_1 \frac{d\phi_{txy1}}{dt} &= \frac{\tau_1}{\tau_1 - \tau_2} U_{xy} \delta T_{xy}(t - t_d) \\ \phi_{txy1} + \tau_1 \frac{d\phi_{txy1}}{dt} &= \frac{\tau_1}{\tau_1 - \tau_2} U_{xy} \delta T_{xy}(t - t_d) \end{aligned} \tag{2.11}$$

2.3.2.2 Mathematical Model of the Heat Flow - Admittance

According to the experimental data that can be seen in Figure 2.9, the total room (interior) admittance may be modelled as a second order differential equation.

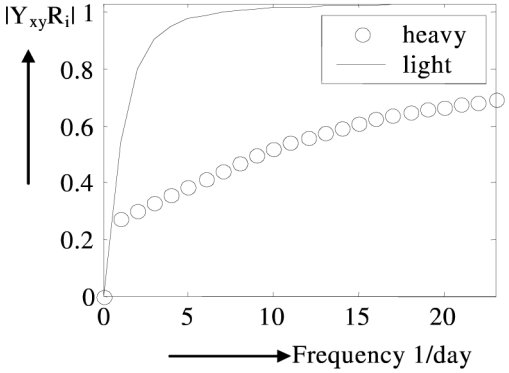

FIGURE 2.9. Cyclic admittance for different walls, L[49]

Figure 2.10 illustrates the relations between variables by using thermal network. Wall is presented with two resistors L_{x1}, L_{x2} and two capacitors C_{x1}, C_{x2}.

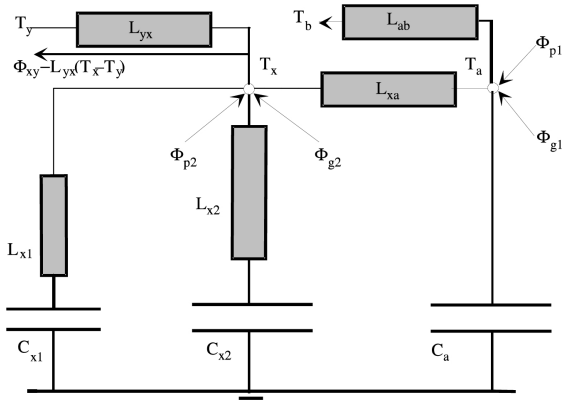

FIGURE 2.10. An indoor thermal model of admittance, L[49]

Following the rules of thermal network graph, the equations may be written as:

$$\begin{aligned} \Phi_{x1} + \frac{C_{x1}}{L_{x1}} \frac{d\Phi_{x1}}{dt} &= C_{x1} \frac{dT_x}{dt} \\ \Phi_{x2} + \frac{C_{x2}}{L_{x2}} \frac{d\Phi_{x2}}{dt} &= C_{x2} \frac{dT_x}{dt} \end{aligned} \tag{2.12}$$

Adding the substitution $\Phi_x = \Phi_{x1} + \Phi_{x2}$ we gain:

$$\frac{C_{x1}C_{x2}}{L_{x1}L_{x2}}\frac{d^2\Phi_x}{dt^2}+\left(\frac{C_{x1}}{L_{x1}}+\frac{C_{x2}}{L_{x2}}\right)\frac{d\Phi_x}{dt}+\Phi_x = (L_{x1}+L_{x2})\frac{C_{x1}C_{x2}}{L_{x1}L_{x2}}\frac{d^2T_x}{dt^2}+(C_{x1}+C_{x2})\frac{dT_x}{dt}\,. \tag{2.13}$$

Equation (2.13) can be written in the following form:

$$k_{a1}\frac{d^2\Phi_x}{dt^2} + k_{a2}\frac{d\Phi_x}{dt} + \Phi_x = k_{a3}\frac{d^2T_x}{dt^2} + k_{a4}\frac{dT_x}{dt}\,. \tag{2.14}$$

where

$$\begin{aligned} k_{a1} &= \tfrac{C_{x1}C_{x2}}{L_{x1}L_{x2}} \\ k_{a2} &= \left(\tfrac{C_{x1}}{L_{x1}}+\tfrac{C_{x2}}{L_{x2}}\right) \\ k_{a3} &= (L_{x1}+L_{x2})\tfrac{C_{x1}C_{x2}}{L_{x1}L_{x2}} \\ k_{a4} &= (C_{x1}+C_{x2}) \end{aligned} \tag{2.15}$$

According to [49] the heat flow through a multilayered wall fit nicely with the solution of the second order equation with a time delay. Similar to the thermal network graph of admittance (see Section 2.3.2.2), the heat balance is also expressed as a sum but with density $q_{xy} = q_{xy1} + q_{xy2}$:

$$\begin{aligned} q_{xy1} + \tau_1\tfrac{dq_{xy1}}{dt} &= \tfrac{\tau_1}{\tau_1-\tau_2}U_{xy}\Delta T_{xy}(t-t_d) \\ q_{xy2} + \tau_2\tfrac{dq_{xy2}}{dt} &= \tfrac{\tau_2}{\tau_2-\tau_1}U_{xy}\Delta T_{xy}(t-t_d)\,. \end{aligned} \tag{2.16}$$

Equations (2.16) may be added together, and if density is expressed through the heat flow $q_{xy} = \Phi_{xy}/A_{xy}$ the following form yields:

$$\tau_1\tau_2\frac{d^2\Phi_{xy}}{dt^2} + (\tau_1+\tau_2)\frac{d\Phi_{xy}}{dt} + \Phi_{xy} = \frac{1}{A_{xy}}U_{xy}\Delta T_{xy}(t-t_d) \tag{2.17}$$

It is more appropriate to group all parameters as shown in:

$$k_{t1}\frac{d^2\Phi_{xy}}{dt^2} + k_{t2}\frac{d\Phi_{xy}}{dt} + \Phi_{xy} = \frac{1}{A_{xy}}U_{xy}\Delta T_{xy}(t-t_d)\,. \tag{2.18}$$

where

$$\begin{aligned} k_{t1} &= \tau_1\tau_2 \\ k_{t2} &= \tau_1+\tau_2 \end{aligned} \tag{2.19}$$

Φ_x is the heat wall directed to the wall, and Φ_{xy} is the heat flow transmitted through the wall. U_{xy} is the total thermal transmittance ($\frac{W}{m^2K}$) of the wall. C_{x1} and C_{x2} are heat capacities of interior corridor surface. L_{x1} and L_{x2} are coupling coefficients. A_{xy} is a

surface of the observed element. τ_1 and τ_2 are parameters of the first and second element of heat transmittance equation (see (2.16)). Variable T_{xy} is the temperature difference between resultant surface temperature T_x and exterior air temperature T_y. T_y may be measured, and T_x may be substituted with admittance part of system equation (2.14). t_d is a time delay (time lag) of temperature difference input that causes an unavoidable nonlinearity in the heat flow. Most of these coefficients cannot be measured directly, and others requires complicated methods for its acquisition. Research [50] propose a combined solution: For all parameters that are considered invariant, values have been taken from standard material specification tables and environmental specification tables for civil engineering. Others, such as τ_1 and τ_2 are calculated by minimizing the error function of the exact solution with the model solution, as the thermal equilibrium must be obtained. Such an approach is necessary to test before applying in control application where the response is much faster.

2.3.3 Heat Transfer through Fenestration

The main focus here is heat flow caused by external temperature variation what may be analysed in an isolated environment. Solar effect is not analysed, and it is left for future research. It should not be concluded that solar is not important because it has the highest influence to the DSF. But, in the sense of control, it is one of many disturbances which is now not a topic of the research.

2.3.4 Heat Transfer through DSF Corridor

Heat transfer through the glass of a DSF's glazed skin can be considered to be one dimensional since the heat transfer through glass will occur predominately in one direction and the heat transfer in other directions is negligible. As also demonstrated in the paper [51], linear relations may be used to calculate the building energy through the DSF. So, the DSF corridor will be represented as thermal network what is shown in Figure 2.11. In the figure, there are three nodes with different temperature: T_e, T_c and T_a. Relation to zero temperature node is not shown. All three nodes are correlated by the law of heat flow equilibrium that may be expressed with relation (2.20).

$$\Phi_{fin} + \Phi_{d2c} = \Phi_{ecd} + \Phi_{fout} \tag{2.20}$$

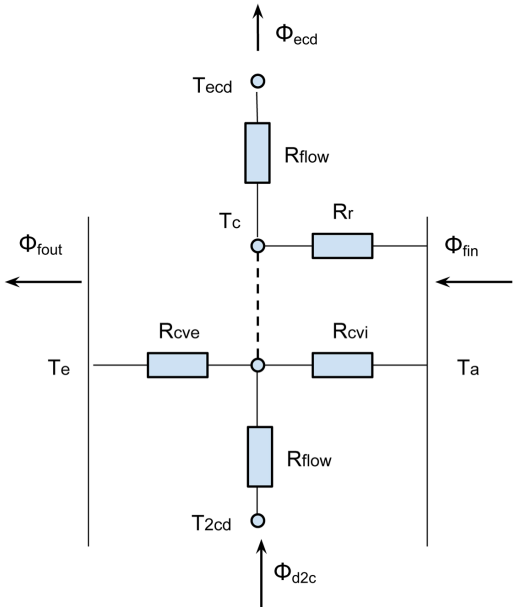

FIGURE 2.11. Thermal network of the corridor

And each heat flow is related with one node.
Node T_e:

$$\Phi_{fout} = R_{cve}(T_c - T_e)\,. \tag{2.21}$$

Node T_c:

$$(R_{cvi} + R_r + R_{flow} - R_{cve})T_c = (R_{cvi} + R_r)T_a + R_{flow}T_{d2c} - R_{cve}T_e\,. \tag{2.22}$$

Node T_a:

$$\Phi_{fin} = (R_r + R_{cvi})(T_a - T_c)\,. \tag{2.23}$$

Node T_{d2c}:

$$\Phi_{d2c} = R_{flow}(T_{d2c} - T_c)\,. \tag{2.24}$$

where:

R_r	thermal resistance by radiation	$\frac{K}{W}$
R_{cv}	thermal resistance by convection	$\frac{K}{W}$
R_{flow}	thermal resistance by airflow through the fenestration	$\frac{K}{W}$
h_r	surface heat transfer coefficient for radiation	$\frac{W}{m^2K}$
h_{cv}	surface heat transfer coefficient for convection	$\frac{W}{m^2K}$
c_p	specific heat of the air	$\frac{J}{kgK}$
Q_m	the air mass flow	$\frac{kg}{m^3}$

Φ_{fout}	the heat flow from fenestration to exterior	W
Φ_{fin}	the heat flow from interior to fenestration	W
Φ_{d2c}	the heat flow to fenestration corridor	W
A	fenestration surface area	m^2
T_e	the exterior (outdoor) temperature	$°C$
T_c	the corridor temperature	$°C$
T_a	the interior air temperature	$°C$
T_{d2c}	the temperature of the air mass that enters the corridor	$°C$

Resistances are calculated by relations:

$$\begin{aligned} R_r &= \tfrac{1}{Ah_r} \\ R_{cve} = R_{cvi} &= \tfrac{1}{Ah_{cv}}\ \Phi_{fin} \\ R_{flow} &\approx \tfrac{1}{2c_pQ_m}. \end{aligned} \tag{2.25}$$

Total heat of the DSF system is the total sum of heat flow (see Figure 2.7)

$$\Phi_{rez} = \sum \Phi_{fin} + \sum \Phi_{d2c} + \sum \Phi_{ecd} + \sum \Phi_{fout}. \tag{2.26}$$

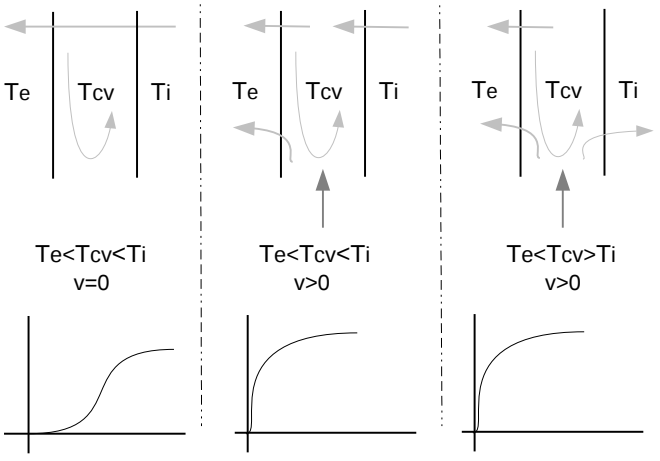

FIGURE 2.12. Heat flux directions in different DSF's work regimes

Analysis of the thermal process inside the DSF corridor shows some similarities with the heat transfer through the wall (see Figure 2.7). Figure 2.12 illustrates three different cases in the corridor of the DSF. In the first case, when there is practically no airflow inside the corridor, a process in DSF is very similar to transmittance part of the equation for heat transfer through the wall.

2.3.5 The Heat Transfer through Air Infiltration

Air infiltration refers to air mass flow through opened doors, windows or gaps between construction elements. To emphasize the heat transfer through elements and to neglect the moisture effect, it is assumed that the interior zone is completely sealed, so air infiltration does not exist in the system.

2.3.6 Hygric Model

Due to the complexity and specific scope of the research, hygric model will not be analysed in details, only some basics will be mentioned. Used hygric model is explained in [49]. Moisture or water vapour moves into building or furniture cavities in three ways: with air currents, by diffusion through materials and by heat transfer. Of these three, air movement accounts for more than 98% of all water vapour movement in buildings [52]. Stored moisture affects the conductivity properties of the construction component and here lies the correlation between thermal and hygric model. As the main generator of hygric dynamics, air infiltration is assumed to be zero, there will not be significant variation of humidity during control, and one important condition may be assumed: In the vicinity of the working regime there are very small variations of hygric conditions. With this assumption, we end up with a linear mathematical model and all benefits of such a model. However, the validity of this linear model is now limited inside the range between 20% and 80% of relative humidity.

During experimental simulations, exterior hygric conditions will not be changed (no hygric disturbance). Consequently, in the case of scaled model and short testing period, the influence of thermal activity to hygric conditions may also be neglected.

2.4 Estimation of the Heat Flow

In order to increase the thermal insulation, efficiency information about the heat flow is required. Measuring the heat flow is still not an appropriate solution due to the absence of adequate sensor, as described in Section 2.7.3. Estimation methods of the heat flow generally may be divided into two groups depending on the level of approximation during the modelling process. In theory, as shown in Section 2.3, a mathematical model based on the heat flow estimation relay on many coefficients what causes complex identification. Even though some relations such as transfer heat flow through the wall are

very simple, in practise, they become very complex due to non-homogeneity of each element. Therefore, an approximation of the physical reality is needed to reduce the required data ([49]. Synthesis of such model for control purposes is a very sensitive task because controlled dynamics should be preserved after all. In the last decade, several papers, such as [53] and [54], described the new estimation method avoiding these shortcomings using neural networks. The neural network is used for feed-forward control with the learning phase. Our propose is to the skip learning phase by using different neural control structure. This strategy has a great advantage in long-term exploitation of the system due to adaptive capability. For instance, the system is capable of adapting its behaviour to ageing, change of parameters or other causes.

Most of the standard building simulation tools (e.g., EnergyPlus, ESP-r, TRNSYS, TAS, IDA ICE, VA114, BSim) developed for conventional building envelopes cannot accurately describe the heat flow and mass transfer phenomena that occur in the complex three-dimensional (3-D) space of DSFs [55], [56]. One solution to yield better results is to include an airflow velocity term in the heat transfer coefficients expression by using CFD analysis tools.

2.5 Numerical Analysis

Numerical methods were used to justify the usage of high approximation relations where experimental verification was not possible. Also, numeric energy simulators where analysed to inspect the possibility of usage in the design of control method.

2.5.1 Computational Fluid Dynamics

Dynamic behaviour of air mass speed and air temperature are all implemented in used numerical model. Due to complexity, assumption related to air mas dynamics were validated by numerical CFD (Computational Fluid Dynamics) analysis. According to the similar CFD analysis done by [57] and [58], the expected difference between the physical measurement and CFD simulation for air velocity is more than 15 $\%$ and less then 20 $\%$. The errors are mainly due to uncontrolled infiltration in the actual zone which is difficult to be quantified for CFD simulation.

The CFD analysis was performed on a scaled segment of the DSF system used in experimental and numerical tests (see Section 2.7). Based on the results of these tests, initial

parameters are defined as follows: Maximum input air speed amounts 0.42 m/s on duct opening and 1.02 m/s directly after the fan. The heater is simulated without dynamics which means that the output is a steady state maximum power of 25 $Watt$.

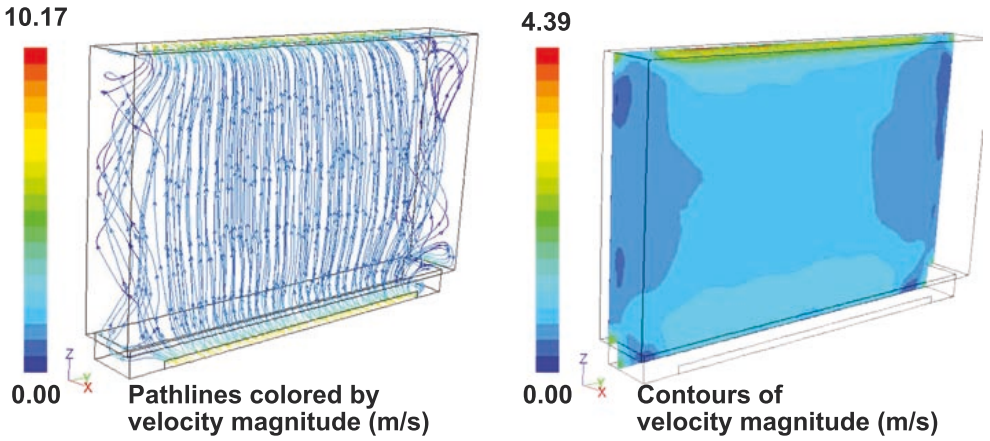

FIGURE 2.13. CFD - airflow velocity vectors and contours

Two different analysises were performed to obtain the airflow behaviour for both DSF configurations: with and without shaft on the diagonally opposite side of the air input. The simulation was influenced by the standard procedures which are defining the geometry of the tested cell, meshing, fluid properties, boundary conditions, solver settings, solution methods and the results are obtained from CFD post which is a common post-processor feature of the fluid dynamics simulation environment. Simulation results of airflow in the corridor area and inlet tube have been obtained using the standard $k - \varepsilon$ model. Curves from Figures 2.13 and 2.17 represents the simulated airflow path lines. Also, contours from Figures 2.13, 2.14, 2.17, 2.16 and 2.15 represents velocity or temperature magnitude. Variable values are indicated by the coloured zones in all figures mentioned above. Figure 2.13 shows results from the test with the shaft opening where the inlet load is ideally spread across the DSF. Plotted path-lines on left image and contours on right images represent velocity values inside the DSF's corridor. It can be seen that the air distribution pattern in the area of low speed flows behaves fairly well for linearization.

Next CFD test is configured without shaft for an outlet, but with the inlet tube, have different results as nonlinearity resulting from shape is more expressed. It can be seen in Figure 2.14 that the warmer air enters the DSF through the lower part of the corridor and spreads to upper parts.

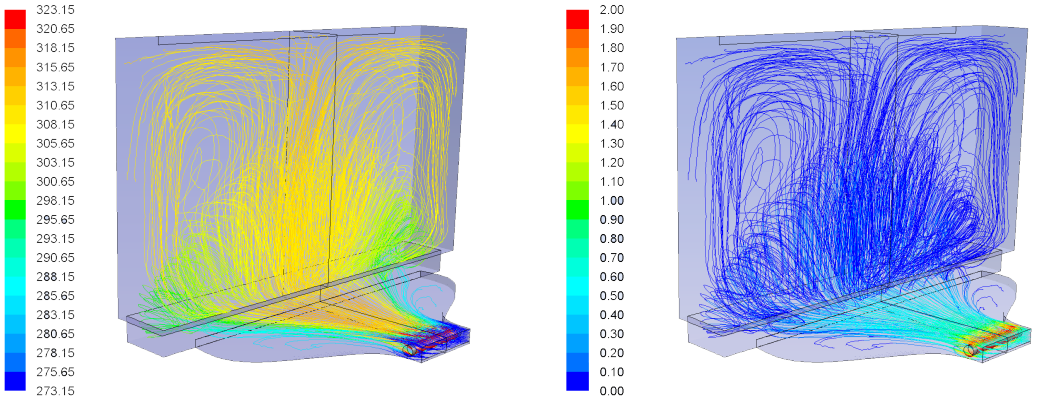

FIGURE 2.14. Pathlines a) Temperatures[K] b) Velocities [m/s]

The central stream splits in two and moves downward by sideways. As noticed, both: thermal and airflow process, are not uniform and linear. At the same time, it can be seen that one temperature dominates the corridor and the velocity is rather low. So, from the control point of view, the mentioned deviation may be neglected. Based upon the calculated temperature across the system's width, temperature contours are shown in Figure 2.15.

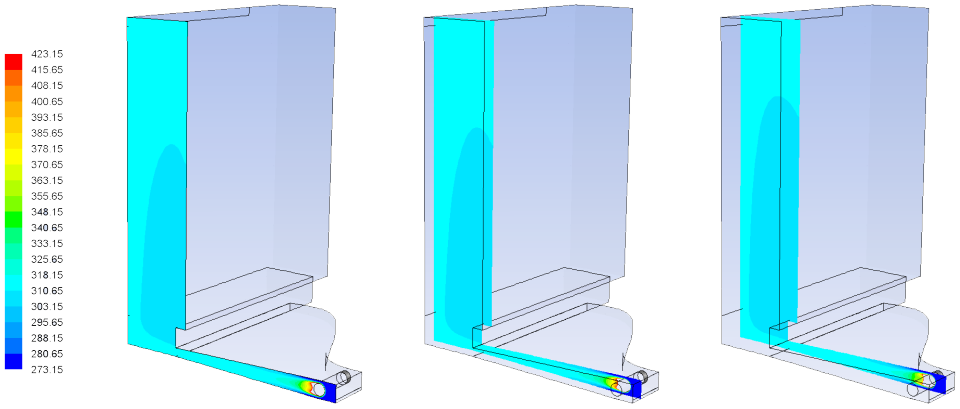

FIGURE 2.15. Temperatures [K] at $y = \{0, 10, 20\}$ mm

Temperature slightly decreases from the centre to lateral even though the airflow velocities are the same as shown in 2.16.

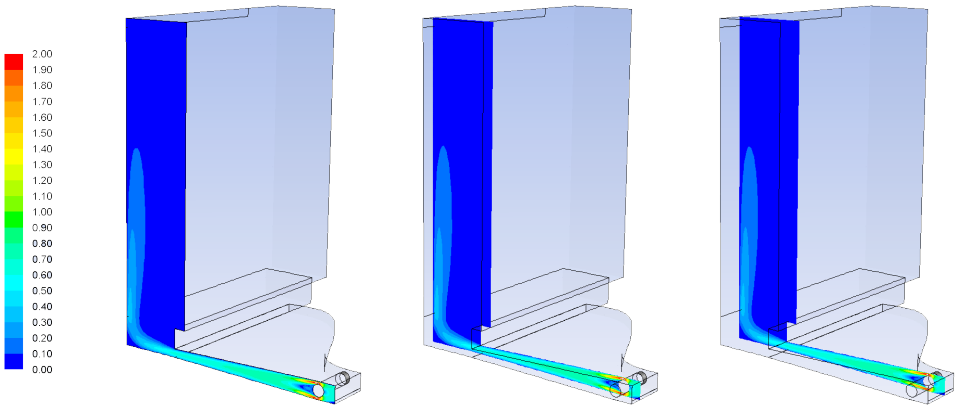

FIGURE 2.16. Velocities [m/s] at $y = \{0, 10, 20\}$ mm

This effect is caused by the shape of the inlet tube: Significant air mass is not under direct airflow stream, yet its results after bending (see Figure 2.17).

At this moment, the preliminary CFD simulation well supports the hypothesis that a vertical upward movement of air mass is almost linearly spread in experimental conditions when the major driving force of airflow is adequate stream source.

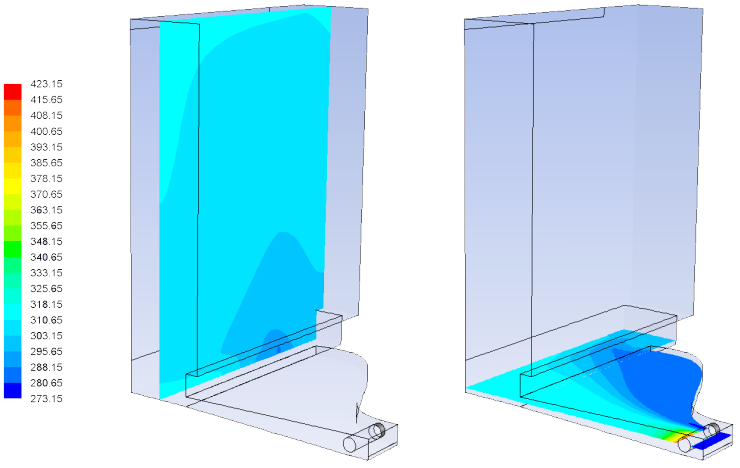

FIGURE 2.17. Velocities [m/s] at $y = \{0, 10, 20\}$ mm

Also, the accuracy of the CFD simulation will be compared against experimental data explained in 2.7. In laboratory experiments, the transient thermal exchange via a single-side ventilation tube was measured using infra-red system (ThermaCam P65, FLIR), and the indoor and outdoor air temperature differences were closely monitored.

2.5.2 Simulation of Energy Consumption

Many common tools for simulation of heat, air and moisture condition of whole buildings [59], where considered. Due to the need for modification, only the free-ware application could take part in this research.

Studied models, in this case, do not have accuracy as the ultimate criterion. Several articles: [60], [61], [62] and [63], points out simplicity as another very important characteristic that enables the practical usage of the model.

2.6 HAMBASE

HAMbase (Heat Air and Moisture model for Building And Systems Evaluation) is an open source simulation model for the heat and vapour flows in buildings. The history of this model starts from 1987 and the used version WAVO [64] is a combination between two separate models: one for modelling thermal network (ELAN described in [65]) and other for simulating the indoor air humidity (AHUM). Separately, a model for simulating the indoor air humidity (AHUM) was developed in 1990 by de Wit [66]. In 1992, the two models were combined and programmed in the *MATLAB* environment [67].

Toolbox HAMBASE is well known for its main advantages:

1. realistic simulation of building system dynamics (time step of one hour)
2. reduced simulation time by modelling the heat flow that varies slowly
3. include the transfer of moisture (water vapour)

However, this software does not take into account a crucial element characteristic of these bio-climatic buildings, the air density [68]. One disadvantage of the HAMBASE is the fact that it has been mainly used in many projects about old buildings: buildings without insulation, with a huge volume (e.g. churches) and a lot of thermal mass. More about these facts will be discussed while analysing simulation result in Chapter 4.

The model was subject to numerical and empirical validation [49]. Numerical validation consisted of comparative testing and analytical verification. For comparative testing, the ASHRAE Bestest is used [69]. Detailed description of the software code may be found in literature [67], [49], [68], [70] and [71]. Settings and changes are described in details.

2.6.1 Parametrisation

The HAMBASE model is analysed to simulate DSF systems. DSF is written as a zone with mainly windows. Interior glassed surface is not defined as window because we don't want to count the heat through the interior wall in losses through the glass. It is described as a very thin wall, made of glass so its capacitive properties will be negligible. A_{tot} is the total surface of the zone. DSF zone does not have ventilation, but heat input.

The influence of the external air temperature upon the building behaviour is analysed using *Matlab*/*Simulink* and toolbox HAMBASE. The shape and dimensions of the tested object in numerical model were limited by experiment that is explained in Section 2.7. However, the simulator enabled manipulations, for instance dimensions are varied from scale 1:1 to scale 1:10 in order to investigate if simulations give appropriate results for high scale. Four variations are exposed to same thermal conditions during the period of 3 days. Temperature of the air in the building and heat were observed. Simulations gave us quite unexpected results, proving that the simulation for the scale 1:10 or higher is not adequate to describe the physical behaviour. Results are shown in 2.18:

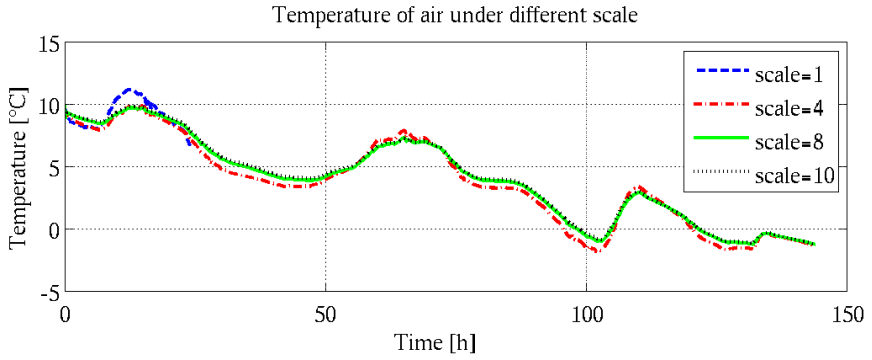

FIGURE 2.18. Influence of dimension variance in scale to air temperature in the zone

By decreasing the dimensions of the building, the influences of the exterior air temperature around the building on the interior air temperature is increasing due to faster dynamics. This should be expected, because for admittance and transmittance process, less time is required if dimensions are smaller. But, the intensity of such effect is too small concerning the scale value.

2.6.2 Implementation

HAMBASE program package is primarily dedicated to energy analysis purposes and not for the purpose of heat regulation. So, few modifications were needed in the HAMBASE program package in order to be explored for the heat regulation purposes. It has been carefully analysed what assumptions are violated and how they influence the model results. However, we have not succeeded to get satisfying results with implemented modifications. One of the reasons is HAMBASE structure: The HAMBASE model calculates the coefficients of a second-order model numerically by searching for ones that gives the same heat flow. The model is excited with a cyclic temperature approximating a triangle with base of two hours each 24 hours. The unknown components of the model network are found by minimizing the error function with respect to heat storage coefficients and heat loss coefficient of the temperature node on the envelope inner surface. In our case, the model is excited with step, process is much faster than one hour, and the mentioned heat coefficients are not precise enough for smaller dimensions. Further on, we can not analyse the impact of the control output to the system with HAMBASE. Consequently, no HAMBASE code will be used in our further experiments, but our mathematical model will be based on HAMBASE. As system identification is now unavoidable, it will be done in following experiments.

2.7 Experimental Analysis

Due to implemented modifications, described in Section 2.7.5, experimental test are required to validate the model's accuracy. These tests were performed on scaled model of the building (scaled mock-up of the building segment, see Figure 2.22). The goal was to isolate interfering disturbances and observe isolated behaviour of the system's response from heat regulation point of view. This is common procedure in commissioning phase while building innovative buildings [72]. Obtained results are used to do calibrations and model corrections that are not possible otherwise. Model has similar construction elements compared to real object. Our intention was to test the numerical model and heat regulation for different conditions. Realized scaled mock-up is made from expanded polystyrene (EPS), bitumen, concrete, glass and paint. The process of the construction is shown in Figures 2.19, 2.20, 2.21, 2.22 and 2.23 as chronological sequence of drawings and photographs.

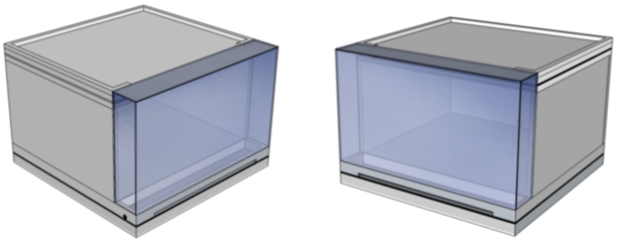

FIGURE 2.19. 3D representation of scaled mock-up

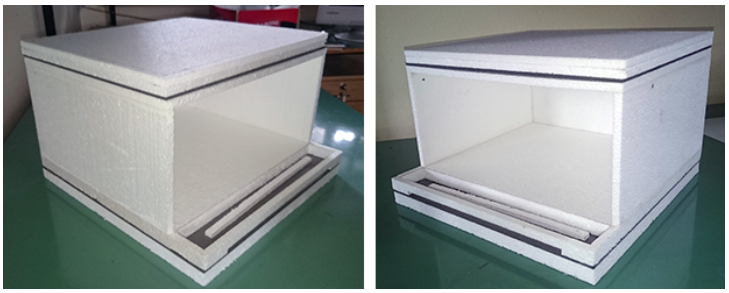

FIGURE 2.20. Photography of scaled mock-up with EPS and bitumen elements

FIGURE 2.21. Photography of painted scaled mock-up with with glazed façade

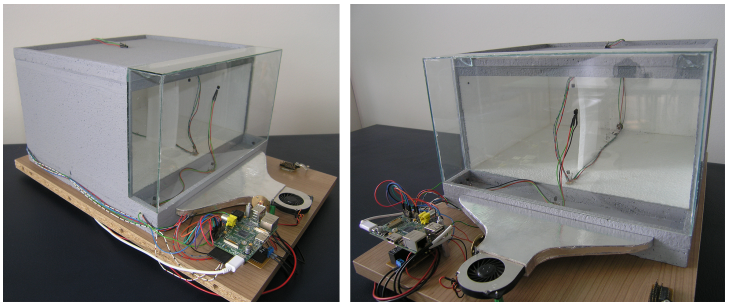

FIGURE 2.22. Photography of painted scaled mock-up with regulating system

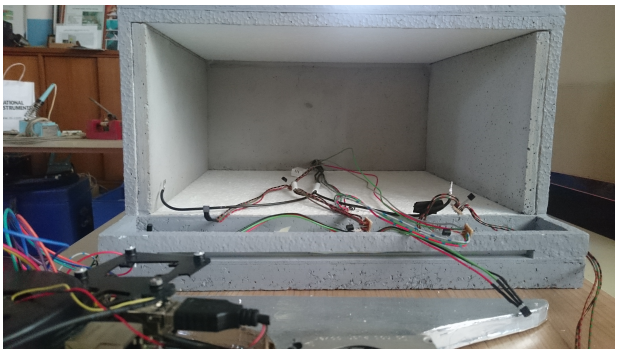

FIGURE 2.23. Photography of scaled mock-up with concrete walls

2.7.1 Experimental set-up

Choosing hardware was demanding due to the limitation of space in the thermal chamber (see Figure 2.29) which was used to produce the desired environmental thermal conditions for the scaled mock-up placed inside the chamber (external disturbances). Data processing has been divided into two separated parts: IO acquisition unit and PC for advanced calculations and control purposes. Sensors, used in experiments, are listed in 2.1.

TABLE 2.1. Equipment list

Item	Producer	Model	Y	Q	Spec.	Un.
Sensors						
Thermographic camera	FLIR	ThermaCAM P65	'07	1	Image output	$\pm 2°C$
Temperature and humidity sensor	DHT22	AOSONG	'14	2	AM2302 chip	$\pm 0.5°C$ ± 5 RH
Temperature sensor	DALLAS	DS18B20	'15	6	digital	$\pm 0.5°C$
Airflow sensor	OMEGA	FLO HH30	'94	1	rotating vans	$\pm 1\%$
Pressure sensor	BOSCH	BMP180	'15	3	digital	± 6 hPa
CPU & Acquisition unit						
Single-board PC	Raspberry Pi	B	'15	1	700MHz 512MB	
Actuators						
Heater	Weller	21 021/50VA	'76	1	12V 25W	
Fan	Sunon	Maglev	'14	1	12V 2.5W	
Thermal chamber	Kottermann	D3165 - 2302		1	-30...+100$°C$ 900W 3x380V 50Hz 4A	$\pm 2°C$

2.7.2 IO Acquisition Unit

Instead of using one of the standard industrial controllers sensor data acquisition is done by developing a simple, low-cost unit based on Raspberry Pi. Communication is done over Ethernet by TCP/IP protocol as time constants are more than seconds.

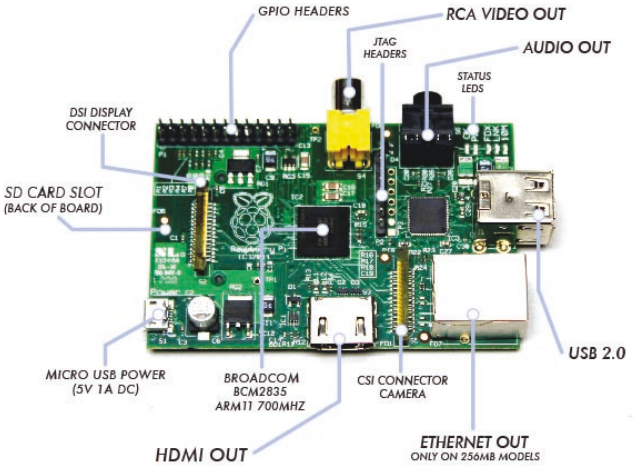

FIGURE 2.24. Low cost single board computer - Rasberry Pi

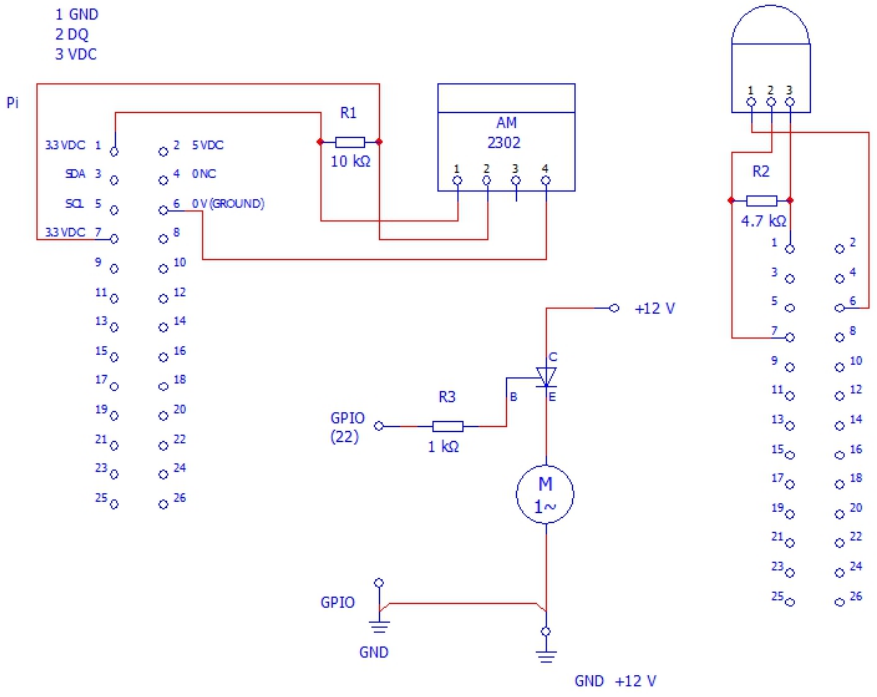

FIGURE 2.25. Electric circuit - schematics

2.7.3 Preparation for Experiments

Collecting data from scaled mock-up has multiple purposes: getting some initial information about the system and validation of the numerical model. Measurements have been taken place from June 2015 till August 2017. at the electro-mechanical laboratory of Brodarski institute. There is no official standard for measuring dynamic characteristics of double skin façades, so practice was to use experiences from other research on the similar topic: [73], [74], [75] and [76].

Dimensions have been carefully chosen to fit testing conditions. For example: the glass width of 36 mm satisfies the conditions of official Code of Practise [77] in civil engineering, so in a scaled version with a ratio of 1:18 the value of the glass width should be 2 mm.

Figure 2.26 represents side-view and top-view projections of the model where the location of measurement points are denoted. Labelled dots stand for sensors, whose purpose, position and type are described in Table 2.2. Due to the projection of 3D to 2D space, some dots represent more than one sensor. At these positions, sensor's labels contain letter x that may have multiple meanings: e.g. T_{c-mx} represents T_{c-mg} and T_{c-mt}.

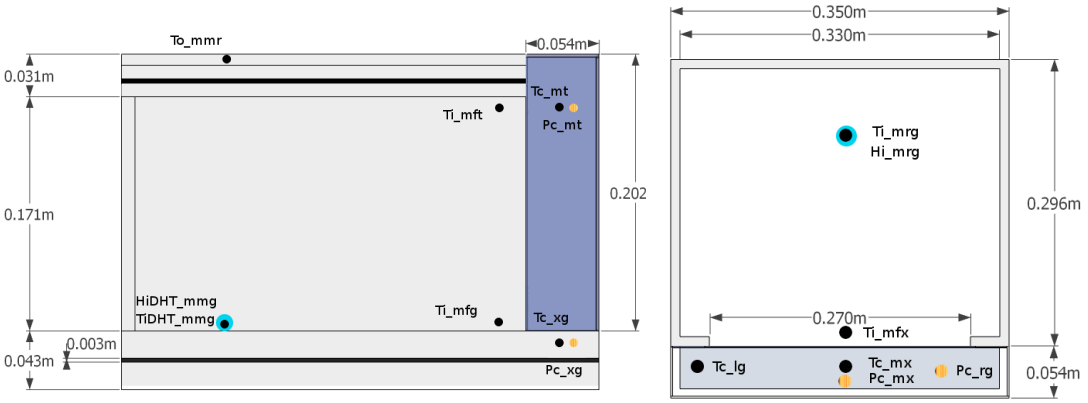

FIGURE 2.26. Dimensions with marked location for sensor deployment a) side view b) top view

Heat flux through building elements can be measured directly on the surface of the element or even inside the element. Such sensors are called heat transducers. Heat flux

TABLE 2.2. Deployment of the sensors

Tag	Property	Location	Deployed position	Type
T_{i-mfg}	temperature	interior	middle, front, ground floor	DS18B20
T_{i-mft}	temperature	interior	middle, front, ceiling	DS18B20
T_{c-mmg}	temperature	corridor	middle, middle, ground floor	DS18B20
T_{c-mmt}	temperature	corridor	middle, middle, ceiling	DS18B20
T_{c-lmg}	temperature	corridor	left, middle, ground floor	DS18B20
T_{o-mmr}	temperature	exterior	middle, middle, ceiling	DS18B20
$T_{iDHT-mmg}$	temperature	interior	middle, middle, ground floor	DHT22
$H_{iDHT-mmg}$	humidity	interior	middle, middle, ground floor	DHT22
P_{c-mmt}	pressure	corridor	middle, ceiling	BMP180
P_{c-mmg}	pressure	corridor	middle, ground floor	BMP180
P_{c-rg}	pressure	corridor	right, ground floor	BMP180

transducers are based on thermocouples. They are used for a variety of applications, for example in the analysis of thermal properties of the soil [78] and in the calculation of thermal resistance or thermal transmittance of the envelope. Depending on the application, such a sensor can measure total heat flux (conductive, convective and radiative part) or single quantity. Since heat flux transducers are very specific and not easy to build, their price is high in comparison to common temperature sensors. Usually, these sensors must be appropriately calibrated, and moreover, high-quality DAQ is needed [79].

2.7.4 Experiments with Thermo-visual Camera

The thermo-visual camera is used to validate equal temperature distribution under dynamic conditions. Scaled mock-up is placed in front of thermo-visual camera listed in Table 2.1. The focus of the camera is set on a duct that connects the model with the source of warm air. During the period of 180 s, the warm air is being delivered into the corridor of the DSF directly through the shaft. Figure 2.27 shows infra-red photos that have been taken during two experiments. The only difference between these two experiments is in the heater position. In the first experiment there is a gap of 1 cm, so the heat flow in the duct is greater on the right side. Comparing both figures it can be observed that a proper experimental design must be ensured to achieve that the heat is spreading equally through the air channel.

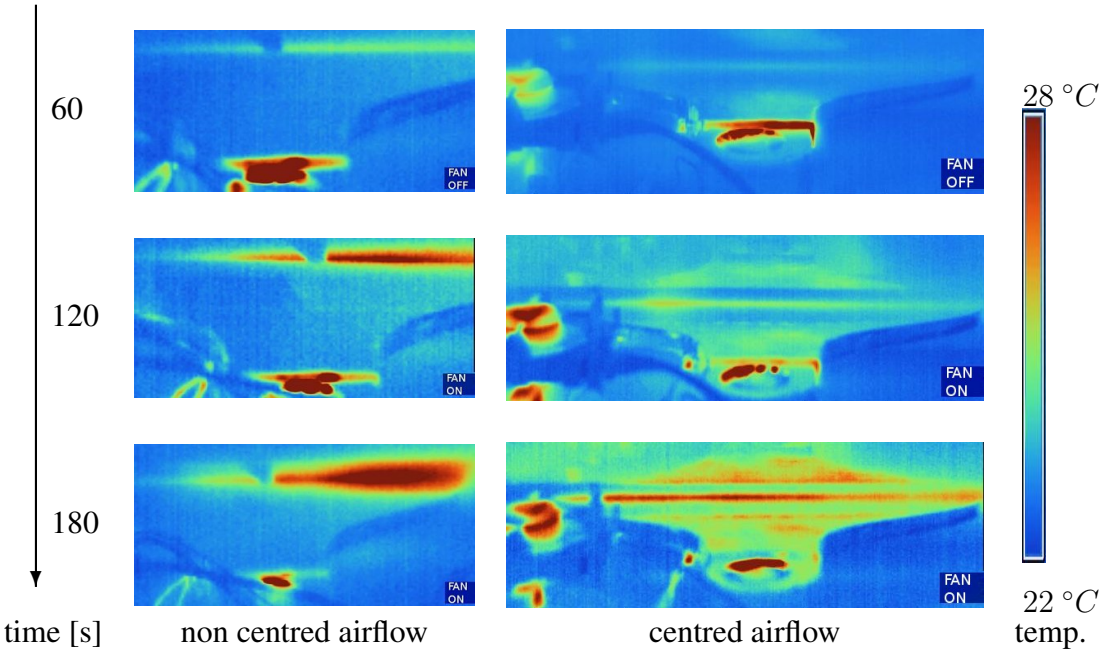

FIGURE 2.27. Thermo-visual tests

2.7.5 Airflow Experiments

Research of [73] demonstrated the extreme difficulty of measuring airflow in naturally ventilated space. Small dimensions of the corridor of scaled mock-up do not allow most of the direct measurements. Miniature pressure sensors from Table 2.1 were installed, but testing yielded very unsatisfactory results.

Airflows caused by mechanical ventilation are much easier to measure. The most common way to get airflow is to measure air speed and then estimate airflow. Air speed is measured directly behind the fan and on the duct opening as in Figure 2.28a. From Figure 2.28b it is evident that the airflow behaviour of the hot-air input system may be linearized around a selected working point. This data is used as an input for the numerical test described in Section 2.5.1.

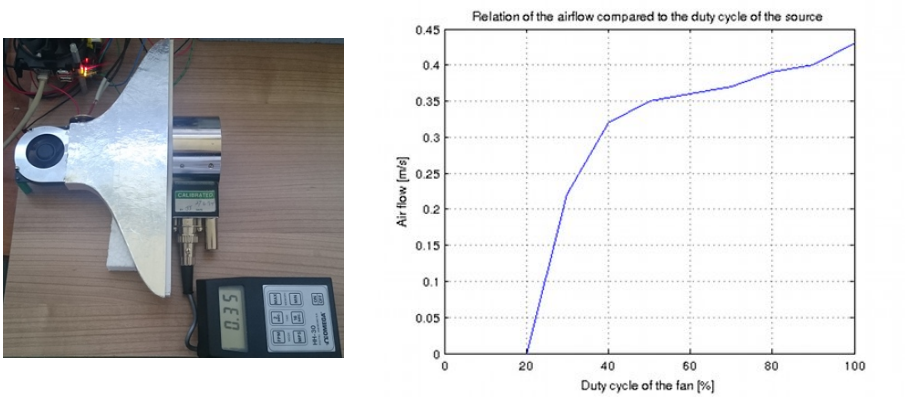

FIGURE 2.28. Air speed measurements a) Sensor position for measurement b) Obtained static characteristic

2.7.6 Heat Transients regarding Heat Inputs

During the experimental measurements, exterior air temperatures varied and the interior air temperature was not conditioned (no HVAC). The experiments were carried out using a thermal chamber to regulate exterior air temperature, and fan with the heater to deliver warm air. Experiment set up is shown in Figure 2.29.

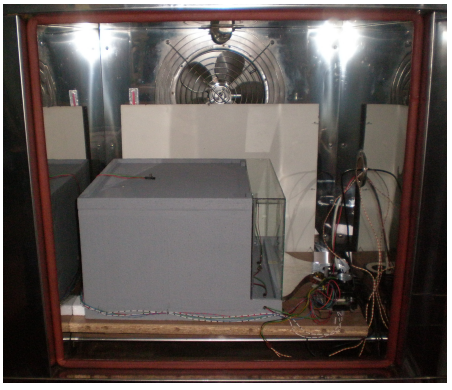

FIGURE 2.29. Thermal chamber with the scaled mock-up inside the chamber

The first test was performed to get some general dynamic properties of the system. The scaled mock-up was excited with negative and positive thermal disturbances. Responses of the air temperatures are shown in Figure 2.30. They are grouped according to zones they belong to. The difference between air temperatures, measured on different positions in the corridor, is very small. This difference is slightly greater in the interior zone. In both cases, these deviations are practically negligible compared to the values

of the adjacent zone and exterior. In the second part of the test, the scaled mock-up was cooled in equal steps of 5 $°C$. Exterior air temperature decreased in steps of 5 $°C$, but this effect did not penetrate the zones.

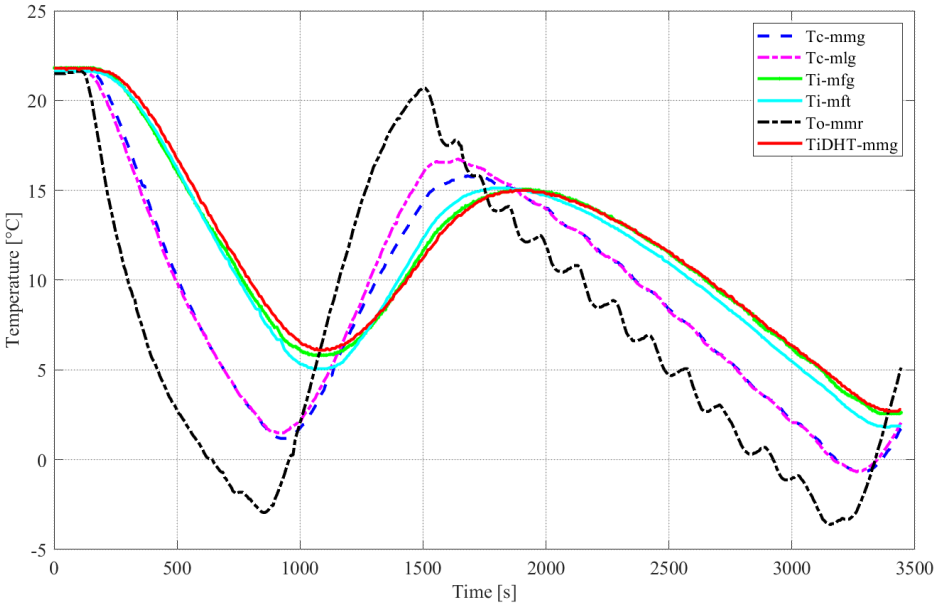

FIGURE 2.30. Air temperatures measured for different zones as a response on dynamic heat flow input in the thermal chamber affected by variation of the input heat flow in the thermal chamber

Figure 2.31 presents temperature of the corridor air and interior air responses to increasing heat-flow steps of 10 $°C$ each. Each figure shows five different responses set to the same scale in order to analyse behaviour under different temperature ranges. Results are very similar for both temperature variables, indicating that thermal resistance of the DSF system in these conditions is constant. Accordingly, the temperature does not affect DSF properties to a significant degree, so that, the system may be treated like a multilayer wall.

The experiment shown in Figure 2.32 has the same set-up and similar scenario as in Figure 2.31, but here thermal disturbance from the thermal chamber has a negative sign. In this case, responses of corridor air and interior air temperature on decreasing heat-flow steps are different from the case of increasing temperature steps (compare time constants and rate of change in Figures 2.31 and 2.32). The reason lies in the cooling process of the thermal chamber which has different time constants in lower temperatures due to the cooler which has different dynamics compared with the heater

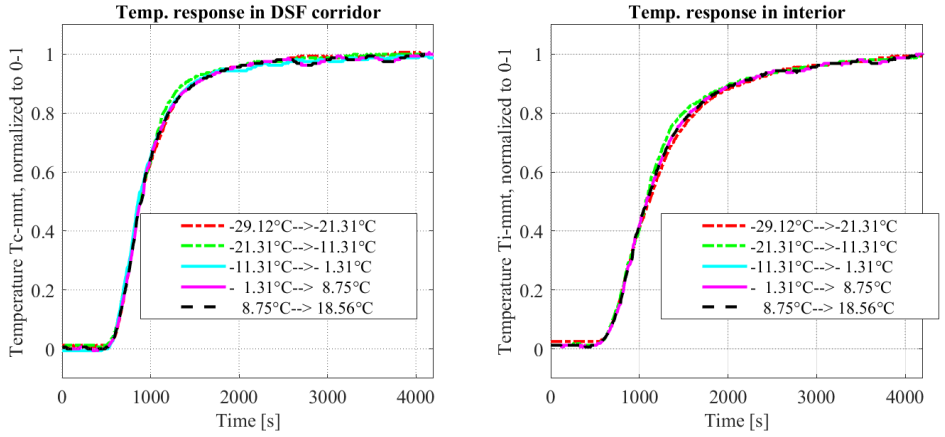

FIGURE 2.31. The air temperature responses to the increasing temperature steps in the thermal chamber a) corridor air b) interior air

in the chamber. This behaviour will be avoided by performing control tests in a range of positive environmental temperatures.

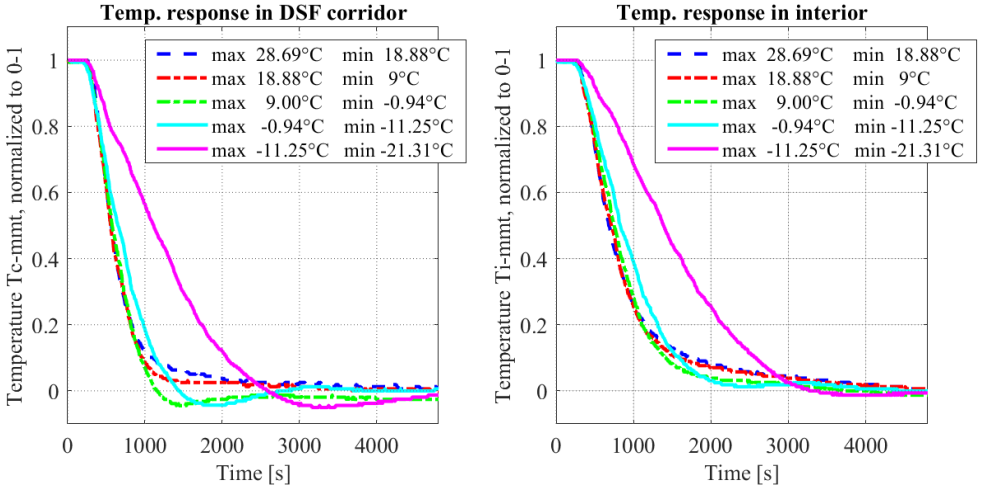

FIGURE 2.32. The air temperature responses to the decreasing temperature steps in the thermal chamber a) corridor air b) interior air

The heater and the fan are placed directly in front of the duct of the scaled mock-up. They represent heating and a cooling actuator for the corridor of the DSF. The efficiency is tested through several experiments shown in Figure 2.33 where scaled mock-up is excited with the hot air that is directly inserted in the corridor. During the experiment, it was detected that the temperature inside the corridor does not behave properly, i.e. do not increase as was expected. For this reason, the thermal chamber was fixed, i.e. the cavity shaft fitting was corrected at approximately 2000 s, and experiment proceeded until 4000 s when the heater and the fan of the scaled mock-up were turned off. At approximately 5000 s the thermal chamber was turned off.

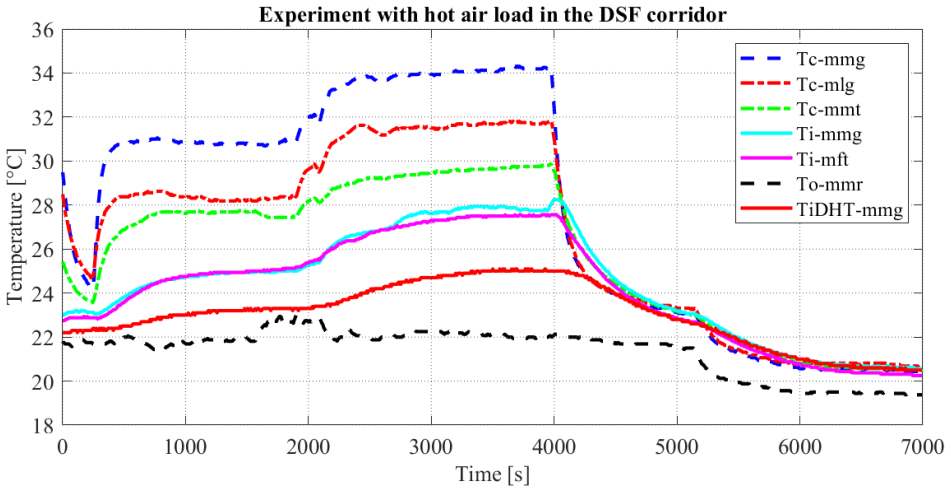

FIGURE 2.33. Temperature responses under hot air input

The heater and the fan (actuator) of the scaled mock-up are jointly modelled as proportional element of the first order[1] (see 2.5.2). Figures 2.34 and 2.35 give their joint responses to the normalized temperature step. Experimental and simulated responses are given for 1 cm and 5 cm corridor. It is logical that the first order approximation is worse for a larger corridor due to nonlinearities of the airflow that is in this case more pronounced.

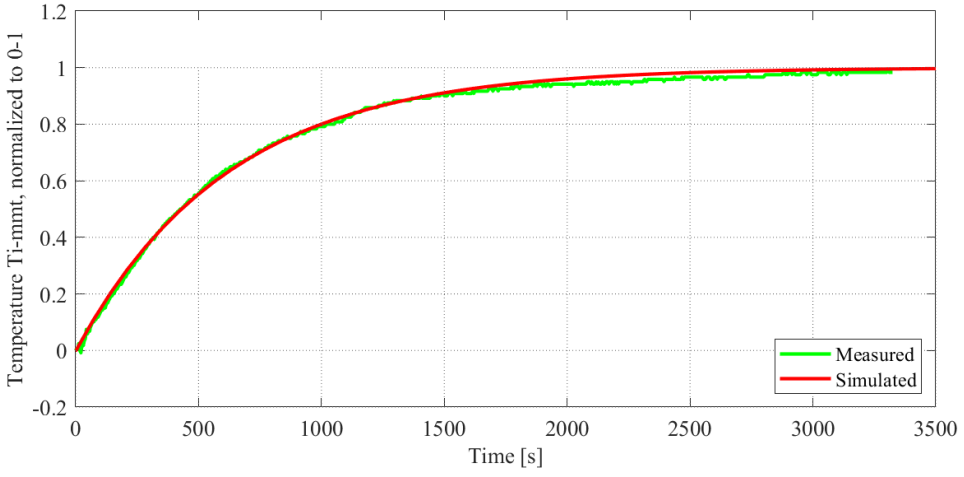

FIGURE 2.34. Comparison of simulated and experimental actuator response, 1 cm DSF

[1]PT1, for 1 cm DSF, $\tau = 620$; for 5 cm DSF, $\tau = 750$

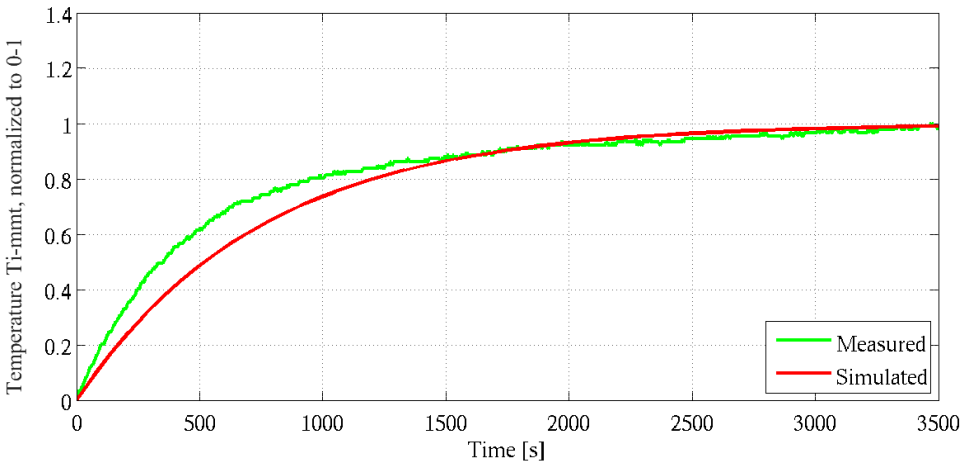

FIGURE 2.35. Comparison of simulated and experimental actuator response, 5 cm DSF

After testing behaviour in different regimes (heating and cooling) the results have shown a similar behaviour of different heat flow direction. This can be seen in Figure 2.36 where responses of different cavities are excited with the same temperature step reference.

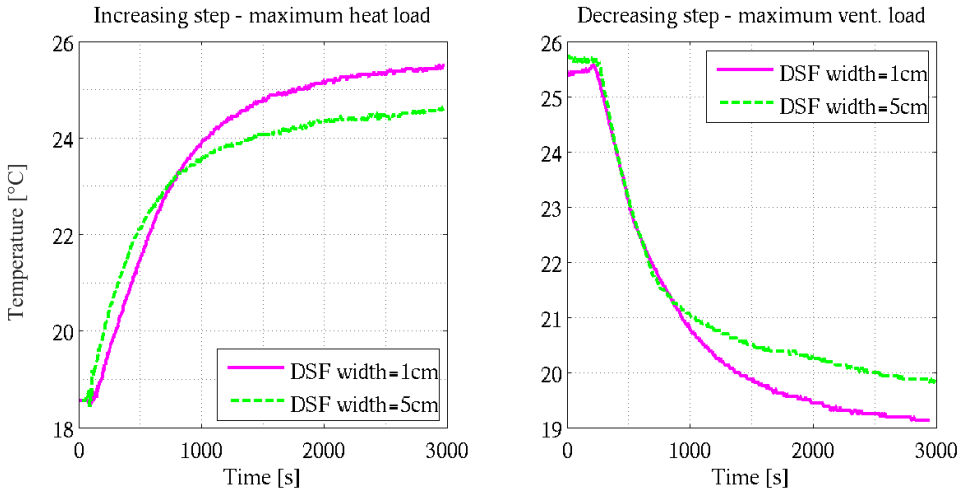

FIGURE 2.36. Comparison of actuator response to maximal temperature step change and different corridor width

2.7.7 Experiments with on-concrete Walls

Even though non equality of interior temperatures in a specific zone are neglected in steady state conditions, the differences are quite significant during the transient state of the heat flow. When the heat transients are of high amplitudes, the distribution is

large enough to be measured. Three sensors (T_{i-mft}, T_{i-mmt} and T_{i-mrt}) where placed inside the inner zone of the scaled mock-up (see Figure 2.26 and Table 2.2). Fourth sensor (T_{e-mrt}) is placed at the exterior side of the right side-wall (T_{c-mmt}) and the fifth one is in the corridor. The distance between two interior sensors and the middle one is approximately 150 mm.

Figure 2.37 shows the temperature differences obtained during experiments. The temperature differences are proportional to the heat flow. Because of the physical relations that exist here between the heat flow and temperature differences, we can perform parameter identification without direct measurement of the heat flow.

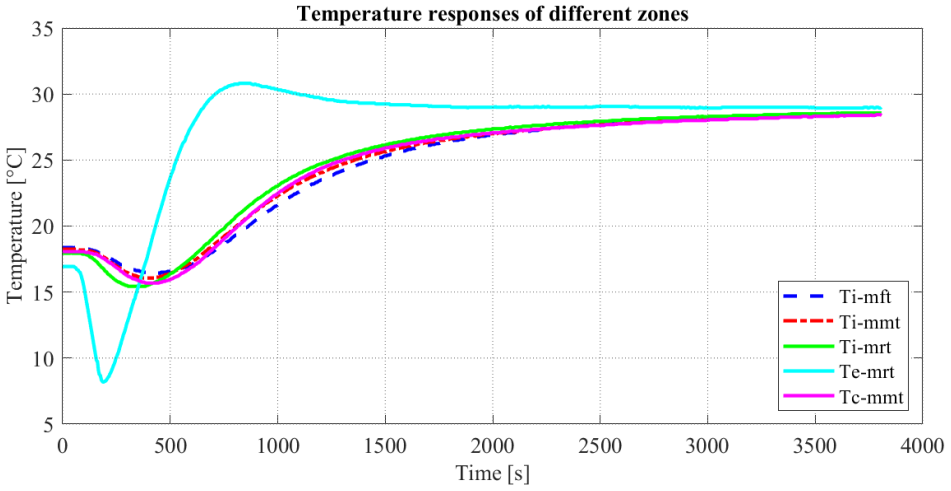

FIGURE 2.37. Temperature responses of different zones

Figure 2.38 shows temperature responses in the different zones and under different experimental conditions. All three tests were obtained with the scale mock-up having no concrete walls, similar starting and ending point, but with a different stream of exterior air or different sensor position. Streamflow of cold air, generated by the thermal chamber is manipulated by the *RaspberryPi* (see Figure 2.29. The third test had the same airflow conditions as the second one, but here the sensors are placed bellow the ceiling. The difference between all test results are small and may be neglected for the scaled mock-up. However, in the real-scale building these differences could be high and consequently transients, i.e. the time constants will be different for each experimental case.

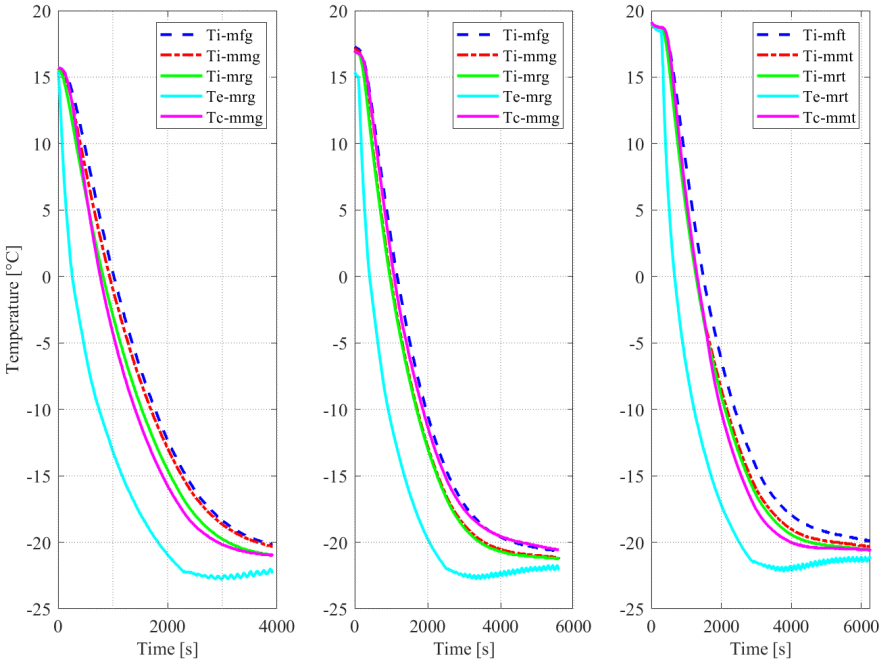

FIGURE 2.38. Temperature responses in different zones under different conditions
a) scaled mock-up is under direct air flow in thermal chamber, sensors are at ceiling
b) scaled mock-up is not under direct air flow in thermal chamber, sensors are at floor
c) scaled mock-up is not under direct air flow in thermal chamber, sensors are at ceiling

Envelope's thickness has the very high effect on experimental results, so in the following tests, width dimensions of wall and DSF element where variated. Because of that, the wall thickness was varied 5, 10 cm (see Figure 2.39), and DSF corridor width was also varied 1, 5 cm. Moreover, DSF was changed in such a way that glazed skin was replaced with various materials: plastic film and cardboard (see Figure 2.40).

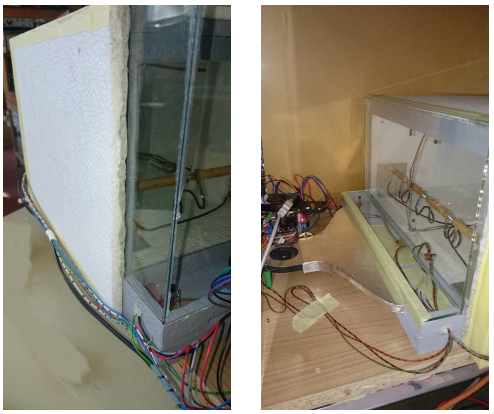

FIGURE 2.39. Parameter variation of scaled mock-up a) double thickness
b) quadruple thickness

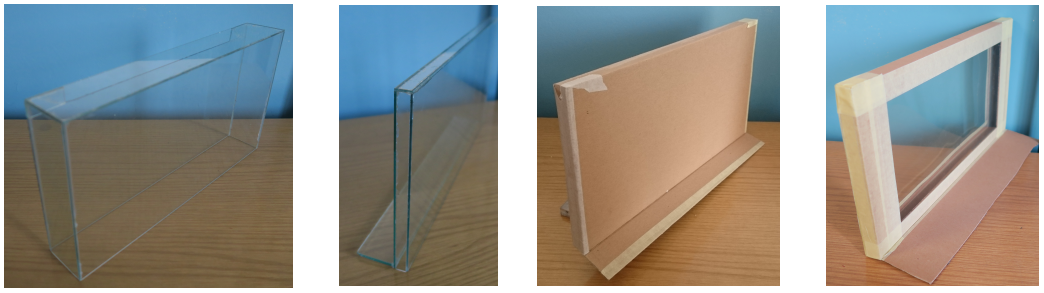

FIGURE 2.40. DSF variation: a) 5 cm wide glazed corridor b) 1 cm wide glazed corridor c) 1 cm wide cardboard corridor d) 1 cm wide plastic and cardboard corridor

Figure 2.41 presents the temperature responses of the scaled mock-up in the inner zone, exterior zone and in the DSF, under a large decrease of the external temperature. The solid curves represent temperatures measured on mock-up that had 1 cm wide walls, and dashed curves represents temperatures measured on mock-up that had 2 cm wide walls. Corridor width was 5 cm for both cases.

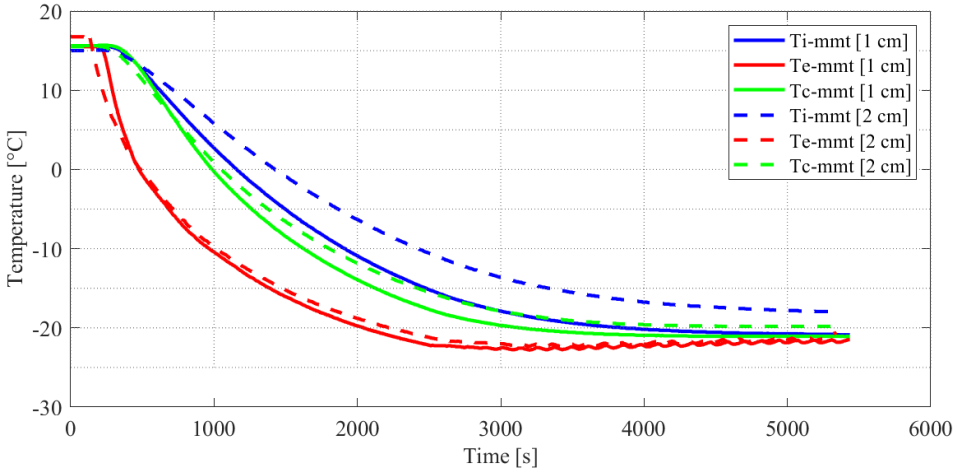

FIGURE 2.41. Temperature responses of the scaled mock-up with different insulation thickness under high temperature decrease

Prior experimental results have shown differences between different sensor location regarding horizontal plane, so it is also necessary to analyse temperature differences regarding vertical plane. Figure 2.42 shows results from experiment where temperature responses are measured at floor and ceiling levels, at the same horizontal position. Only the first part of response is shown because there is only difference. Initial temperature for experiment with glass DSF and paper-plastic DSF was $20/pm1$ degrees, and initial temperature for experiment with paper DSF was 12 degrees. The reference temperature of the thermal chamber for all three experiments was -20 degree, so settling times of

all experiments were similar. But temperatures at different positions during first part of response are significantly different.

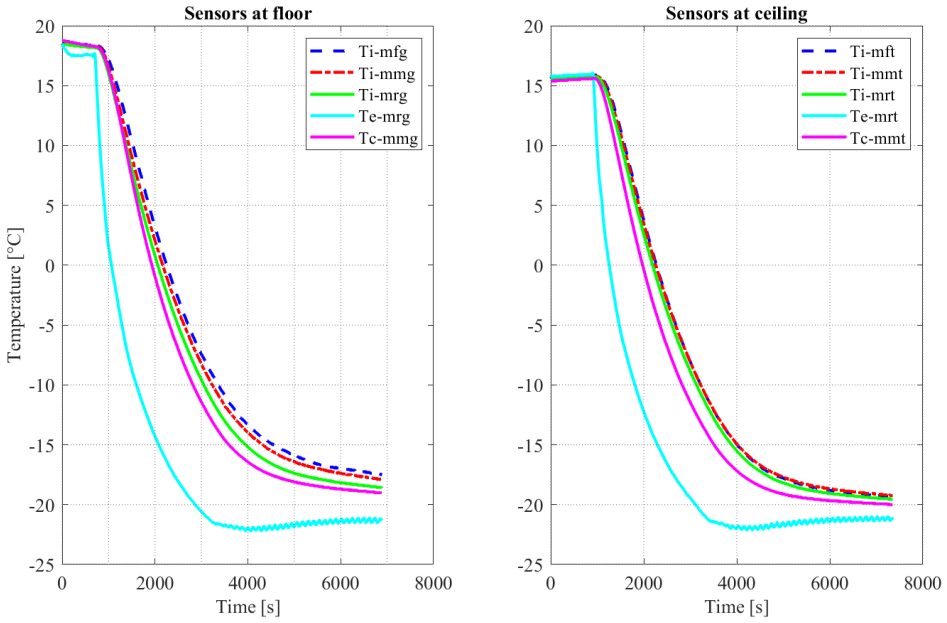

FIGURE 2.42. Temperature responses of the scaled mock-up with 1 cm wide DSF corridor: different vertical positions of the sensors

To emphasize the influence of the DSF parameters, the experiment was carried out with very thick wall insulation: 3 layered 40 mm thick wall. Temperature responses of different DSF is shown in Figure 2.43.

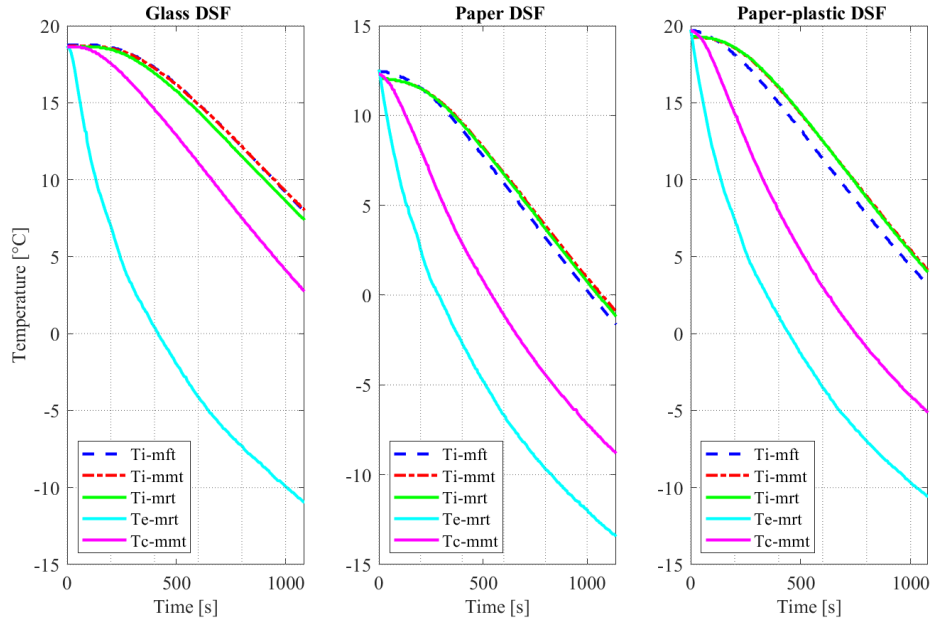

FIGURE 2.43. Temperature responses of the scaled mock-up with various DSF a) glass DSF with 1 cm wide corridor b) paper DSF with 1.5 cm wide corridor c) paper-plastice DSF with 2 cm wide corridor

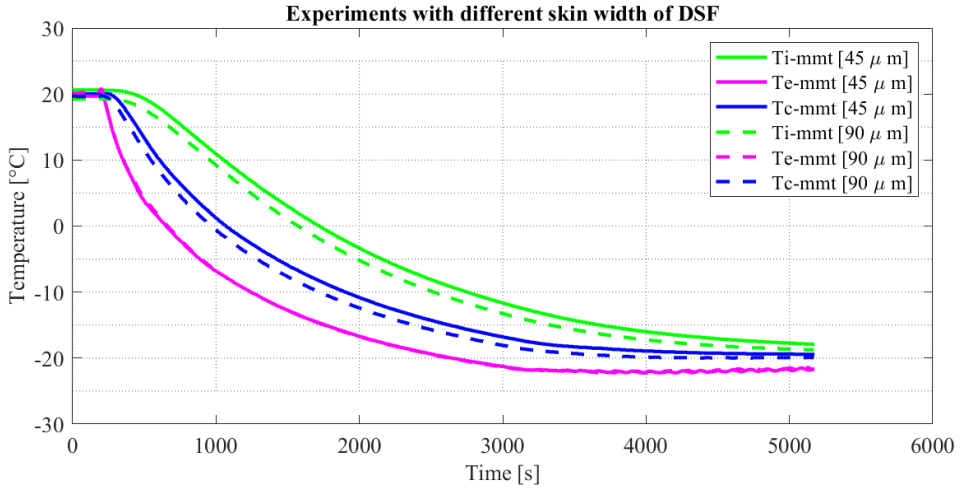

FIGURE 2.44. Temperature responses of the scaled mock-up with various plastic DSF

Temperature responses of the DSF zone of the scaled mock-up with different thickness of the DSF skin and high external temperature decrease are given in Figure 2.44. DSF is structured similarly to a double window where thin plastic film substitutes the glazed area. The frame is made of 1.5 mm carton. Two different thickness of plastic films are used in experiments: 45 μm and 90 μm thick plastic films.

2.7.8 Experiments with Scaled Mock-up with Concrete Walls

The concrete has a higher thermal capacity. Experiments were performed with different scaled mock-up parameters to detect the influence of the thermal capacity. Figure 2.45, Figure 2.46 and Figure 2.47 measured temperatures for three different cases.

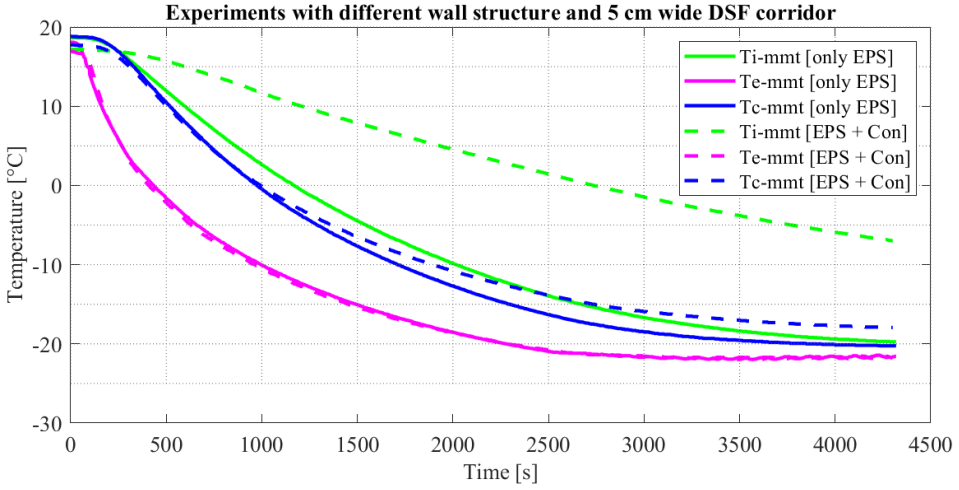

FIGURE 2.45. Temperature responses of the scaled mock-up with and without concrete walls, with DSF width = 5 cm

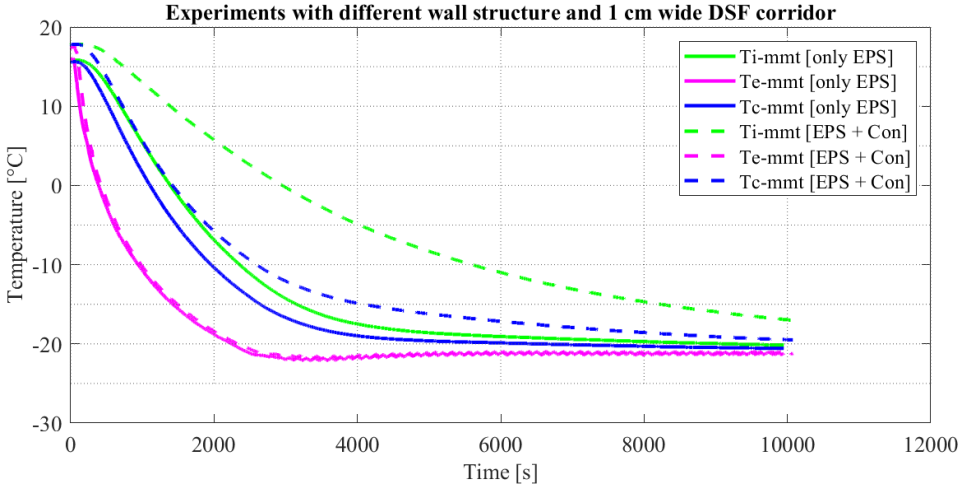

FIGURE 2.46. Temperature responses of the scaled mock-up with and without concrete walls, with DSF corridor width = 1 cm

As it can be seen in Figure 2.46 temperature in DSF with smaller DSF width drops faster than in a full-scale model.

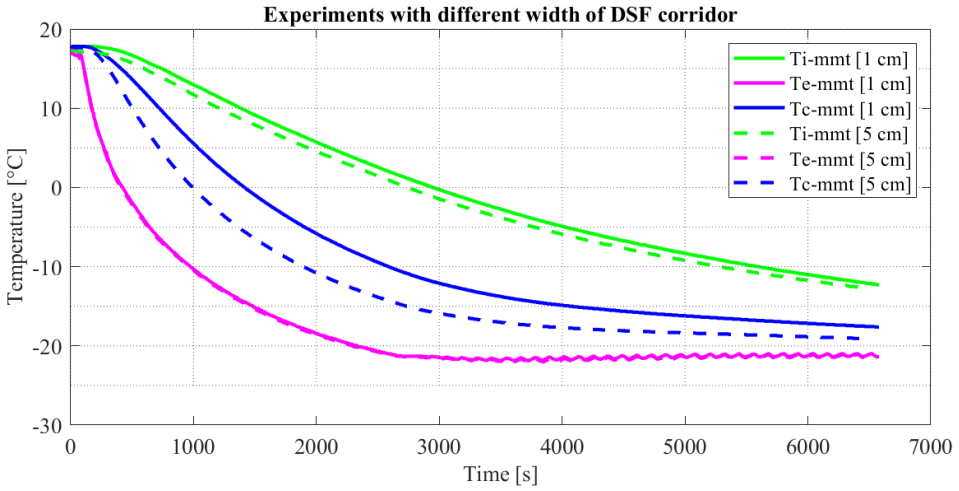

FIGURE 2.47. Temperature responses of the scaled mock-up with walls made of 1 cm wide concrete and 1 cm wide EPS insolation, various DSF width: 1 cm wide corridor and 5 cm wide corridor

2.7.9 Parameter Identification and Verification

Experimental results described earlier were also used to verify parameters of the HAMBASE model. Fig. 2.48 a) shows a comparison of measured and simulated response on the negative step of exterior temperature. Exterior temperatures have been oscillating in steady state because the thermal chamber has the precision of 1 $°C$. However, due to slow nature of the process, the response of the internal temperature of the scale mock-up is quite smooth and not affected. Simulated and measured temperature response of the scale mock-up differs a lot. Considering the experimental results explained earlier, we may assume that the problem is not caused by incorrect relations, but false parameters. By decreasing the sampling time, HAMBASE limitation (T_d=1 hour) is violated, so standard parameters given in the literature [25],[56], [80], [69] and [48] are not precise enough. Because of that, it was chosen to create improved model. The improved model is using similar relations as HAMBASE, but parameters have been identified directly from measured temperature response of the scaled mock-up.

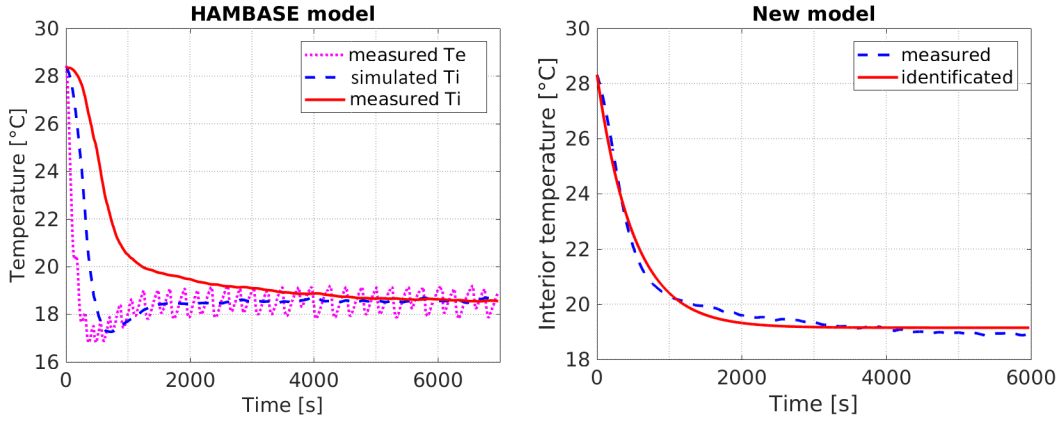

FIGURE 2.48. Interior temperature response of the scaled mock-up to external temperature step change a) HAMBASE model b) improved model

Fig. 2.48 b) shows the better correspondence of the improved model with the measured internal temperature of the scaled mock-up. The improved model explore measured signals and consequently better results from the model are expected. To justify the usage of the improved model, the experiments should be performed for various external temperature step changes. Figures 2.49 and 2.50 show temperature response of 6 different parameter sets excited by three different external temperature steps. In Figures 2.49 and 2.50, graphs on the left side represent interior air temperatures, while graphs on the right side represent the error between models with different parameters. Unlike the experimental results shown in Figure 2.48, where the internal temperature of improved model closely resembles the measured internal temperature of the scale mock-up, here the simulated internal temperature responses can't appropriately resemble the measured internal temperature of the scale mock-up in all possible external temperature ranges. Note that, the performance at larger transients has more energy, the faster response at the start, and also more deviation from real situation due to nonlinear effects. We thus conclude that the linear model is not appropriate to simulate the internal temperature of the scale mock-up to ranges of the external temperature exceeding those used for the parameter identification of the improved model. The order of the transfer function is identical for all cases but parameters are different [81].

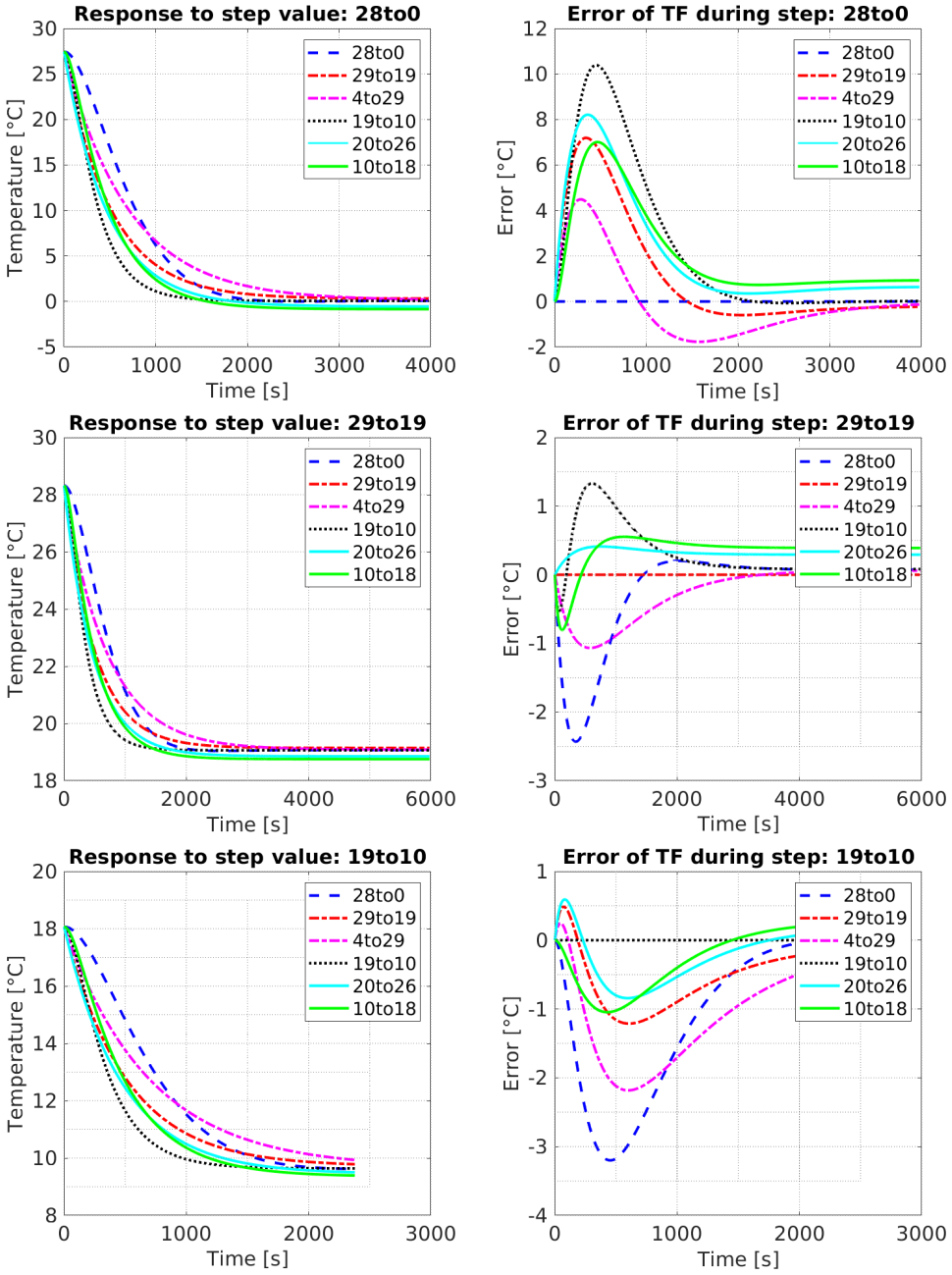

FIGURE 2.49. Comparison of experimental and simulated response through different regions, negative step

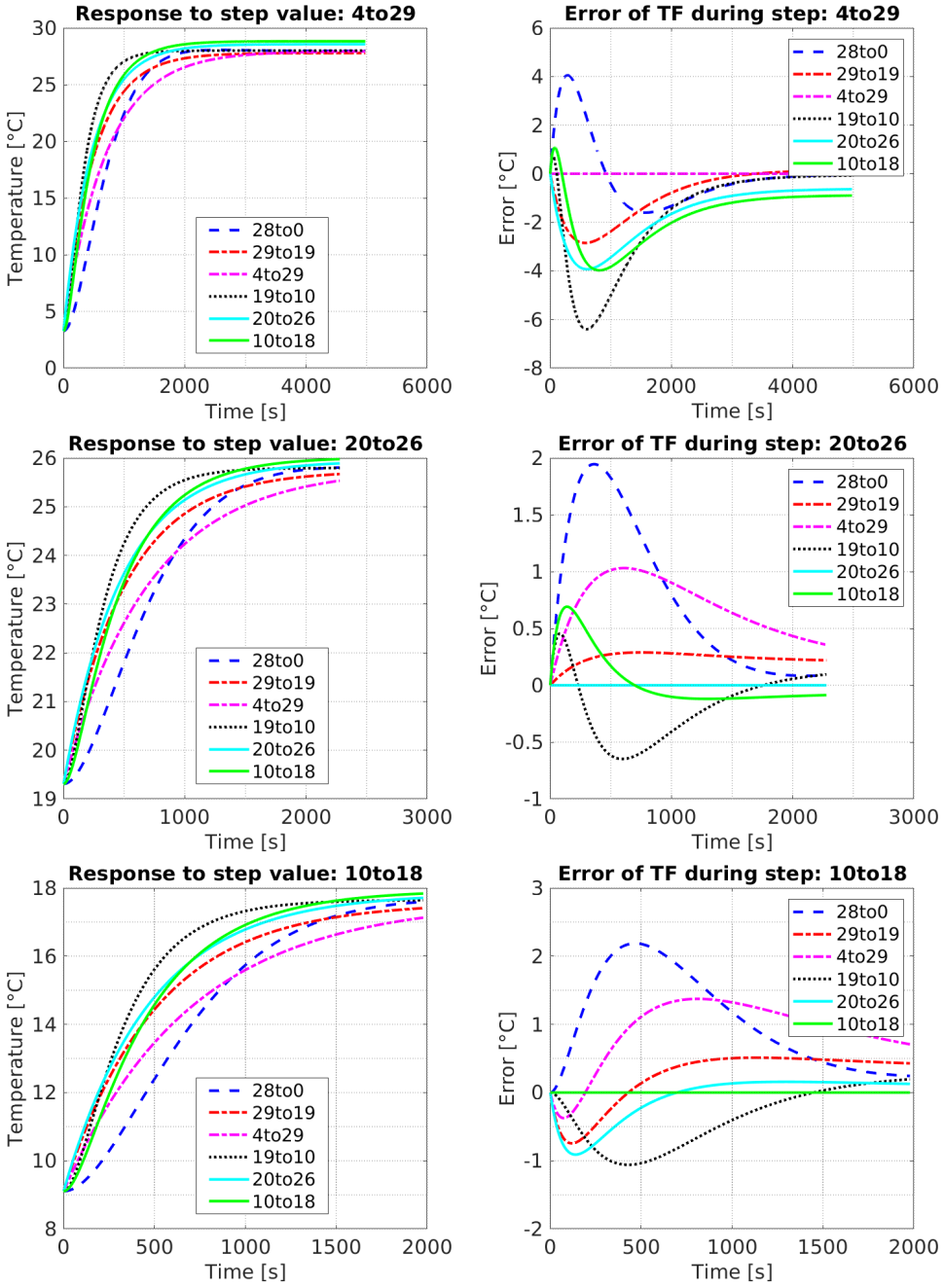

FIGURE 2.50. Comparison of experimental and simulated response through different regions, positive step

2.8 Open-loop Stability

Stability analysis of the open-loop system will be given in this chapter. The focus will be placed on the thermal system consisting of the thermal chamber, scaled mock-up, heaters, fans and sensors. Passivity approach will be used.

The heat transfer model, described in Section 2.3 is based on thermal resistance and capacitance. These elements form all components of the building that are finally lumped together into the thermal network.

2.8.1 Passivity-Based Approach

If it is shown that the thermal system is strictly passive, then many non-conventional controllers[2] can be used, [82]. The heat transfer problem is modelled using the electrical analogy so that, passivity will be proved in the domain of electrical circuit network.

According to [83], the heat transfer network is shown in Figure 2.7 and described with (2.9) may be simplified. The thermal network is represented as in Figure 2.51.

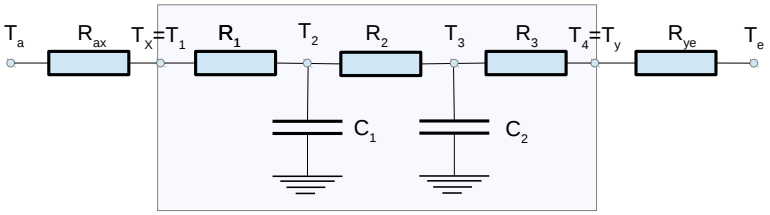

FIGURE 2.51. R3C2 model of the envelope

In general, all main thermodynamic properties have been kept. The thermal process between two zones is represented with Resistor–Capacitor (RC) circuits. By using dynamic consensus protocol as in [84], standard $3R2C$ model of the heat flow in internal zone Q_i may be expressed in following form:

$$Q_i = C_i\dot{T}_i = \sum_{j\in\mathcal{N}_i} R_{ij}^{-1}(T_i - T_j) + Q_i^e + Q_i^c \tag{2.27}$$

where $\mathcal{N}_i$ denotes neighbours of observed capacitor i. In other words, $\mathcal{N}_i$ represents set of capacitors j adjacent to capacitor i that have a link that originates from capacitor i. Each link has an associated weight valued by resistor R_{ij}. $Q_i^{(e)}$ is external heat input:

$$Q_i^{(e)} = \begin{cases} -R_{i0}^{-1}(T_i - T_e) & if\ adjacent\ to\ ambient \\ 0 & other \end{cases} \tag{2.28}$$

[2]NN, fuzzy etc.

, and $Q_i^{(c)}$ denotes external heat output:

$$Q_i^{(c)} = \begin{cases} u_i & if\ node\ is\ heated \\ 0 & other \end{cases} \tag{2.29}$$

The passivity of the system is to prove the convergence of the state variables in steady state. The simplest way to solve such a problem is by graph theory, and this is allowed because of the system properties: thermal network, including all building components, may be represented as a graph. Graph, in this context, is a mathematical structure used to model pairwise relations between objects. Objects are temperature nodes that are mutually connected. As energy flows between them in both directions, such graphs are also called undirected graphs [85]. An orientation is assigned to the link between two nodes when one of them have a positive end. Let the positive end of the *i*th node be denoted with $\mathcal{L}_i^+$ and negative end with $\mathcal{L}_i^-$. To show the relationship between two nodes, the incident matrix is defined. The incident matrix for a connected graph with a reference node has a value expressed with the relation:

$$D_{1_{i,j}} = \begin{cases} +1 & if\ j \in \mathcal{L}_i^+ \\ -1 & if\ j \in \mathcal{L}_i^- \\ 0 & other \end{cases} \tag{2.30}$$

Graph of the scaled mock-up must be specified now to determine dimensions of the incident matrix. Envelope elements of the scaled mock-up are given in Table 2.3. These elements are presented in Figure 2.52 as a thermal network graph. Thermal connection between floors, ceilings and walls are represented using 3R2C wall model, while the connection between single glass surface may be represented by a single resistance: corresponding to the inverse of the conductive heat transfer coefficient of glass. Node 1 corresponds to the room thermal capacitance. Nodes 2 and 3 denote thermal capacities in walls, 4 and 5 in cavities of the double skin glass façade, 6 and 7 in the ground floor and at last 8 and 9 roof ceiling. The corridor is an only active element with

TABLE 2.3. Scaled mock-up - envelope types

	Envelope type	Number of layers
1	ground floor	3
2	roof	3
3	wall	1
4	ground floor in DSF	2

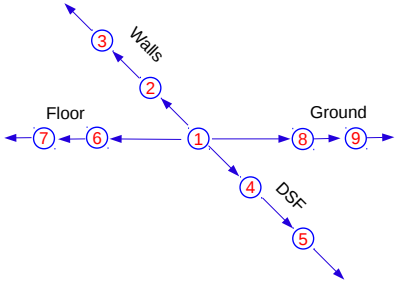

FIGURE 2.52. Thermal graph representation of the building segment

control input. Activity here, has the meaning of any regulation. If winter conditions are analysed, heat flow has a direction to the exterior, and that defines the direction of the thermal graph. Considering that the scaled mock-up has only one room, one double-skin façade, one ceiling and one floor, the number of capacitive elements is $N = 1\ room + 2\ capacities * 4\ "walls" = 9$. The number of thermal resistance elements $L = 12$. Hence, the dimension of the incidence matrix without ambient node is $\mathbf{D}_1 = L \times N = 108$.

According to Property 1.5 in [82] rank of $\mathbf{D}_1$ is at most $N - 1$ and the rank of $\mathbf{D}$ is $N - 1$ if and only if the graph shown in 2.52 is connected. Further on, it follows that if the graph is connected, the only null space of $\mathbf{D}^T$ is spanned by 1_N. Reference node temperature is externally imposed, so the first row is independent related to another matrix. Hence, if the first row is noted as $\mathbf{d}_0$ may be extracted from the incident matrix as:

$$\mathbf{D}_1 = \begin{bmatrix} \mathbf{d}_0 \\ \mathbf{D} \end{bmatrix} \tag{2.31}$$

The reduced incident matrix $\mathbf{D}$ has full row rank N. Proof is given in [83]. As the state space matrix form is required for further analysis, new variables are defined: where:

$$\mathbf{C} = \begin{bmatrix} C_2 \\ \vdots \\ C_N \end{bmatrix} \quad \dot{\mathbf{T}} = \begin{bmatrix} T_2 \\ \vdots \\ T_N \end{bmatrix} \quad \mathbf{R} = \begin{bmatrix} R_{22} & \dots & R_{2N} \\ \vdots & \ddots & \vdots \\ R_{N2} & \dots & R_{NN} \end{bmatrix} \quad \mathbf{T} = \begin{bmatrix} T_{22} & \dots & T_{2N} \\ \vdots & \ddots & \vdots \\ T_{N2} & \dots & T_{NN} \end{bmatrix} \tag{2.32}$$

$\mathbf{C}$ is a diagonal, positive definite matrix consisting of the wall capacitances, $\mathbf{R}$ is a diagonal, positive definite matrix consisting of the link thermal resistances.

Thermal network graph may also be expressed as Laplacian matrix $\mathbf{L}$ whose elements are calculated by:

$$l_{ij} = \begin{cases} |\mathcal{N}_i| & \textbf{if } \ j = i \\ -1 & \textbf{if } \ j \in \mathcal{N}_i \\ 0 & \textbf{otherwise} \end{cases} \tag{2.33}$$

We denote by $\mathcal{N}_i$ the set of *neighbours* of node j. The Laplacian matrix is used to find properties of a graph that are related to the incidence matrix. According to Property 1.2 from [82] an undirected graph is symmetric and positive semidefinite. Another Property (1.5) states that graph Laplacian matrix $\mathbf{L}$ satisfies:

$$\mathbf{L} = \mathbf{D}\mathbf{D}^T \tag{2.34}$$

Considering properties 2.8.1 and 2.34, relation (2.27) may be rewritten as

$$C\dot{T} = -\mathbf{D}\mathbf{R}^{-1}\mathbf{D}^T + \mathbf{B}_0\mathbf{T}_e + \mathbf{B}\mathbf{u} \tag{2.35}$$

where $\mathbf{B}_0 = -\mathbf{D}\mathbf{R}^{-1}\mathbf{d}_0^T$ is a column vector with non-zero elements as the thermal conductance of nodes connected to the exterior node. $\mathbf{u}$ is the heat input vector, and $\mathbf{B}$ is the corresponding input matrix. It is shown that $\mathbf{D}\mathbf{R}^{-1}\mathbf{D}^T$ is positive definite. The detailed proof that the open-loop system in the steady state is exponentially stable, is given in [83].

2.9 Summary

The chapter describes the Double Skin Façade concept and all its components. The mathematical representation of all system's elements is given in Section 2.3. The DSF system was analysed, and its appropriate model was proposed. The main focus is on the system's behaviour. Two different types of numerical simulations were carried out to justify such an approach: CFD analysis and advanced energy calculation. Results of the CFD analysis have shown that the shape of the corridor and the airflow intensity has the main role in defining the mathematical model. Simulations were validated by experiments with thermal a camera. The scaled mock-up model was adjusted by changing the shape of the ducts, the position of the heater, the dimension of the DSF corridor, the material of the walls and DSF, etc. The reason for that was to be able to

explore the linearized mathematical thermal model. The thermal mathematical model, that was used in the dissertation, explores the equations of the simulator (HAMBASE). HAMBASE is used in civil engineering for energy analysis for buildings. Limitations of the HAMBASE were recognized, and only thermal transients were adjusted for our purposes. The heat flux and pressure sensor turned out not to be adequate for providing feedback information. However, temperature sensors provided enough information to estimate behaviour. Experimental tests were performed in order to prove the quality of the improved thermal model. Open-loop stability is confirmed by the passivity-based approach.

Chapter 3

Design of the Closed-Loop Thermal Control of DSF System

In this Chapter, existing control strategies for DSF heat flow regulation will be given. The new strategy and corresponding regulator is proposed for the thermal process of DSF systems. The goal is to equalize the building heat losses for the situation where there is only one critical element (DSF). The problem of global stabilization of the system will be studied. Passive stability of the open-loop system, proven in Chapter 2, guarantees that the closed-loop system will also inherit the passivity properties. The passivity approach also leads to a systematic construction of tuning law for the regulator, based on Lyapunov function.

3.1 Overview of Strategies for Regulating the Heat Flow in DSF

The double skin façade (DSF) requires an automated building management system (BMS) to reach its full potential. BMS aims to satisfy the required indoor climate conditions and also to save energy. These two goals are opposed, especially in cases when the double skin façade is integrated with the air conditioning system. This conflict can be avoided by use of two separate systems, one for air conditioning and another for insulation (DSF). However, these separated systems increase initial and maintenance costs.

The BMS control strategy depends on buildings design and requirements. In [41] four different strategies are described:

- Airflow and temperature control with the use of passive components
- Night cooling with predictive control
- Daylight control level by opening and closing window blinds
- Integrated control (all building systems are interconnected for the purpose of control)

These control strategies are generally based on hysteresis regulators (i.e. [32] and [26]. Proportional or other advanced regulators are very rare. However, the energy efficiency trend motivated a few types of research to use advanced regulators. We can mention here [86], [53], [41] and [87]. One of the difficulties is the identification procedure of the parameters. Most of the control designers try to avoid this by using standard ratings to determine DSF properties, so the accuracy of the identification process is limited. Also, there are differences between North American and European standards[1] that may cause mistakes during identification. DSF has a similar structure as airflow window, so an overview of ([88] and [89]) is performed and four conclusions are extracted as useful for DSF analysis:

1. The dual airflow window can conserve energy by using the window panes as a heat exchanger. The window can improve indoor air quality (IAQ) by supplying fresh outdoor air to the indoors. The interior surface temperature is closer to the room air temperature when compared to a single airflow window, so thermal comfort can be also improved.
2. By using fans to supply and extract air through the window corridor, forced convection effects dominate. This approach leads to a nearly identical thermal performance for the supply and exhaust air windows. The window performed better for sunny and calm conditions in the winter and cloudy and calm conditions in the summer. The airflow rate should be low, and the corridor width should be small to improve the performance.
3. With the optimal design of 10 L/s flow rate and 9 mm corridor width, the heat exchange efficiency of the dual airflow window varies from 29.9 % for a cloudy

[1] National Fenestration Rating Council (NFRC), Canadian Standard Association (CSA), International Standard Organisation (ISO) and Passive House Institute (PHI)

and windy winter day to 56.2 % for a sunny and calm winter day, and from 19.8 % for a sunny and windy summer day to 27.7 % for a cloudy and calm summer day. Solar radiation increases efficiency by up to 20 % under winter conditions.

4. Condensation risk exists in the middle glass pane. During winter conditions, exhausted indoor air may condense if the indoor air humidity exceeds 48.5 % at 22 °C; during summer conditions, the outdoor air may condense if the humidity exceeds 68.1% at 37 °C.

In DSF systems airflow is usually the mix of three different airflow types:

- Buoyancy-driven airflow, in specially designed structures stack effect, enables that the temperature difference between the highest and lowest position occur.
- Wind-driven airflow
- Mechanically driven airflow

First two flows are considered as natural ventilation. Buoyancy-driven ventilation occurs as a result of the directional buoyancy force that results from temperature differences between the interior and exterior [90]. The flow in naturally ventilated double skin façade systems is usually regulated by adjustable shaft opening. Controlling shafts opening requires observation of the airflow. According to research [41] total airflow through the window can be calculated if the wind speed and temperatures are measured under the assumption that all dimensions and system coefficients are known. Here, the identification of these parameters presents the main problem in the real environment. Third version of DSF system is the climate façade. As defined in [41], this is an active façade that has a combination of functions of the façade as a mechanical exhaust duct and a heat recovery system. A big disadvantage, compared to the classic DSF, is worsened performance concerning the reduction of the cooling load and lack of natural ventilation. The most often role of the DSF system is to equalize the airflow and drain undesired air mass replacing it with the fresh airflow. Thus, the airflow ventilation is natural, but if specific conditions occur the DSF system loses its functionality. For example, if there is not enough temperature difference between exterior and interior temperature, and no wind, only possibility to inject the air mass and generate the airflow is by using the fan. When the airflow is mechanically driven in DSF (by the fan), additional energy consumption exists. So, the increased heat loss by convection

and energy loss due to fans are not an efficient strategy. In some cases, thermal storage would be an interesting solution[2].

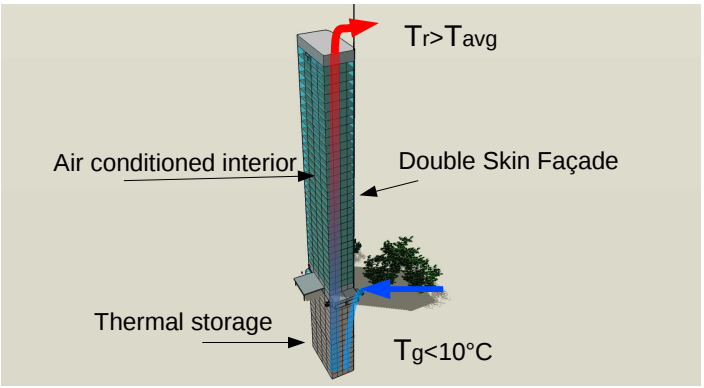

FIGURE 3.1. Energy saving concept

Figure 3.1 nicely visualizes an idea for energy saving concept. Unfortunately, the initial costs are increased. The first idea was to use the garage as air mass storage, but the problem appeared because air has very low specific heat capacity, and also, in civil engineering practice, there is no perfect sealing, so this exhaust air would eventually infiltrate to the interior and contaminate the breathing air.

Design methods for regulating the heat flow in the corridor area of DSF buildings, that are given in this section, are still not generally accepted as their use highly depends on DSF design. Thus, the new control method is proposed here. Our goal is to improve temperature transient properties of building elements and not to replace the HVAC role.

3.2 DSF System Dynamics

Double skin façade system has multiple operating modes due to different seasonal dynamics and different HVAC requirements. Only the heating season has been chosen for testing, even though the numerical simulator could handle all seasons. The scaled mock-up is a segment of the building discussed in Section 2.7. The design of active DSF is presented in figure 3.2. The heater with the fan is mounted in the external duct (see Figure 2.28) and placed at the bottom of the corridor to generate warmer air mas. Upper shaft opening is closed to maximize thermal efficiency, so the ventilation shaft effect is excluded. The airflow is forced by the fan and not by natural buoyancy. The

[2] geothermal heat exchanger, pools as heat storage, solar panels etc.

natural flow without the heater can be used in real applications, but in this research it was not used due to scaled mock-up [3].

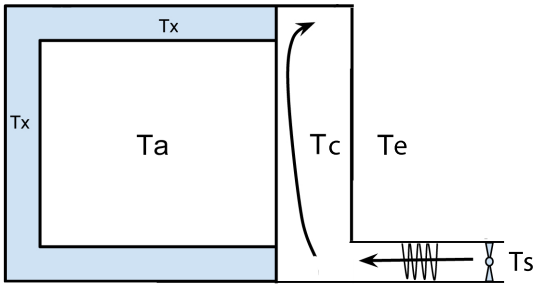

FIGURE 3.2. Schematic diagram for heating the scaled mock-up

The scaled mock-up consists of the zone with internal temperature T_a and the DSF system representing the second zone with the temperature of the corridor T_c. Exterior temperature is designated as T_e, and in our experiments, this temperature represents disturbance influencing the temperatures of both zones. With the use of the air mass temperature T_s, we can regulate temperatures in both zones. If T_s is greater than T_e we are rising temperatures in both zones. Zones will be analysed as areas with constant temperatures in steady state (see Section 2.7). The variable temperature T_x is introduced as a result of the numerical calculation. T_x represents the surface temperature of the wall. This temperature is obtained from the heat balance equation for the scaled mock-up. According to relations (2.26) and (2.9) and corresponding block diagram given in

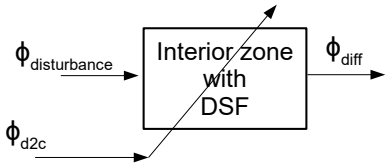

FIGURE 3.3. DSF block diagram

Figure 3.3, heat flow difference in the interior zone of the building with the DSF can be written as follows:

$$\Phi_{diff} = F_{\phi}\{\Phi_{corridor}, \Phi_{disturbance}\} = F_T\{T_x, T_y, T_a, T_c, T_e, T_{d2c}\} \tag{3.1}$$

[3] no multi-floor mock-up, no real scale, not enough height for buoyancy

Values of T_x, T_y and T_c are strongly coupled and also sensitive to external disturbances such as T_e. Block diagram of the closed-loop control for DSF system is shown in Figure 3.4.

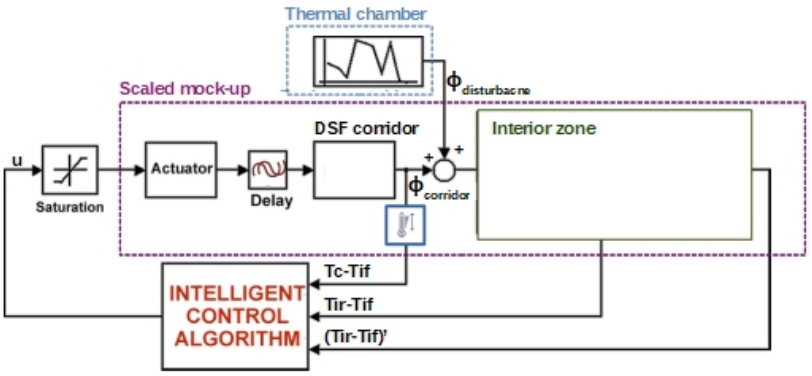

FIGURE 3.4. Block diagram of DSF control

According to analysis, done in earlier sections, the most efficient option of DSF regulation is to decrease the heat loss of DSF to the level of walls[4] of the scaled mock-up. In this set-up, the complete system without actuator is simplified to the second order function. Even-thought there are other nonlinearities, only saturation[5] and delay[6] are included in the analysis as they have significant influence. Conventional control methods based on the known mathematical model of the process couldn't be used here because the mathematical model of our process is absent and moreover change over time and due to seasonal effects ([91], [92], [9], [86] and [93]). Thus, the intelligent control methods should be used because they do not rely on a mathematical model of the process. Variables that will be used for feedback depends on the type of intelligent control used. Three states that can be measured, should be used for feedback if the neural network controller is used. As shown in Figure 3.5, these states are differences in air temperature measurements inside scaled mock-up and derivations of their differences. Heat flow measurements are not available in experiments, so the non equality of both zone temperatures are used to estimate heat flows in the scaled mock-up. When HVAC is turned off, directly measured temperatures may be used as feedback information.

The standard requirements for office spaces in buildings with DSF system are thermal and air regulation of inner space for the certain daily period. Hence, reference temperature (i.e. $20°C$) is achieved by HVAC (i.e. PID regulation) during the working hours,

[4]three walls, ceiling and the floor of the scaled mock-up
[5]Saturation comes from limited output of installed heater and fan
[6]Delay mainly comes from transmittance properties of the scaled mock-up

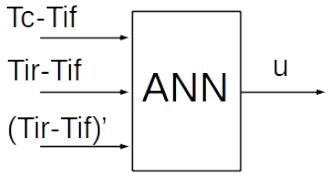

FIGURE 3.5. Block diagram of the intelligent control with designated states

and during the night the HVAC is turned off. For better illustration, these two different operating modes of the heating regime are shown in Figure 3.6. The heat transfer process has similar characteristics in both cases (same energy directions and similar temperatures), but there is a huge difference in a level of temperature dissipation. Temperature differences between the air inside the same zone are significantly larger and do not have the same behaviour. Also, different HVAC design generate completely different dynamics which makes this heat flow equalization very demanding task.

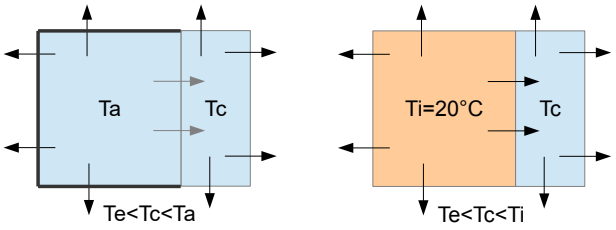

FIGURE 3.6. Different control modes a) HVAC OFF b) HVAC ON

To summarize, HVAC output directly affects the heat flow of the walls and DSF system. In the case when HVAC is active, the differences between air temperatures of different position is not only caused by differences in heat loss, but it is also caused by the non-homogeneous distribution of HVAC output[7]. So, to regulate the heat flow of the DSF system when HVAC is active, states of the HVAC system must be available.

DSF system is analysed with ANN regulator but without HVAC. A linear mathematical model will be in state space form. According to [49], DSF that is used in experiments may be modelled as a zone with additional heat input (see Figure 3.2). This linear mathematical model will be used for stability analyses. So-called DSF zone is coated with a single layered wall. The equation for the wall's heat flow (2.9) will be applied to describe thermal dynamics in DSF as follows:

[7]HVAC delivers output through ventilation draft opening, radiator, supplying ducts etc.

$$\begin{aligned} k_{a1}\frac{d^2\Phi_x}{dt^2} + k_{a2}\frac{d\Phi_x}{dt} + \Phi_x &= k_{a3}\frac{d^2T_x}{dt^2} + k_{a4}\frac{dT_x}{dt} \\ k_{t1}\frac{d^2\Phi_{xy}}{dt^2} + k_{t2}\frac{d\Phi_{xy}}{dt} + \Phi_{xy} &= A_{xy}U_{xy}\Delta T_{xy}(t-t_d)\,, \end{aligned} \tag{3.2}$$

where

$$\begin{array}{ll|ll} k_{a1} = \frac{C_{x1}C_{x2}}{L_{x1}L_{x2}} & & k_{a2} = \left(\frac{C_{x1}}{L_{x1}} + \frac{C_{x2}}{L_{x2}}\right) & \\ k_{a3} = (L_{x1}+L_{x2})\frac{C_{x1}C_{x2}}{L_{x1}L_{x2}} & & k_{a4} = (C_{x1}+C_{x2}) & \\ k_{t1} = \tau_1\tau_2 & & k_{t2} = \tau_1+\tau_2\,. & \end{array} \tag{3.3}$$

The system output is the difference between heat flow of the DSF and walls: Φ_{xy}. In the case of DSF, the control variable is the temperature of the corridor T_c. So, the heat loss through the DSF is only the transmitted heat and not admitted one. Because of that, Φ_{xy} in relation (3.2) is expressed through T_x. T_x may be replaced with substitution derived from relation (2.6).

$$C_{ca}\frac{dT_{ca}}{dt} = L_{xa}(T_x - T_{ca}) + \Phi_{cg} \tag{3.4}$$

where Φ_{cg} is the heat flow as a result of all common heat gains in the system

$$\Phi_{cg} = \Phi_{cv} - \frac{h_{cv}}{h_r}\Phi_r\,, \tag{3.5}$$

where Φ_{cv} is convective part of the heat flow.

Also, an assumption is made here: There is no air infiltration from other zones, or through open window or doors $\sum \Phi_{ab} = 0$. If T_x is extracted in relation (3.4) we get T_x

$$T_x = \frac{C_{ca}}{L_{xa}}\frac{dT_{ca}}{dt} + T_a - \frac{1}{L_{xa}}\Phi_{cg} \tag{3.6}$$

and after substitution of relation (3.6) in second equation of (3.2), the differential equation of system output may be written as:

$$\tau_1\tau_2\frac{d^2\Phi_{xy}}{dt^2} + (\tau_1+\tau_2)\frac{d\Phi_{xy}}{dt} + \Phi_{xy} = \frac{1}{A_{xy}}U_{xy}\left[T_x(t-t_d) - T_y(t-t_d)\right] \tag{3.7}$$

and after substitution of T_x with $f(T_a)$:

$$\tau_1\tau_2\frac{d^2\Phi_{xy}}{dt^2}+(\tau_1+\tau_2)\frac{d\Phi_{xy}}{dt}+\Phi_{xy}=A_{xy}U_{xy}\frac{C_{ca}}{L_{xa}}\frac{dT_{ca}(t-td)}{dt}+A_{xy}U_{xy}T_a(t-t_d)$$
$$-A_{xy}U_{xy}\frac{\Phi_{cg}(t-t_d)}{L_{xa}}-A_{xy}U_{xy}T_y(t-t_d) \tag{3.8}$$

Dividing (3.8) by $\tau_1\tau_2$ we will get:

$$\frac{d^2\Phi_{xy}}{dt^2}+\frac{\tau_1+\tau_2}{\tau_1\tau_2}\frac{d\Phi_{xy}}{dt}+\frac{1}{\tau_1\tau_2}\Phi_{xy}=\frac{A_{xa}U_{xy}C_{ca}}{\tau_1\tau_2L_{xa}}\frac{dT_{ca}(t-td)}{d_t}+\frac{A_{xa}U_{xy}T_{ca}(t-t_d)}{\tau_1\tau_2}$$
$$-\frac{A_{xa}U_{xy}\Phi_{cg}(t-t_d)}{\tau_1\tau_2L_{xa}}-\frac{A_{xa}U_{xy}}{\tau_1\tau_2}T_y(t-t_d) \tag{3.9}$$

Equation (3.9) can be given in the form:

$$\frac{d^2\Phi_{xy}(t)}{dt^2}+a_1\frac{d\Phi_{xy}(t)}{dt}+a_0\Phi_{xy}=b_1\frac{dT_{ca}(t-t_d}{d_t}+b_0T_{ca}(t-t_d)+g_0\Phi_{aux}(t-t_d) \tag{3.10}$$

where:

$$\begin{aligned}
a_1&=\tfrac{\tau_1+\tau_2}{\tau_1\tau_2}\\
a_0&=\tfrac{1}{\tau_1\tau_2}\\
b_1&=\tfrac{A_{xy}U_{xy}C_a}{L_{xa}\tau_1\tau_2}\\
b_0&=\tfrac{A_{xy}U_{xy}}{\tau_1\tau_2}\\
g_0&=-\tfrac{A_{xy}U_{xy}}{\tau_1\tau_2}\\
\Phi_{aux}&=\tfrac{\Phi_{cg}(t-t_d)}{L_{xa}}+T_y(t-t_d)
\end{aligned} \tag{3.11}$$

Equation (3.10) may be written in shorter form:

$$\ddot{\Phi}_{xy}(t)+a_1\dot{\Phi}_{xy}(t)+a_0\Phi_{xy}(t)=b_1\dot{T_{ac}}+b_0T_{ac}+g_0\Phi_{aux}(t) \tag{3.12}$$

The function $\Phi_{aux}(t-t_d)$ represents external disturbance to the system. If there are no disturbances, this function has fixed values. Also, we may introduce control signal u and output signal y:

$$\ddot{y}(t)+a_1\dot{y}(t)+a_0y(t)=b_1\dot{u_1}(t-t_d)+b_0u_1(t-t_d)+g_0u_2(t-t_d) \tag{3.13}$$

where:

$$\begin{aligned} y(t) &= \Phi_{xy}(t) \\ u_1(t-t_d) &= T_{ca}(t-t_d) \\ u_2(t-t_d) &= \Phi_{aux}(t-t_d) \end{aligned} \tag{3.14}$$

Heat input through the air loaded into corridor may be modelled as the first order differential equation [49]:

$$C_{ca}\frac{dT_{ca}}{dt} = \frac{C_{ca}}{L_{d2c}}\frac{d\Phi_{d2c}}{dt} + \Phi_{d2c} \tag{3.15}$$

Relation (3.13) may be written in the form:

$$\dddot{y}(t) + a_1\ddot{y}(t) + a_0\dot{y}(t) = b_1\ddot{T}_{ca}(t-t_d) + b_0\dot{T}_{ca}(t-t_d) + g_0\dot{\Phi}_{aux}(t-t_d) \tag{3.16}$$

and now we substitute T_{ca} by using relation (3.15):

$$\begin{aligned} \dddot{y}(t) + a_1\ddot{y}(t) + a_0\dot{y}(t) = \tfrac{b_1}{L_{ca}}\ddot{\Phi}_{d2c}(t-t_d) + \left(\tfrac{b_1}{C_{ca}} + \tfrac{b_0}{L_{ca}}\right)\dot{\Phi}_{d2c}(t-t_d) \\ + \tfrac{b_0}{C_{ca}}\Phi_{d2c}(t-t_d) + g_0\Phi_{aux}(t-t_d) \end{aligned} \tag{3.17}$$

and finally we get:

$$\dddot{y}(t) + a_1\ddot{y}(t) + a_0\dot{y}(t) = c_2\ddot{u}_1(t-t_d) + c_1\dot{u}_1(t-t_d) + c_0u_1(t-t_d) + g_0u_2(t-t_d) \tag{3.18}$$

where:

$$\begin{aligned} c_2 &= \tfrac{b_1}{L_{ca}} \\ c_1 &= \tfrac{b_1}{C_{ca}} - \tfrac{b_0}{L_{ca}} \\ c_0 &= \tfrac{b_0}{C_{ca}} \\ u_1(t-t_d) &= \Phi_{d2c}(t-t_d) \\ u_2(t-t_d) &= \Phi_{aux}(t-t_d) \end{aligned} \tag{3.19}$$

3.2.1 State space representation

Relation (3.13) can be written in state space form:

$$\begin{aligned} x_1(t) &= y(t) = \Phi_{xy}(t) \\ \dot{x}_1(t) &= x_2(t) + b_1u_1(t-t_d) \\ \dot{x}_2(t) &= b_0u_1(t-t_d) + g_0u_2(t-t_d) - a_0x_1(t) - a_1x_2(t) \end{aligned} \tag{3.20}$$

Relation (3.13) will be transformed into state space representation by using the standard method of transforming the differential equation to state space (see [92] - Section 8.6.1. The state space form of (3.13) is thus given by:

$$\begin{aligned}\dot{\mathbf{x}}(t) &= \begin{bmatrix} 0 & 1 \\ -a_0 & -a_1 \end{bmatrix} \mathbf{x}(t) + \begin{bmatrix} b_1 & 0 \\ b_0 & g_0 \end{bmatrix} \mathbf{u}(t - t_d) \\ \mathbf{y}(t) &= \begin{bmatrix} 1 & 0 \end{bmatrix} \mathbf{x}(t)\end{aligned} \tag{3.21}$$

where:

$$\dot{\mathbf{x}}(t) = \begin{bmatrix} x_1(t) \\ x_2(t) \end{bmatrix} \qquad \mathbf{u}(t - t_d) = \begin{bmatrix} u_1(t - t_d) \\ u_2(t - t_d) \end{bmatrix} \tag{3.22}$$

To define the DSF system with control signal, we need to add the heat input to the state space form (3.18):

$$\begin{aligned} x_1(t) &= y(t) = \Phi_{xy}(t) \\ \dot{x}_1(t) &= x_2(t) + c_2 u_1(t - t_d) \\ \dot{x}_2(t) &= x_3(t) + (c_1 - a_1 c_2) u_1(t - t_d) \\ \dot{x}_3(t) &= -a_0 x_2(t) - a_1 x_3(t) \\ &\quad + (a_1^2 c_2 + c_0 - a_1 c_1 - a_0 c_2) u_1(t - t_d) + g_0 u_2(t - t_d) \end{aligned} \tag{3.23}$$

Finally we have the mathematical model in state space form for the temperature transients through DSF system:

$$\begin{aligned}\dot{\mathbf{x}}(t) &= \begin{bmatrix} 0 & 1 & 0 \\ 0 & 0 & 1 \\ 0 & -a_0 & -a_1 \end{bmatrix} \mathbf{x}(t) + \begin{bmatrix} c_2 & 0 \\ c_1 - a_1 c_2 & 0 \\ a_1^2 c_2 + c_0 - a_1 c_1 - a_0 c_2 & g_0 \end{bmatrix} \mathbf{u}(t - t_d) \\ \mathbf{y}(t) &= \begin{bmatrix} 1 & 0 & 0 \end{bmatrix} \mathbf{x}(t)\end{aligned} \tag{3.24}$$

where:

$$\dot{\mathbf{x}}(t) = \begin{bmatrix} x_1(t) \\ x_2(t) \\ x_3(t) \end{bmatrix} \qquad \mathbf{u}(t - t_d) = \begin{bmatrix} u_1(t - t_d) \\ u_2(t - t_d) \end{bmatrix} \tag{3.25}$$

3.3 Artificial Neural Network

Artificial Neural networks (ANNs) are a special sort of nonlinear networks. Their design is inspired by the nervous systems of the brain. As documented in [94], ANN has been successfully applied in research in various disciplines such as the economy, biochemical research, ecology and many researches in computing and engineering, science and nanotechnology. Every field has its own modification to fit the right form, but they all have two common properties: learning and the approximation. There are many descriptions of the structure of the neural network (NN). One of these is given in [95]. There, the NN consists of an interconnected group of artificial neurons, and it processes information using a confectionist approach to computation. For an artificial neuron, the weight is a number, and represents the synapse. A negative weight reflects an inhibitory connection, while positive values designate excitatory connections. All inputs are summed altogether and modified by the weights and refer as a linear combination. Finally, an activation function controls the amplitude of the output. For example, an acceptable range of output is usually between 0 and 1, or it could be -1 and 1.

A neuron y_j is given by (3.26)

$$y_j = \sum_{i=1}^{k} w_{ij} x_i \tag{3.26}$$

where w_{ij} is the weight value of input i and neuron j, and k is the number of inputs. A graphical presentation of a simple neural network is given in 3.7, where $f(y_j)$ is the output of the simple NN. Mathematically a multi-Layer perceptron network is a function consisting of compositions of weighted sums of the functions corresponding to the neurons.

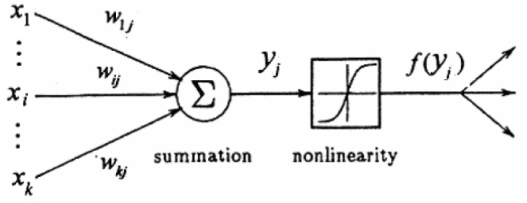

FIGURE 3.7. Graphical presentation of neuron, L[95]

The discussion that follows, refers only to NN as a controller, also called neural controller in [96]. Especially attractive aspects of neural control are abilities:

- to identify any nonlinear single-valued function and control processes with these functions

- ability to control SISO or MIMO systems

Due to its approximation ability, neural control has difficulties in controlling systems where global stability is not ensured. Assuming that controllability and observability conditions are met, the ANN controller can be used. Neural control methods ([95],[96],[97],[94], [98], [99] and [100]) are presented in Table 3.1 and Table 3.2.

TABLE 3.1. Neural control methods with heuristic algorithm

Control Methods			
Type	**Method**	**Description**	**Block scheme**
Heuristic control methods	Expert emulator	Learning existing controller	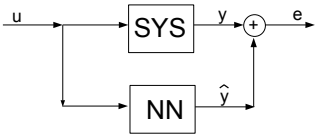
	Inverse control	Open-loop control	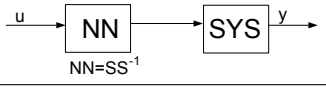
	Neural aid to feedback	Feedback control used to improve classical methods	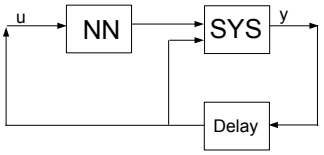

TABLE 3.2. Neural control methods with feedback

Control Methods			
Type	**Method**	**Description**	**Block scheme**
Neural feedback control methods	Feed-forward Networks	Open-loop network that requires independent learning by some method, usually by backward propagation (BP) of error	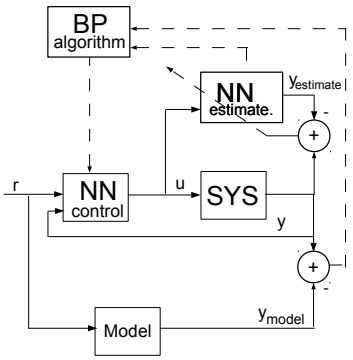
	Recurrent Neural Networks	Thanks to internal closed-loop in the network there is internal memory that enables giving a desired response to each time step	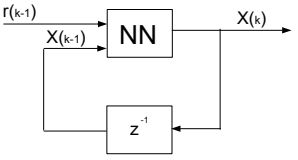
	Adaptive critic control	Two neural networks where one NN is an action generator network and another NN evaluates the performance and adjust the weight of another	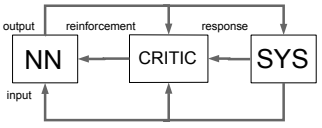

Adaptive critic NN has high-level topology design with the objective of learning how to generate the best control action in the absence of detailed knowledge of system parameters. The choice of critic signal and NN weights tuning function are both results of stability analysis of the system. These functions should be designed in a way to ensure the convergent and bounding behaviour of the resulted output. Adaptive critic allows all kind of modifications such as fuzzy component instead of the second neural network. This is analysed and tested in [10]. The guaranteed performance of the adaptive neural network with a similar approach but only with activation neural network is given in [101] and [102]. Another adaptive solution is described in [103], and this one is more

general and proves that the adaptive law assures bounded solutions without prior information about perturbations. In adaptive control theory, stated in [104], when both, the plant and the disturbance model are linear, it is known that satisfactory results can be achieved by increasing the dimension of the controller. If only linear adaptive control is used, the errors do not tend to zero due to the presence of the nonlinear terms. Because of that, the NN is used to compensate the nonlinearities in the process and make the control error tend to zero. To assure that the approximation is sufficiently accurate, the neural networks must be adjusted on a slower time scale.

In [93] neural network is used for parameter identification of nonlinear process and control of complex thermal plants. From a control point of view in thermal systems, the essential impact occurs due to time delays and natural operating modes. ANN can be used for learning process dynamics properties and parameter identification as well as for estimation of time delays, or bounds of input and output signals. Despite their popularity in the research community, NN has a bad reputation in industrial automation because there are misconceptions regarding how neural networks work [105]. This can be attributed to poor network design and its misuse. Nevertheless, there are few papers ([11],[9]) that represent novel design in industrial control. The use of adaptive ANN (AANN) is justified whenever conventional control methods cannot adapt to the process parameter change. The proposed solution in this dissertation represents AANN as universal approximation property that identifies the whole process under control rather than process parameters.

Parameter configuration of ANN may be divided into two steps. First, we have to determine structural design[8] Then we design the mechanism for tuning weights. Weights are tuned in the learning process or during the regulation process. The learning process usually consists of finding an optimum set of weights and thresholds, that minimize the error between the system output and the network response ([93]). The mechanism is achieved by minimization of the sum of squared errors, which is the most common criterion for minimization in ANNs. In the research, tuning weights of ANN are being done constantly, so there is no learning phase. This mechanism update weights through the weighting function which will be described in the following sections.

[8]choice of ANN type, number of layers, number of nodes, choice of activation functions etc.

3.3.1 Adaptive Tuning of AANN

According to [106] there are six categories of the adaptive control system with parameter tuning. The neural network may be categorized as adaptive control of the stochastic process. The proof will be given about the convergence of the error signal. AANN weights will be tuned in each iteration depending on disturbance which is a stochastic but bounded process. The justification for adaptivity requirements of the HVAC system lies in the lack of a suitable mathematical model. Parameter tuning in any process (in our case tuning of weights of AANN) will be possible if PE is ensured. In thermal processes a disturbance input is characterized by oscillations of bounded amplitudes and because of this PE condition is satisfied. However, the quality of temperature regulation depends on the quality of sensors used, their deployment, initial set-up and good calibration.

3.4 Neural Network Design

Neural networks can be used for control purposes whenever the mathematical model of the process do not exist or is inadequate to describe the dynamics of the process. This is very often the case in situations whenever process parameters are changing due to various reasons. AANN is universal approximator, as shown by [107] and [108], [96], [98] and [10]. It can approximate every smooth function with the desired accuracy. However, there are certain prerequisites to enable control with AANN. The main prerequisite is a stability of the open-loop controlled system or at least passivity of the system, [82] and [83]. The passivity of the open-loop system has been shown in Section 2.8.1. To show passivity we used the mathematical model of the thermal process. The same mathematical model can be explored for deciding on the topology of the AANN. When the topology of the AANN is fixed, it can be used for controlling the thermal process whose dynamics could change due to change of parameters or any other cause. The closed-loop system with chosen AANN, sensors and actuators is analysed by using the Lyapunov stability criterion (as in [107]). Design of neural network also refers to the choice of a number of layers, number of nodes, and type of activation functions. There is no general recommendation for selecting the optimum numbers and types. However, there exist a couple of methods and a few heuristic rules:

- In [9], the number of nodes is estimated by picking the representative transfer function of the process and then the process is persistently excited. By analysing

the simulated closed-loop responses and approximation errors the number of nodes can be finally defined.

- Non-linear functions have been used as activation functions[9]. Sigmoid is commonly used as transfer function because it is nonlinear and continuously differentiable which is desirable for network learning.

Weight update mechanism for AANN is based on defining the differential equation that describes the performance of the controlled process (process model). Proper settings of the weighting function can be defined only if initial conditions for the mathematical model of the process are known. Also, disturbances, constraints on process signals and all signals in the closed-loop has to be taken into account.

Time delays are common nonlinearity in thermal processes. The time constant of the scaled mock-up is about one minute so that, we can expect much larger lags in real scale building. The thermal lag (time delay) of the heating process to any input has been found in the thermal analysis of the real scale building heating system in [109]. Accordingly, particular attention is devoted to compensation of thermal leg. The design of the AANN control system for regulating heat flow in the scaled mock-up will proceed without the thermal leg, which will be included afterwards.

3.4.1 Mathematical Background

Matrix norms will be used in solving stability issues because they are well suited in cases where we have to define boundaries [110]. An induced norm is defined by the following

$$\|\mathbf{A}\| = sup\,\{\|\mathbf{Ax}\| \mid \|\mathbf{x}\| = 1\} \tag{3.27}$$

what means that $\|\mathbf{A}\|$ on the left side is matrix norm , while$\|\mathbf{Ax}\|$ on the right side denotes the vector norm [111]. Property of induced norms of the identity matrix I and matrices **A** and **B** are:

$$\|\mathbf{I}\| = 1 \tag{3.28}$$

$$\|\mathbf{Ax}\| < \|\mathbf{A}\|\|\mathbf{x}\|,\ for\ all\ \mathbf{A}, \mathbf{x} \tag{3.29}$$

$$\|\mathbf{AB}\| < \|\mathbf{A}\|\|\mathbf{B}\|,\ for\ all\ \mathbf{A}, \mathbf{B} \tag{3.30}$$

[9]sigmoid, hyperbolic tangent rectified linear unit, leaky relu, swish etc.

Let $R^{m\times n}$ be vector space of dimension $m \times n$, then magnitudes of matrices $\mathbf{A} \in R^{m\times n}$ can be "measured" by employing any vector norm on $R^{m\times n}$. Frobenius norm is a special matrix norm defined as

$$\|\mathbf{A}\|_F = \sqrt{\sum_{ij} |\mathbf{A}_{ij}|^2} = \sqrt{Tr(\mathbf{A}\mathbf{A}^H)} \tag{3.31}$$

3.4.2 Stability Proof

As the system have time-delay component, closed-loop system will be first analysed as a time-delay-free system, and then the system delay will be added into account as in Chapter 8 of [96].

3.4.2.1 Delay-free-function

The system (3.23) without time delay may be written as

$$\dot{\mathbf{x}}(t) = \mathbf{A}\mathbf{x}(t) + \mathbf{B}\mathbf{u}(t) \tag{3.32}$$

or:

$$\dot{\mathbf{x}} = \mathbf{A}\mathbf{x} + \mathbf{B}\mathbf{u} \tag{3.33}$$

The NN is described by the control variable Φ_{d2c} and states $\mathbf{x}$ as inputs ([9]):

$$\Phi_{d2c} = \mathbf{W}^T \varsigma(\mathbf{x}) \tag{3.34}$$

where Φ_{d2c} represent the injected heat flow of the DSF corridor and ς is activation function used in the neural network. The last hidden layer weights (V) are fixed ,so (3.34) may be written as:

$$\Phi_{d2c} = \mathbf{W}^T(\varsigma(\mathbf{V}^T\mathbf{x})) = \mathbf{W}^T\varphi(\mathbf{x}(t)) \tag{3.35}$$

where $\varphi(\mathbf{x})$ is basis function vector. Basis function may be any smooth, monotone increasing function [9]. Lyapunov candidate is defined as:

$$L = \frac{1}{2}\mathbf{x}^T\mathbf{P}\mathbf{x} + \frac{1}{2}\mathbf{W}^T\mathbf{F}^{-1}\dot{\mathbf{W}} \tag{3.36}$$

where P is symmetric positive definite matrix satisfying the Lyapunov equation:

$$\mathbf{A}^T\mathbf{P} + \mathbf{PA} + \mathbf{Q} = 0 \tag{3.37}$$

and Q is a symmetric positive definite matrix. Variable F is any symmetric positive definite matrix and also has to be invertible to satisfy:

$$\frac{d}{dt}(\mathbf{W}^T\mathbf{F}^{-1}\mathbf{W}) = \mathbf{W}^T\mathbf{F}^{-1}\dot{\mathbf{W}} = \dot{\mathbf{W}}^T\mathbf{F}^{-1}\mathbf{W} \tag{3.38}$$

A derivative of 3.36 is as follows:

$$\dot{L} = \frac{1}{2}\left(\dot{\mathbf{x}}^T\mathbf{Px} + \mathbf{x}^T\mathbf{P}\dot{\mathbf{x}} + \dot{\mathbf{W}}^T\mathbf{F}^{-1}\mathbf{W} + \mathbf{W}^T\mathbf{F}^{-1}\dot{\mathbf{W}}\right) \tag{3.39}$$

From (3.38) it follows

$$\dot{L} = \frac{1}{2}\left(\dot{\mathbf{x}}^T\mathbf{Px} + \mathbf{x}^T\mathbf{P}\dot{\mathbf{x}}\right) + \dot{\mathbf{W}}^T\mathbf{F}^{-1}\mathbf{W} \tag{3.40}$$

Using (3.33), equation (3.40) can be rewritten as:

$$\dot{L} = \frac{1}{2}\left(\mathbf{x}^T\mathbf{A}^T\mathbf{Px} + \mathbf{u}^T\mathbf{B}^T\mathbf{Px} + \mathbf{x}^T\mathbf{PAx} + \mathbf{x}^T\mathbf{PBu}\right) + \mathbf{W}^T\mathbf{F}^{-1}\dot{\mathbf{W}} \tag{3.41}$$

By grouping (3.41) we gain:

$$\dot{L} = \frac{1}{2}\left(\mathbf{x}^T(\mathbf{A}^T\mathbf{P} + \mathbf{PA})\mathbf{x} + \mathbf{u}^T\mathbf{B}^T\mathbf{Px} + \mathbf{x}^T\mathbf{PBu}\right) + \mathbf{W}^T\mathbf{F}^{-1}\dot{\mathbf{W}} \tag{3.42}$$

From (3.37) follows that $\mathbf{A}^T\mathbf{P} + \mathbf{PA} = -\mathbf{Q}$ and from (3.42) follows:

$$\dot{L} = -\frac{1}{2}\mathbf{x}^T\mathbf{Qx} + \frac{1}{2}\mathbf{u}^T\mathbf{B}^T\mathbf{Px} + \frac{1}{2}\mathbf{x}^T\mathbf{PBu} + \mathbf{W}^T\mathbf{F}^{-1}\dot{\mathbf{W}} \tag{3.43}$$

The result of $\mathbf{u}^T\mathbf{B}^T\mathbf{Px}$ and $\mathbf{x}^T\mathbf{PBu}$ are scalars. So, their sum may be written as $2x^TPBu$. Applying this substitution in 3.43 we may write:

$$\dot{L} = -\frac{1}{2}\mathbf{x}^T\mathbf{Qx} + \mathbf{x}^T\mathbf{PBu} + \mathbf{W}^T\mathbf{F}^{-1}\dot{\mathbf{W}} \tag{3.44}$$

In order to ensure Lyapunov stability, the ANN weights updating should be chosen in such a way to set $\dot{L}$ negative:

$$\dot{W} = \mathbf{F}\varphi(\mathbf{x})\Phi_{diff} - k_w\|\mathbf{x}\|\mathbf{FW} \tag{3.45}$$

where k_w is a positive design parameter, and ϕ_{diff} is the difference in interior heat flow (see Figure 3.3). After substitution of (3.45) in (3.44) we get:

$$\dot{L} = -\frac{1}{2}\mathbf{x}^T\mathbf{Q}\mathbf{x} + \mathbf{x}^T\mathbf{P}\mathbf{B}\mathbf{u} + \mathbf{W}^T\varphi(\mathbf{x})\Phi_{diff} - \mathbf{W}^T k_w\|\mathbf{x}\|\mathbf{W} \tag{3.46}$$

According to (3.19), vector **u** consists of the control signal and disturbance, so we may write $\mathbf{u} = c_0 u_1 + d$, where d is a disturbance. If (3.34) is used to substitute the control signal u_1, then we may write:

$$\dot{L} = -\frac{1}{2}\mathbf{x}^T\mathbf{Q}\mathbf{x} + \mathbf{x}^T\mathbf{P}c_0\mathbf{W}^T\varphi(\mathbf{x}) + \mathbf{x}^T\mathbf{P}d + \mathbf{W}^T\varphi(\mathbf{x})\Phi_{diff} - \mathbf{W}^T k_w\|\mathbf{x}\|\mathbf{W} \tag{3.47}$$

If (3.47) is rewritten into

$$\dot{L} = -\frac{1}{2}\mathbf{x}^T\mathbf{Q}\mathbf{x} + \mathbf{x}^T\mathbf{P}d + \mathbf{W}^T\varphi(\mathbf{x})(\mathbf{x}^T\mathbf{P}c_0 + \Phi_{diff}) - \mathbf{W}^T k_w\|\mathbf{x}\|\mathbf{W} \tag{3.48}$$

If we want that the closed-loop system is asymptotically stable, the derivative of Lyapunov candidate function should be negative or equal to zero.

$$0 \geq -\frac{1}{2}\mathbf{x}^T\mathbf{Q}\mathbf{x} + \mathbf{x}^T\mathbf{P}d + \mathbf{W}^T\varphi(\mathbf{x})(\mathbf{x}^T\mathbf{P}c_0 + \Phi_{diff}) - \mathbf{W}^T k_w\|\mathbf{x}\|\mathbf{W} \tag{3.49}$$

The inequality (3.49) has to be valid in all working regimes, and this is ensured by bounding state vector **x** and weight matrix **W** in respect of thermal process characteristics (**P**, **Q**, **B** etc.). Positive definite matrices **P** and **Q** are variant, so we must consider the worst scenario where matrix **Q** has the minimum value and matrix **P** has the maximum value. Therefore, matrix norms and singular values are used to define inequality:

$$0 \geq -\frac{1}{2}\|\mathbf{x}\|^2\lambda_{min}(\mathbf{Q}) + \|\mathbf{x}\|\|\mathbf{W}\|D + \|\mathbf{x}\|\lambda_{max}(\mathbf{P})d_M + \|\mathbf{W}\|^2 k_w\|\mathbf{x}\| \tag{3.50}$$

where:

$$D = max(\|\varphi(\mathbf{x})\|(\|\mathbf{P}c_0\| + 1)) \tag{3.51}$$

$\|\mathbf{x}\| \geq \|\Phi_{diff}\|$ as $\|\Phi_{diff}\| \leq \|\Phi_{xy}\|$ and $y = \Phi_{xy}$ (see (3.23))
$\lambda_{max}(\mathbf{P})$ is the maximum singular value of matrix **P**
$\lambda_{min}(\mathbf{Q})$ is the minimum singular value of matrix **Q**
d_M maximum disturbance

According to relations given so far, the system is asymptotically stable as long as:

$$\|\mathbf{x}\| > \frac{d_M \lambda_{max}(\mathbf{P}) + \frac{D^2}{4k_w}}{\frac{1}{2}\lambda_{min}(\mathbf{Q})} \tag{3.52}$$

and

$$\|\mathbf{W}\| > \frac{D}{2k_w} + \sqrt{\frac{D^2}{4k_w^2} + \frac{d_M \lambda_{max}(\mathbf{P})}{k_w}} \tag{3.53}$$

In practice, it is not unusual to have unknown disturbances, [96]. These disturbances are usually bounded by some known amount. Increase of bound value affects the increase of ratio $\frac{\lambda_{max}(\mathbf{P})}{\lambda_{min}(\mathbf{Q})}$ which is a standard result on norms of Lyapunov solution.

3.4.2.2 Function with Delay

The linearized thermal process with time delay in state space form is:

$$\dot{\mathbf{x}}(t) = \mathbf{A}\mathbf{x}(t) + \mathbf{B}\mathbf{u}(t - t_d) \tag{3.54}$$

Component $k_d\mathbf{F}\mathbf{W}(t)$ is added to the weighting function update mechanism (3.45) to compensate time delay effects. The function is defined as:

$$\dot{\mathbf{W}}(t) = \mathbf{F}\varphi(\mathbf{x})\Phi_{d2c}(t) - k_w\|\mathbf{x}(t)\|\mathbf{F}\mathbf{W}(t) - k_d\mathbf{F}\mathbf{W}(t) \tag{3.55}$$

where $k_d > 0$ is a scalar design parameter added to compensate delay.

Although the thermal process has only control signals with time delays, the control signals in the closed-loop system will be realized by AANN for which the tuning of weights will compensate for this time delays (k_d), and we will have effect as time delays are not present. Lyapunov candidate function for our thermal process, taking into account present time and time delay, is then:

$$\begin{aligned} L \;=\; & \tfrac{1}{2}\mathbf{x}^T(t)\mathbf{P}\mathbf{x}(t) + \tfrac{1}{2}\mathbf{W}^T(t)\mathbf{F}^{-1}\mathbf{W}(t) + \mathbf{x}^T(t - t_d)\mathbf{P}\mathbf{x}(t - t_d) \\ & + \tfrac{1}{2}\mathbf{W}^T(t - t_d)\mathbf{F}^{-1}\mathbf{W}(t - t_d) \end{aligned} \tag{3.56}$$

and derivatives of these states are described as:

$$\dot{\mathbf{x}}(t) = \mathbf{A}x(t) + \mathbf{B}u(t) \tag{3.57}$$

$$\dot{\mathbf{x}}(t - t_d) = \mathbf{A}\mathbf{x}(t - t_d) + \mathbf{B}\mathbf{u}(t - t_d) \tag{3.58}$$

The derivative of Lyapunov function ends up as:

$$\begin{aligned}\dot{L} &= -\tfrac{1}{2}\mathbf{x}^T(t)\mathbf{Q}\mathbf{x}(t) + \tfrac{1}{2}\mathbf{u}^T(t)\mathbf{B}^T\mathbf{P}\mathbf{x}(t) + \tfrac{1}{2}\mathbf{x}^T(t)\mathbf{P}\mathbf{B}\mathbf{u}(t) \\ &\quad +\mathbf{W}^T(t)\mathbf{F}^{-1}\dot{\mathbf{W}}(t) \\ &\quad -\tfrac{1}{2}\mathbf{x}^T(t-t_d)\mathbf{Q}\mathbf{x}(t-t_d) + \tfrac{1}{2}\mathbf{u}^T(t-t_d)\mathbf{B}^T\mathbf{P}\mathbf{x}(t-t_d) \\ &\quad +\tfrac{1}{2}\mathbf{x}^T(t-t_d)\mathbf{P}\mathbf{B}\mathbf{u}(t-t_d) + \mathbf{W}^T(t-t_d)\mathbf{F}^{-1}\dot{\mathbf{W}}(t-t_d)\end{aligned} \tag{3.59}$$

Derivatives of state space matrices may be substituted as in (3.57) and (3.58). After substitution, Lyapunov derivative becomes:

$$\begin{aligned}\dot{L} &= -\tfrac{1}{2}\mathbf{x}^T(t)\mathbf{Q}\mathbf{x}(t) + \mathbf{x}^T(t)\mathbf{P}\mathbf{B}\mathbf{u}(t) + \mathbf{W}^T\varphi(\mathbf{x}(t))\phi_{d2c}(t-t_d) \\ &\quad -\mathbf{W}^T(t)k_w\|\mathbf{x}(t)\|\mathbf{W}(t) - \mathbf{W}^T(t)k_d\mathbf{W}(t) \\ &\quad -\tfrac{1}{2}\mathbf{x}^T(t-t_d)\mathbf{Q}\mathbf{x}(t-t_d) + \mathbf{x}^T(t-t_d)\mathbf{P}\mathbf{B}\mathbf{u}(t-t_d) \\ &\quad +\mathbf{W}^T(t-t_d)\varphi(\mathbf{x}(t-t_d))\phi_{d2c} - \mathbf{W}^T(t-t_d)k_w\|\mathbf{x}(t-t_d)\|\mathbf{W}(t-t_d) \\ &\quad -\mathbf{W}^T(t-t_d)k_d\mathbf{W}(t-t_d)\end{aligned} \tag{3.60}$$

Derivation of the Lyapunov candidate function should be negative:

$$\begin{aligned}0 > &-\|\mathbf{x}(t)\|\left(\tfrac{1}{2}\lambda_{min}(\mathbf{Q})\|\mathbf{x}(t)\| - \|\mathbf{W}(t)\|D - Pd_M + \|\mathbf{W}(t)\|^2k_w\right) \\ &-\|\mathbf{W}(t)\|^2k_d \\ &-\|\mathbf{x}(t-t_d)\|\left(\tfrac{1}{2}\lambda_{min}(\mathbf{Q})\|x(t-t_d)\| - \|\mathbf{W}(t-t_d)\|D - Pd_M + \|\mathbf{W}(t-t_d)\|^2k_w\right) \\ &-\|\mathbf{W}(t-t_d)\|^2k_d\end{aligned} \tag{3.61}$$

Equation (3.61) may be written as:

$$\begin{aligned}0 > &-\|\mathbf{x}(.)\|\left(\tfrac{1}{2}\lambda_{min}(\mathbf{Q})\|\mathbf{x}(.)\| - \|\mathbf{W}(.)\|D - \lambda_{max}(\mathbf{P})d_M + \|\mathbf{W}(.)\|^2k_w\right) \\ &-\|\mathbf{W}(.)\|^2k_d\end{aligned} \tag{3.62}$$

where $\|\mathbf{x}(.)\|$ and $\|\mathbf{W}(.)\|$ are notations for *Frobenius norms* that includes both moments: t and $t - t_d$. In (3.62) two inequalities can be identified. First, the inequality with $\|\mathbf{W}\|$ will be extracted:

$$\frac{1}{2}\lambda_{min}(\mathbf{Q})\|x\| - \|\mathbf{W}\|D - \lambda_{max}(\mathbf{P})d_M + \|\mathbf{W}\|^2k_w > 0 \tag{3.63}$$

and then with $\|\mathbf{x}\|$:

$$\frac{1}{2}\lambda_{min}(\mathbf{Q})\|x\|^2 - (\|\mathbf{W}\|D + \lambda_{max}(\mathbf{P})d_M + \|\mathbf{W}\|^2k_w)\|\mathbf{x}\| + \|\mathbf{W}\|^2k_d > 0 \tag{3.64}$$

In order to satisfy inequality in (3.64) the following condition must be met:

$$k_d - k_w > 0 \tag{3.65}$$

Finaly we conclude the closed-loop system is stable as long as:

$$\|\mathbf{W}(.)\| > \frac{D}{2k_w} + \sqrt{\frac{D^2}{4k_w^2} + \frac{\lambda_{max}(\mathbf{P})d_M}{k_W}} \tag{3.66}$$

and

$$\|\mathbf{x}(.)\| > \frac{\lambda_{max}(\mathbf{P})}{\lambda_{min}(\mathbf{Q})}d_M + \sqrt{\frac{\lambda_{max}^2(\mathbf{P})}{\lambda_{min}^2(\mathbf{Q})} + \frac{1}{2}\frac{D^2}{(k_d - k_w)\lambda_{min}(\mathbf{Q})}} \tag{3.67}$$

3.5 Summary

The chapter listed known control strategies of DSF systems and proposed a novel one, focusing on critical temperature differences. The special case of DSF without natural ventilation was analysed because there is a static air buffer that can be used for control purposes. The control is achieved by adding extra heat load into its corridor. The challenging goal of the control system is to maintain the equal heat flow of DSF and all walls. As described in Chapter 2, it is possible but not practical to measure scaled mock-up state variables, so estimation is required. AANN was proposed as a regulator for temperature control of the scaled mock-up with DSF. Tuning of the adaptive neural network is based on Lyapunov function. This tuning ensures desired performance for the scaled mock-up and can be proposed for the real buildings with DSFs if appropriate AANN preparation is performed. Time delays are analysed as a response to disturbances and control signals. The chapter concludes with providing a theoretical proof of the stability and efficiency of the proposed AANN.

Chapter 4

Analysis of Thermal Control System by Simulation

In the following part, the proposed control systems are simulated to test the performance. As concluded, based on experiments (see Chapter 2.7), the heat flow cannot be properly estimated by using linearized mathematical model and only temperature measurement data. Therefore, simulation aim is to justify the usage of simplified equations for AANN weight tuning and proof of stability as described in Chapter 3. In other words, simulations are here to give us the answer to what transients we can expect. Simulations will not give us precise answers because we are using a linearized mathematical model. The scaled mock-up with corridor DSF is also investigated, and the comparison is made between controlled and non-controlled DSFs. The contribution of such comparative study is in verification of efficiency of controlled DSF.

4.1 Simulation Setup

Our goal is to investigate important features and behaviours of DSF system. In order to analyse these features and behaviour, several assumptions must be made. For instance, it is useful to eliminate disturbances such as human presence, stationary devices, HVAC, solar radiation etc. The solar radiation is omitted due to the lack of detailed information about received direct and diffuse solar radiation. This assumption is necessary, even though the solar radiation in real buildings have quite dominant effects because in an experimental set-up that we use, solar radiation is quite difficult to generate. However, for performance comparison between controlled and uncontrolled DSF, this assumption

can be justified. We can assume that we have a cloudy day. Both, simulated and measured weather data[1] are used in simulations. The same mathematical model is used with different simulation set-ups, depending on the test objective. Our simulation set-up is in fact hardware in-the-loop setting, where the real building or in our case scaled mock-up is replaced with the linearized mathematical model. The versatility of this set-up has been facilitated by the choice of the programme packages, namely the MATLAB and LINUX/PYTHON, which allows rapid prototyping and easy interfacing, using suitable hardware, between the virtual world and the real one.

4.2 Simulations Results

Simulations are presented in chronological order. At first, preliminary tests were performed with the HAMBASE model. Unavoidable drawbacks were revealed, so we created new improved model. The improved model was designed by using HAMBASE equations an identification was based on measurements of desired temperature response. Different regulators were simulated.

4.2.1 Preliminary Tests

Preliminary tests are designed to provide answers about the quality and adequacy of the mathematical model. During these tests, no modification is done to the HAMBASE model.

4.2.1.1 Test 1 - Variations of Parameters

At first, the simulation is done without any regulation (open-loop system) while environment temperature changes. The weather data, used in this test, are from a site at 15.98° longitudes and 45.82° latitudes, Above Mean Sea Level (AMSL) height 157 m, station ”Maksimir”, Zagreb, Croatia. Basic simulation parameters are shown in Table 4.1.

[1] measured weather data are taken from statistical tables of meteorological stations: outdoor temperature, relative humidity, air velocity, etc.

TABLE 4.1. Simulink parameters

Purpose	**Period [h]**	**Step type**	**Step size**	**Solver**
Open-loop test	72	fixed	0.0166666	4th order Runge Kutta

Impacts of input heat value, corridor ventilation value and model size value were monitored during testing. The set-up of the first simulation series may be illustrated with the simple schematics shown in 4.1, where two detached squares represents a building's zone with DSF system. Inner temperature T_i should be greater than the temperature of the corridor T_c during the transient event of negative gradient of exterior temperature T_e.

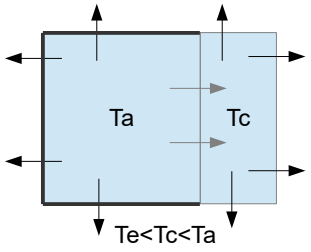

FIGURE 4.1. Set-up without temperature regulation

The period of simulation corresponds to three days of real operations (72 hours-see Table 4.1), during which different conditions are considered. Influence of changing corridor ventilation and input heat to air temperature in the zone is shown in Figure 4.2. The tested model is described in more details in previous Section 2.3.

At first, simulation tests were performed on the mathematical model of the real building by simple variation of different parameters such as ventilation or heat input. When these variable values exceed the limitations, responses drastically changes - see Figure 4.2, where the same tests were performed. Results are shown in Figure 4.3: Variation of the ventilation input does not significantly change temperature response.

Building scale variation from 1 (18 times smaller size than real scale) to 10 (1.8 times smaller size then real scale) will give us quite different results shown in Figure 4.3. Variation of the scale from 1 to 18 ends up with quite different results. Results are shown in Figure 4.3:

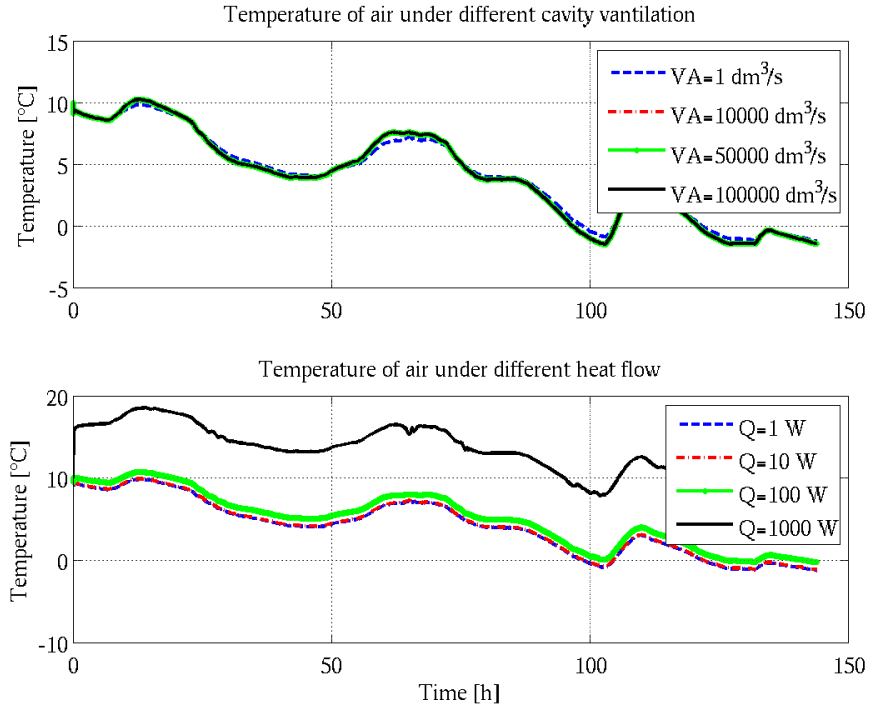

FIGURE 4.2. Influence of corridor ventilation and input heat to air temperature in the zone

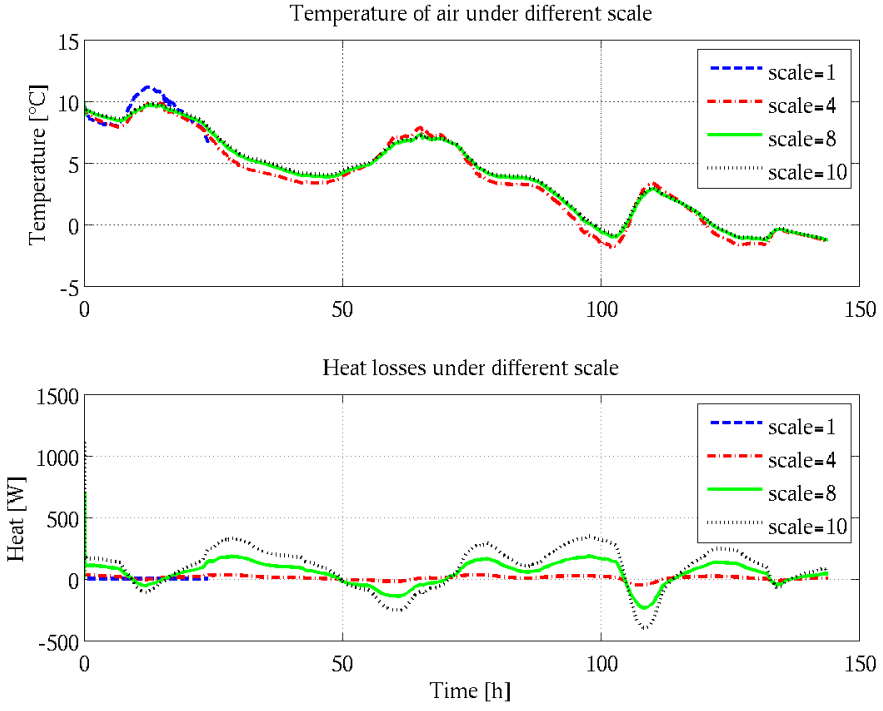

FIGURE 4.3. Influence of dimension variance in scale to air temperature in the zone

Temperature transients with scaled building model are not realistic because there is no significant phase shift. The fix would require changes in parameter calculation. Real-scale model preserves appropriate response, but it has an issue with adjusting parameters. Longer simulation times are required due to slower system's response.

4.2.1.2 Test 2 - Heat Flow Response to Temperature Variation

Instead of using real measured data from weather stations, the environmental disturbances will be simulated as a sinusoidal wave function. The regular sinusoidal signal has been chosen due to easier detection of differences between responses. The amplitude is set to a value similar to real weather data amplitudes. Tests were carried out on the scaled mock-up, as presented in Figure 2.26.

Since the scaled mock-up envelope is not made of the same material and thickness, the heat flow response will vary in amplitude and shape - see Figure 4.4.

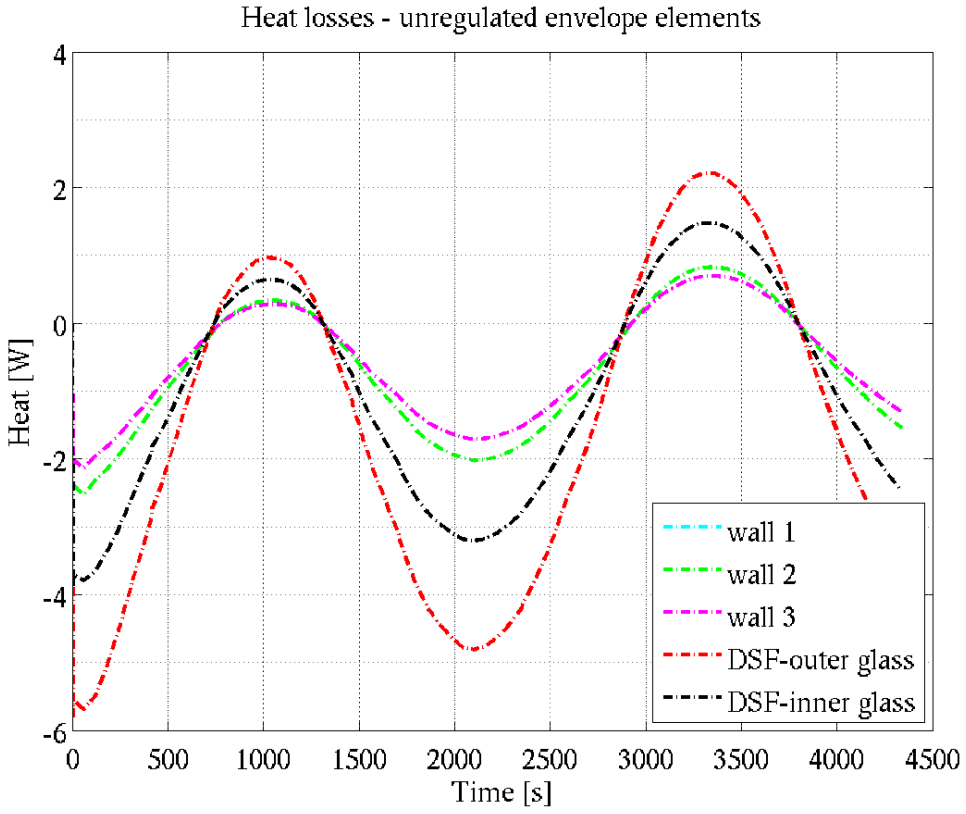

FIGURE 4.4. Heat losses of scaled mock-up

Simulation results with non-regulated DSF system coincide with experimental results where temperatures had been measured while changing exterior conditions (see Figure

2.45). Heat flows (heat losses) of walls and DSF skins are presented separately. Simulated heat flow responses and measured thermal responses confirms that glazed element is critical as it generates significantly larger heat losses then walls.

4.2.2 Analysis with the improved Model

The improved model is also not good enough to independently represent the system, but due to the proven fact that behaviour is similar, simulations with the improved model is used for testing functionality of designed regulator. First, the frequency response of the thermal transient through the wall is analysed. The temperature variance is presented as a disturbance. Figures 4.5 and 4.6 shows the frequency responses (Bode) of the open-loop system. Frequency responses are given for different mathematical models. Table 4.3 gives relative stability (amplitude and phase margins) for these models. Amplitude frequency responses (4.3) are similar for all models. However, phase frequency characteristics (4.5) show greater differences between models. This indicates that the adaptive controller will be needed. Bode diagram demonstrates that the dimension of the building affects temperature responses significantly, while the stability is not affected so much.

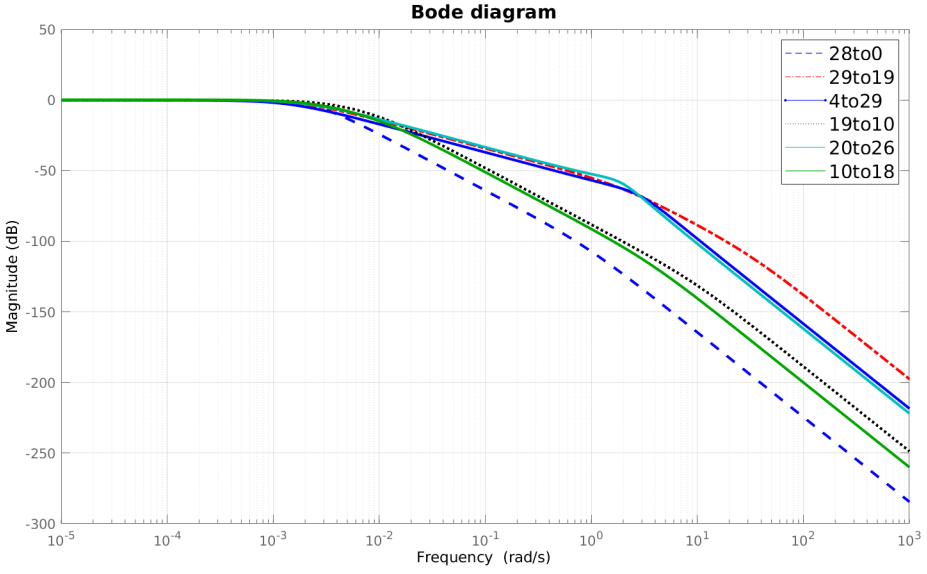

FIGURE 4.5. Bode diagram - magnitude plot

Because of our interventions (heat pumping), parameters in buildings can change, so LTI transfer function can't appropriately describe the dynamics of the building. However, if we can start our simulation with LTI transfer function and during simulation

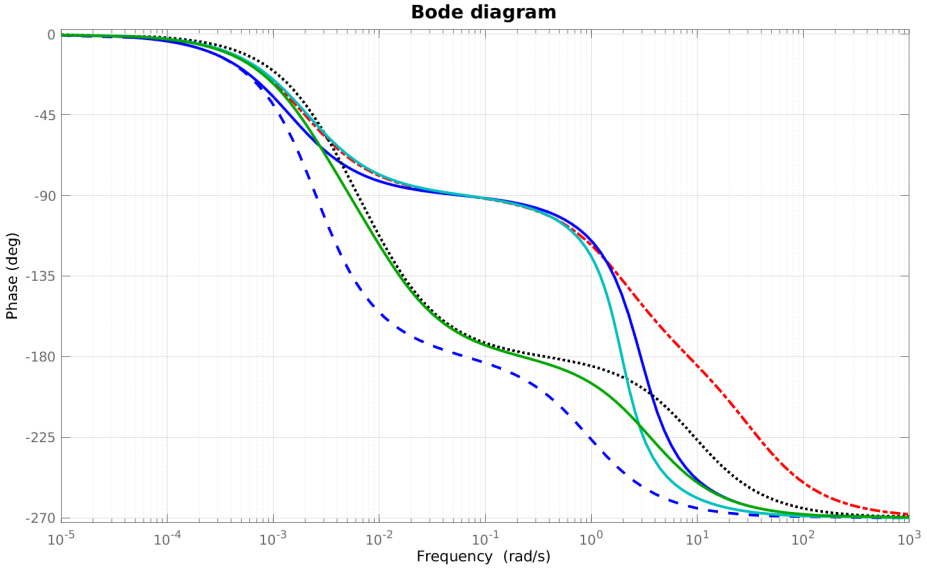

FIGURE 4.6. Bode diagram - phase plot

slowly change mathematical model parameters we can come closer to the real situation. This capability is now possible in *Simulink* (see Figure 4.7). The usage of the continuous-time transfer function with varying coefficients is limited since it is assumed that these varying coefficients are time-independent, [112]. If in Figure 4.7, instead of a slow change of parameters, fast change is used, we will end-up with errors that can't be overcome and our simulation will not give us appropriate results. However, the research is using neural networks which do not use mathematical models, so detailed analysis, that covers parameter identification and all working regimes, is not necessary. Figure 4.7 shows the *Simulink* diagram used for our simulations. Temperature responses to thermal disturbance (caused by T_e) in scaled mock-up are presented with four transfer functions, listed in Table 4.2.

TABLE 4.2. List of transfer functions presented in Figure 4.7

Transfer Function	*Simulink* Block Type	Color
$F(T_e, T_{ir})$	Transfer Fcn	Skyblue
$F(Ref, \phi_{d2c})$	Transfer Fcn	Black
$F(T_e, T_{if})$	Varying Transfer Function	Red
$F(T_e, T_c)$	Varying Transfer Function	Orange
$F(T_e, T_{d2c})$	Transfer Fcn	Blue

Functions $F_t(T_e, T_if)$ and $F_t(T_e, T_c)$ have variant coefficients as the change in control signal directly affect them. For our purpose the following physical variables are important and measured (see Table 2.2):

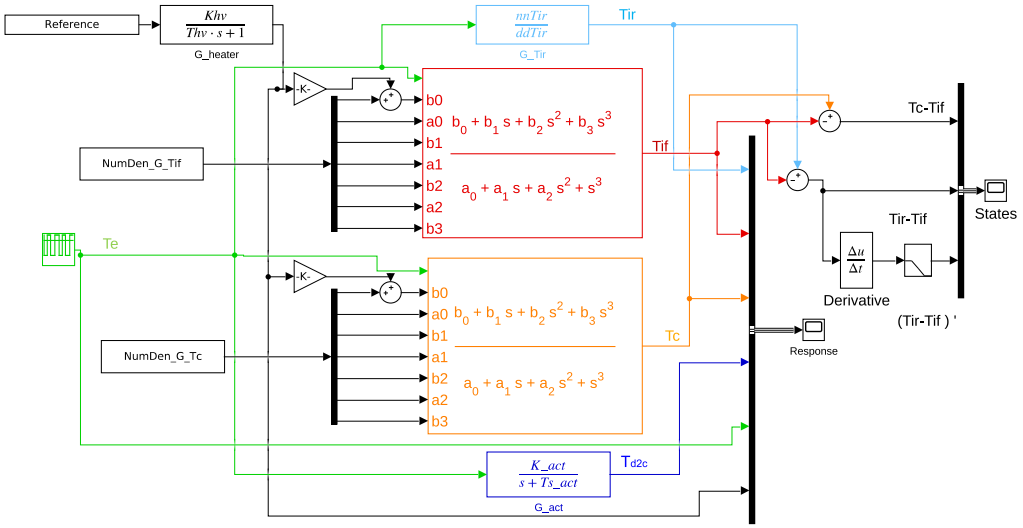

FIGURE 4.7. Block diagram of the improved model presented in *Simulink*

- T_{if} - Temperature of interior air directly behind the glazed surface of the DSF
- T_{ir} - Temperature of interior air in front of the right wall, close to the centre of the wall
- T_c - Corridor temperature
- T_{d2c} - Temperature of air inserted into the corridor

Scaled mock-up disturbance is a regular quadratic signal with constant cycles. The disturbance generates steep thermal variations and significant difference between temperatures in the same zone, even if the dimensions are very small. Temperature differences will be explored for estimation purposes. Thus, the state vector consists of:

- $T_c - T_{if}$ - Thermal difference between the corridor and front interior temperature
- $T_{ir} - T_{if}$ - Thermal difference between front and rear-side temperature
- $(T_{ir} - T_{if})'$ - Derivation through a time of the thermal difference between front and rear-side temperature.

TABLE 4.3. Magnitude and phase margins

	28to0	29to19	4to29	19to10	20to26	10to18
Magnitude marging	671.8889	0.9729	0.9806	0.9824	1.0041	1.0146
Phase marging	Inf	-2.8826	-0.4003	-2.0881	-2.7174	-2.8905

4.2.2.1 Test 3 - open-loop response

The values for the scaled mock-up parameters given in 2.3 were selected as in [51]. The temperature disturbance signal is a square wave with a period of 30 minutes. This period is chosen to get a response that is capable of reaching a steady state. Figure 4.8 shows responses of the scaled mock-up without temperature regulation. Measured responses differ in various areas of the scaled mock-up.

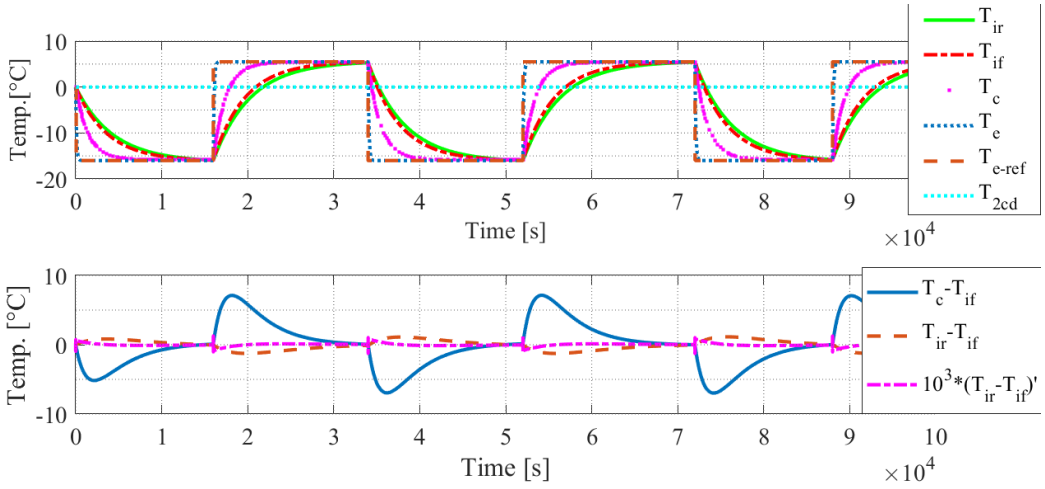

FIGURE 4.8. Simulated temperature responses of the scaled mock-up

Temperature deviation in interior air is small, with a maximum value around 1.2 $°C$ (0.5% compared to the value of the maximum variation of external temperature). Considering that dimension of the scaled mock-up is 18 times smaller than the real building, this difference is not negligible. Large temperature deviation is not just uncomfortable but in combination with humidity may cause condensation and mould growth what is extremely unhealthy. The derivation of the difference between T_{ir} and T_{if} is quite small, so to show it on the graph (Figure 4.8), it was multiplied by 1000.

4.2.2.2 Test 4 - Closed-loop with P Regulator and Improved Mathematical Model

The results of closed-loop system with P regulator are shown in 4.9. The internal thermal difference ($T_{ir} - T_{if}$) is reduced by using P regulator, but benefits are modest.

Controlled signal (temperature of inserted air) T_{2cAct} appears not to be appropriate for regulating thermal difference $T_{ir} - T_{if}$.

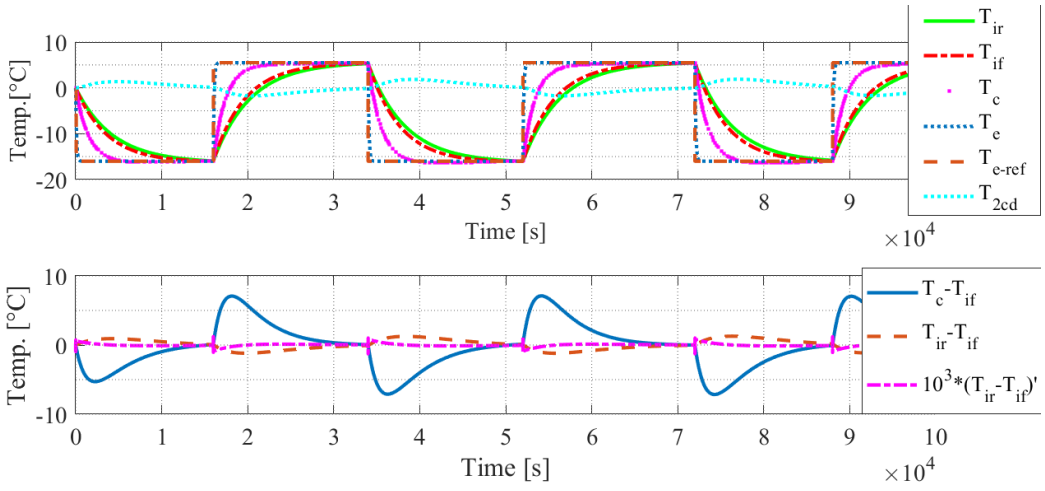

FIGURE 4.9. Simulated temperature responses of scaled mock-up with P regulator

One may notice that the control signal is quite similar to internal thermal difference response. P regulator tries to eliminate feedback error which is the internal thermal difference ($error = T_{ir} - T_{if}$). Simulation experiments with P regulator and improved mathematical model of the scaled mock-up have shown that with P regulator results are not as we would expect. The reason for this is that P regulator use only one signal (error signal) to improve dynamics, but in our case, the error signal is the internal thermal difference ($T_{ir} - T_{if}$) which do not have enough information in it to get better results.

4.2.2.3 Test 5 - Closed-loop System with AANN and Improved Mathematical Model of the Scaled Mock-up

A linear mathematical model of the scaled mock-up can-not cover all temperature ranges of interest. Thus, P regulator that is properly tuned for one temperature range should be re-tuned for another temperature range. We need the adaptive capability of our regulator if we want it to be appropriate for temperature ranges of interest. Thus, we propose an adaptive artificial neural network (AANN) and hope that it can give performances that we need. We will test it by simulation and experiments. In order to ensure asymptotic stability of the closed-loop system AANN weighting coefficients will be tuned by use of Lyapunov theory of stability (see Section 3.4.2). At the beginning, there is not much improvement in the performance of internal thermal difference, but performance is rapidly improving through the next few cycles of square disturbance

temperature. This is especially evident in Figure 4.12 where ISA and IAE are shown respectively to all three cases (Test 3, Test 4 and Test5).

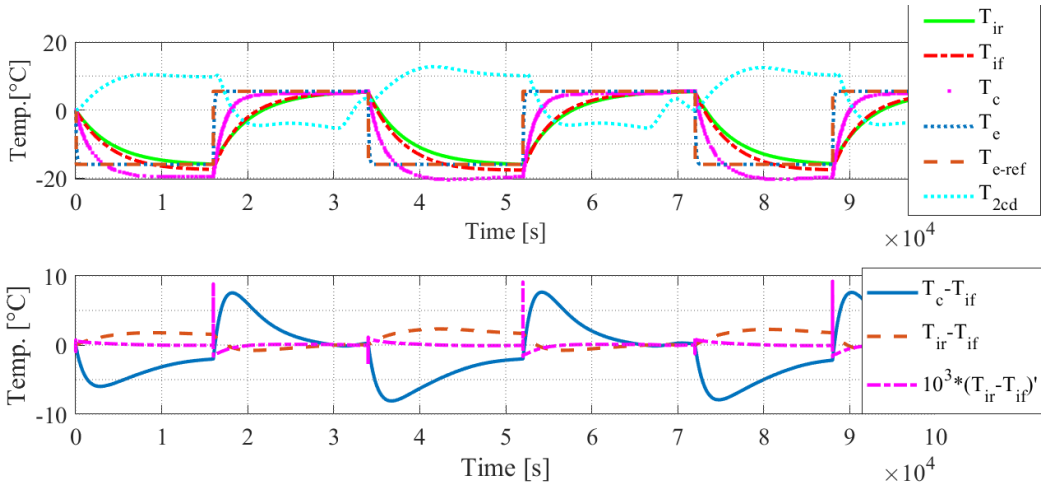

FIGURE 4.10. Simulated response of scaled mock-up with AANN regulator

AANN topology consists of 4 layers: two hidden layers with 5 neurons, input layer with 3 neurons and output layer with 1 neuron. The activation function in AANN is the sigmoid function. In this case, the AANN weights are bounded.

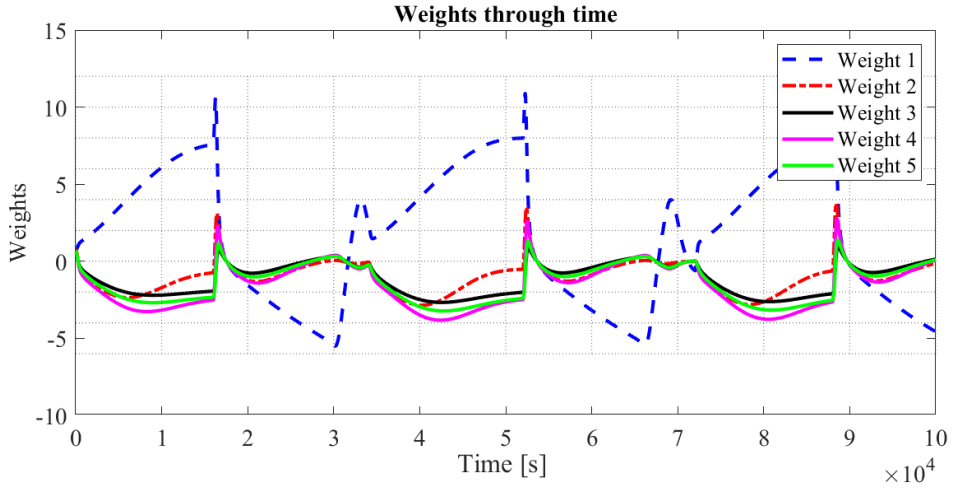

FIGURE 4.11. Weights of the AANN hidden layer during simulation

The weighting function update mechanism (see Section 3.4.2) consists of the back-propagation term ($\mathbf{F}\varphi(\mathbf{x})(T_{ir}-T_{if})$) and robustifying term ($-k_w\|\mathbf{x}\|\mathbf{FW}$). Back-propagation term is also called modification term because it contains thermal difference $T_{ir} - T_{if}$. The robustifying term is needed to overcome high-order modelling error terms. The tuning of the weighting coefficients in the hidden layer makes the AANN strictly passive,

and because of this, weights are bounded which is very important in practical non-ideal situations.

4.2.2.4 Comparison of PI and AANN

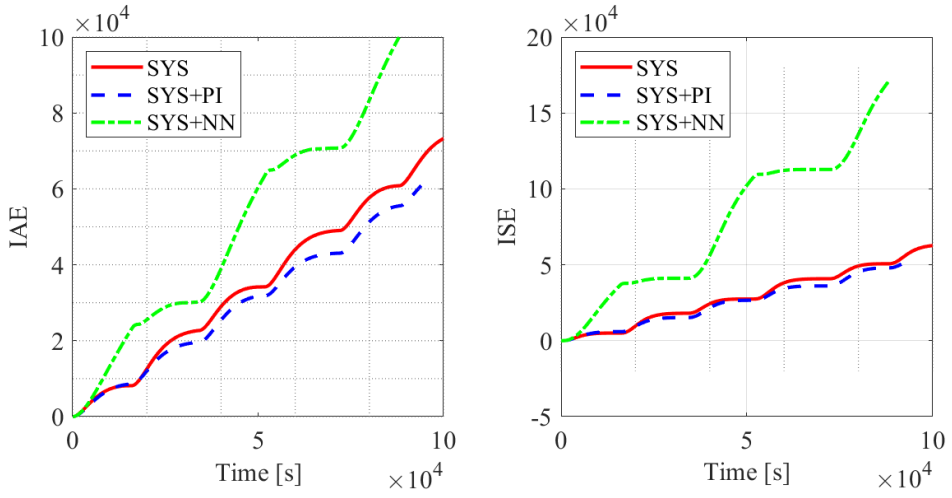

FIGURE 4.12. IAE and ISE comparison for different control methods

4.3 Summary

Common practice in civil and control engineering is to simulate novel methods before implementation [72], [113]. Simulations are performed in Chapter 4. Our goal was to examine dynamics and analyse stability. Even though, the analysis in Chapter 2 has shown that linear mathematical model of the scaled mock-up can't describe dynamics in all temperature ranges, and that nonlinear mathematical model is needed, we tested our regulators with linear models. The reason for this is in the fact that the nonlinear model of the scaled mock-up is not available and even if we do have the nonlinear model of the scaled mock-up it will significantly differ from the nonlinear model of the real building. So, our simulations serve the purpose only to inform us about what we could expect in the real situation. Experiments in the laboratory with the scaled mock-up will show in more detail the dynamics and capability of our regulators to deal with the unknown process. We suppose that if the AANN is capable of regulating temperature for the scaled mock-up, it will be capable also of regulating temperature in the real building. AANN could learn and adapt and with proper adjustment can be used to control any stable process. Test 1 to Test 5 covers various set-ups and control topologies. In Test 1

and Test 2 HAMBASE model was simulated. It was shown that this HAMBASE model is not appropriate and that the improved model of the scaled mock-up is what we need. Test 3 shows an open-loop system response to square temperature disturbance. In Test 4 P regulator was introduced and closed-loop response analysed. In Test 5 proposed AANN was introduced and analysed. Finally, comparative analysis was performed by comparison of IAE and ISE criterion (Section 4.2.2.4). The comparison shows that AANN is to be recommended.

The number of the highest derivative in a differential equation should be sufficient information required to set up the AANN regulator what will be described in the following chapter. Thus, simulated responses in this chapter should be observed qualitatively and not quantitatively. AANN is used to minimize unwanted internal thermal difference ($T_{ir} - T_{if}$) during thermal transients. Required persistence of excitation was ensured by the sinusoidal temperature change which is also common in the real environment. Stability is rigorously proven and synthesis procedure is straightforward and simple to use. No knowledge of the details of the building's dynamics is needed, and no regression matrices had to be found to design the AANN regulator.

Chapter 5

Analysis of Thermal Control System by Experiment

Experimental tests were carried out with the scaled mock-up as shown in Section 2.7.3. The control loop consists of AANN regulator, sensors, actuators and scaled mock-up (HIL[1] configuration). The AANN regulator is introduced in Section 3.4 and simulated in Section 4.2.2. Neural control performance was validated by Integral Absolute Error (IAE) and Integral of Squared Error (ISE) as described in [9].

5.1 Adjustment to Hardware-in-the-loop Set-up

To experiment with the scaled mock-up, controlled by AANN, we needed appropriate interfaces among all components of the closed-loop system. The important step is the right choice of the appropriate software and acquisition unit. Few choices for software modification for data acquisition are available:

- Converting *Matlab* code into some language understandable to specified logic controller i.e. $SIEMENS\ Step7^{®}$.
- Integrating *Matlab* code with $dSpace^{®}$ - real-time interface for running models or prototypes during HIL tests.
- Running *Matlab* code in $Octave^{®}$ and wrapping it into *C++* library, using *Ethernet* connection protocol for communication with sensors and actuators.

[1] Hardware In the Loop

- Running *Matlab* code from remote PC connected by TCP protocol with single-board PC such as Raspberry.

The first solution is a standard industrial solution characterized as robust and well-known concept described in [114]. A faster alternative is the integration of *Matlab* code directly by using new *Matlab* toolbox or some additional application such as *dSpace*. Octave is a free-ware numerical computational package that has many of the same features as *Matlab* [115]. Unlike *Matlab*, *Octave* is open-source software with all benefits and drawbacks of such software.

Set-up with remote PC is the last option, and it is applicable only when the controlled process is quite slow. This solution appears to be the most convenient for our case, especially because we required a proof-of-principle prototype [116]. Communication between PC and *RaspberryPi* was made with *TCP* implemented as *Python* function. *Matlab* and *Simulink* were running on the PC while on the *RaspberryPi* is *Python* application. AANN was realized on the PC with *Matlab*/*Simulink* program package with *s-function*. Data acquisition was realized in *Python* on *RaspberryPi*. Sampling time was set up to 4 seconds.

5.1.1 Experimental Setup

Numerical calculation parameters have an important role for quality of obtained results. Various methods can be used, but numerical stability must be preserved whatever method is used. As *Matlab*'s *s-functions* are used as alternative solution for data acquisition during these tests, the numerical method has to be one of fixed-step type. Namely, in the case of AANN, which we use, the tuning of weights operates in constant time steps.

The low-pass filter transfer function is:

$$H(s) = \frac{1}{1 + \tau s} \tag{5.1}$$

where s is Laplace operator and τ is time constant. Figure 5.1 shows temperature step response and corresponding derivative of internal temperature difference $T_{ir} - T_{if}$ of the scaled mock-up. Also, corresponding filtered signals are also given. Signal labelled as *Offline* represents temperature difference $T_{ir} - T_{if}$, filtered in the off-line procedure by using *Matlab* function *filter*[2] where the size of the window is 50, [117]. The resulted

[2]One-dimensional digital filter based on rational transfer function and designed by window method

signal is very smooth, but this filter introduces constant lagging. The third signal in Figure 5.1 is labelled as *Online* and represents the temperature difference filtered by *Simulink* block that implements a first order low pass filter, [118], [112].

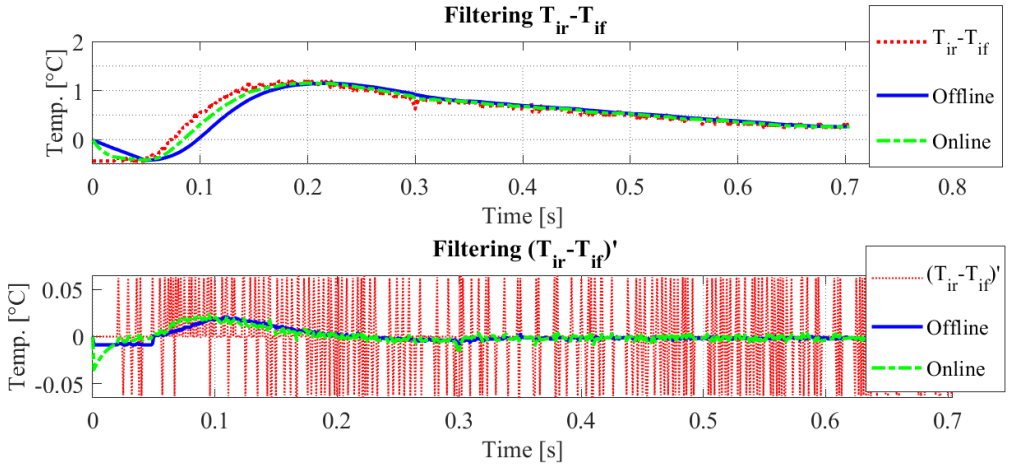

FIGURE 5.1. Thermal responses of the scaled mock-up with low-pass filters

First order low pass filter has been chosen due to lower lagging, even though the temperature response is not so smooth as *Offline* signal. Filter parameters are shown in Table 5.1. The block *First Order Low Pass Filter* in *Simulink* realize the low-pass filter transfer function (5.1).

TABLE 5.1. Filter properties

Parameter	Value
Filter type	lowpass
AC initial input: $[MagPhase(degrees)Freq(Hz)]$	[10 -25 60]
DC Initial input:	-0.4
Frequency range $[Hz]$: $[StartEndInc.]$	[12001]

After filter settings, next is to set-up sources of hot and cool air. Heating/cooling actuator has physical constraints. In practical situations, these constraints can change and cause various limitations for control signals (see Chapter 2). Position and shape of ducts that deliver warm or cold air from the actuator to the DSF corridor are designed carefully to reduce complex dynamics of the heat flow in the corridor. We have accomplished to approximate this heat/cold delivery process with the first order function (see Section 2.7).

5.1.2 Experimental Tests

Exhaustive experimentation was performed before the set-up was properly done. Two main tests with PI and with AANN regulator were analysed. Our main goal in both tests were to maintain thermal difference ($T_{ir} - T_{if}$) at zero value which means that scaled mock-up internal right temperature is equal to scaled mock-up internal temperature in front of the double skin façade (DSF), i.e. we end up with homogeneous thermal conditions inside scaled mock-up (interior of scaled mock-up).

5.1.2.1 Test 6 - Closed-loop System of the Scaled Mock-up with the PI regulator

Before testing closed-loop dynamics with the PI regulator, tuning of proportional and integral coefficients are needed first. According to [119], [120] and [121], best candidates for PI tuning methods ended up to be Cohen-Coon, Ziegler-Nichols and Lambda method. Tuning of PI regulator parameters are based on transient response and because dynamics of the heating and cooling transients are different PI regulator which is tuned for heating will not have appropriate parameters for cooling. Consequences of this disadvantage are in the inability of the PI regulator to regulate this process and necessity of process parameter identification to overcome this by the self-tuning PI regulator. Unfortunately, due to the complexity of dynamics of the building, nonlinearities and dependences of parameters to various external and internal conditions this solution is not possible. [121] claims that the Ziegler-Nichols method works well only on processes with smaller dead time such as less than half the length of the process time constant while the Cohen-Coon tuning rules is more flexible with dead time limitation (two times the length of the time constant). The *Cohen-Coon* tuning rules use three process characteristics: process gain, dead time, and time constant. These are determined by doing a step test and analysing the results. The Cohen-Coon tuning rules are suitable for use on self-regulating processes if the control objective is having fast response. *Lambda* tuning rules [120] are considered because their aim is first-order response to a step change of reference[3]. The drawback of *Lambda* tuning rules is that the regulator's integral time had to be set as equal to the process time constant. If a process has a very long time constant, the controller will consequently have a very long integral time. Long integral times make a recovery from disturbances very slow [121].

[3] no overshoot of reference, less sensitivity to errors of process dead time determination

The *Cohen-Coon* tuning rules were chosen for tuning PI regulator parameters. The temperature step response ($T_{ir} - T_{if}$) of the scaled mock-up without PI regulator (open-loop) was performed - see Figure 5.2. From Figure 5.2 we get enough information to perform *Cohen-Coon* tuning. If only the first heating part in Figure 5.2 is used, the PI

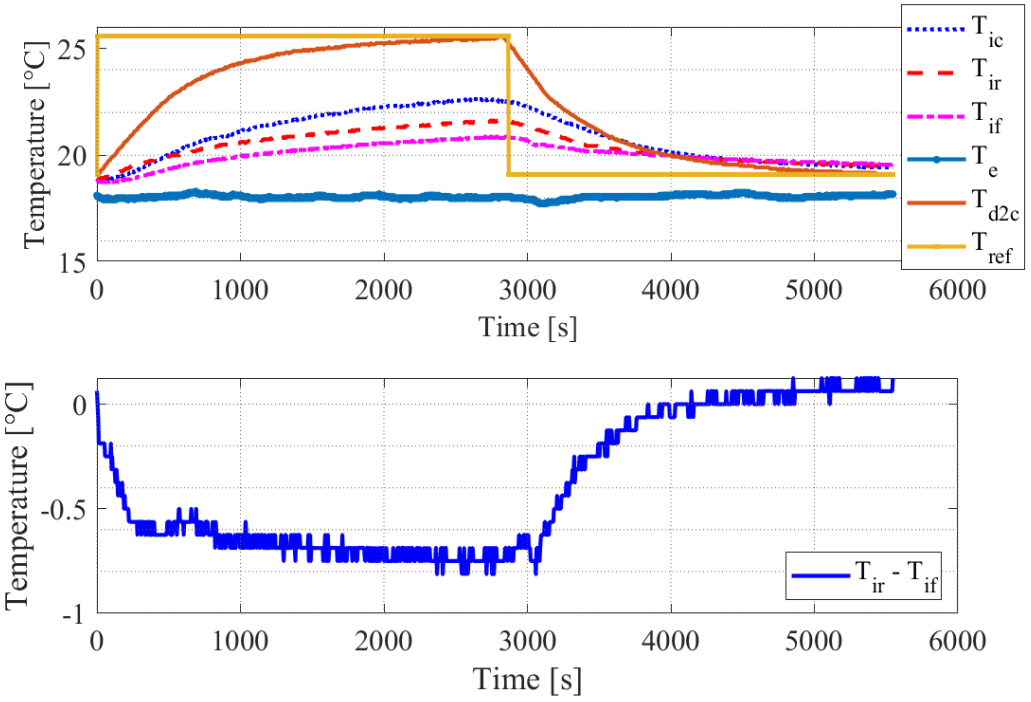

FIGURE 5.2. Temperature response ($T_{ir} - T_{if}$) on maximum and minimum step reference of actuator's reference (heating and cooling)

parameters can be tuned, and the result is shown in Table 5.2 and by (5.2). by equations

TABLE 5.2. PI parameters set by Cohen-Coon method

A	B	t_1	t_2	t_3	K	I
100.00	-1.44	150.86	193.20	893.21	-1041.27	125.16

shown in (5.2):

$$\begin{aligned} t_1 &= \tfrac{t_2-(ln(2)t_3)}{1-ln(2)} \\ \tau &= t_3 - t_1 \\ \tau_{del} &= t_1 - t_0 \\ K &= \tfrac{B}{A} \\ r &= \tfrac{\tau_{del}}{\tau} \\ P &= \tfrac{1}{rK}(0.9 + \tfrac{r}{12}) \\ I &= \tau_{del}\tfrac{30+3r}{9+20r} \end{aligned} \tag{5.2}$$

Figure 5.3 gives measured responses of various signals during the closed-loop experiment with PI regulator tuned by Cohen-Coon method.

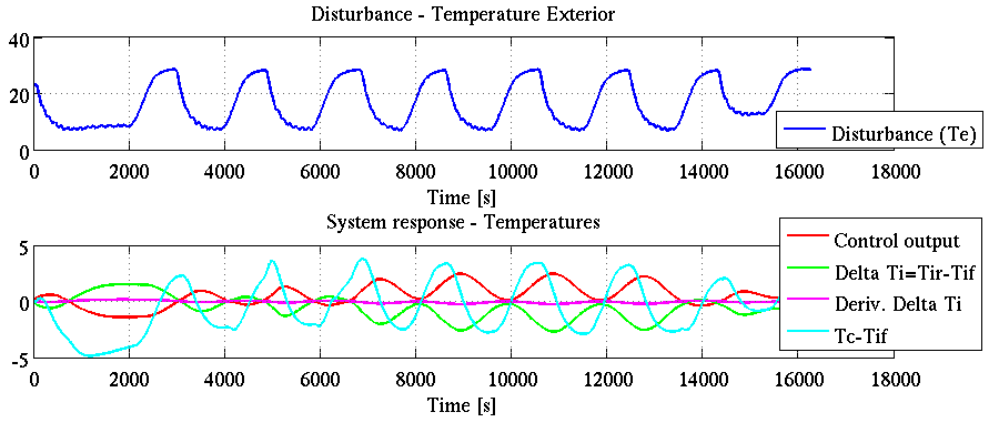

FIGURE 5.3. Results of an experiment with the PI regulator

5.1.2.2 Test 7 - Closed-loop System of the Scaled Mock-up with AANN

The performance of the AANN is shown in Figure 5.4. The feedback error converges to a smaller value as expected from the stability analysis. This effectively eliminates large error even though there is no reliable mathematical model of the scaled mock-up system and significant time delay in the feed-forward loop. This behaviour is due to the inherent memory of the AANN which comes from the robust part of the weight tuning update mechanism. The proposed weight tuning update mechanism of AANN has an advantage compared with the PI regulator, because it enables cancelling the effects of the nonlinearities of the scaled mock-up. These nonlinearities are changing due to various conditions (humidity, temperature, airflow, etc.) and because of this are not known during the heat flow control. The proposed algorithm has good performance in cancelling the nonlinearities in the controlled system which are completely unknown to the controller. For the weighting function only a few parameters must be selected: F matrix elements which are defining the tuning rate for the part of the AANN that defines change of the hidden layer parameters, kv - gain coefficient of the excitation part of the hidden layer (see Section 3.4.2) and kd - gain coefficient of the part of the weighting update mechanism which neutralizes time delay of the scaled mock-up.

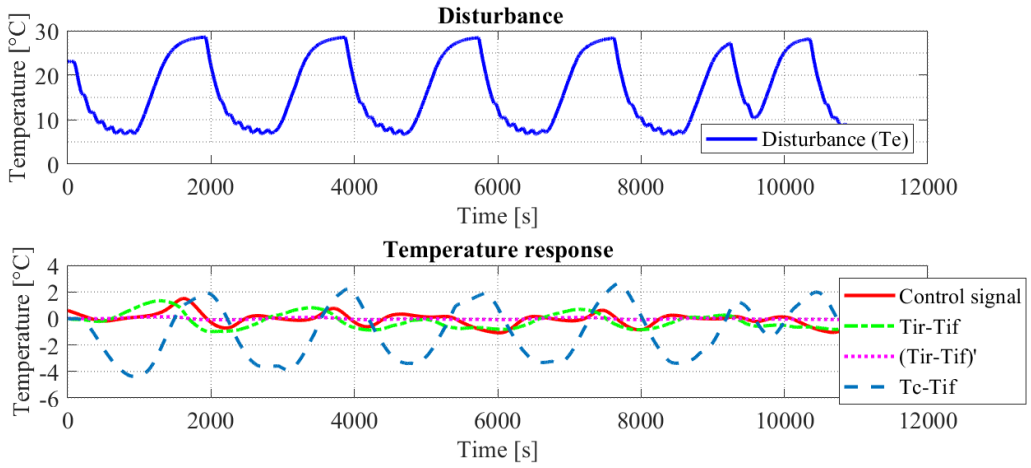

FIGURE 5.4. Results of the experiment with AANN.

Recorded performance indices were Integral of Absolute Error and Integral of Squared Error (ISE)like in [11] and [9].

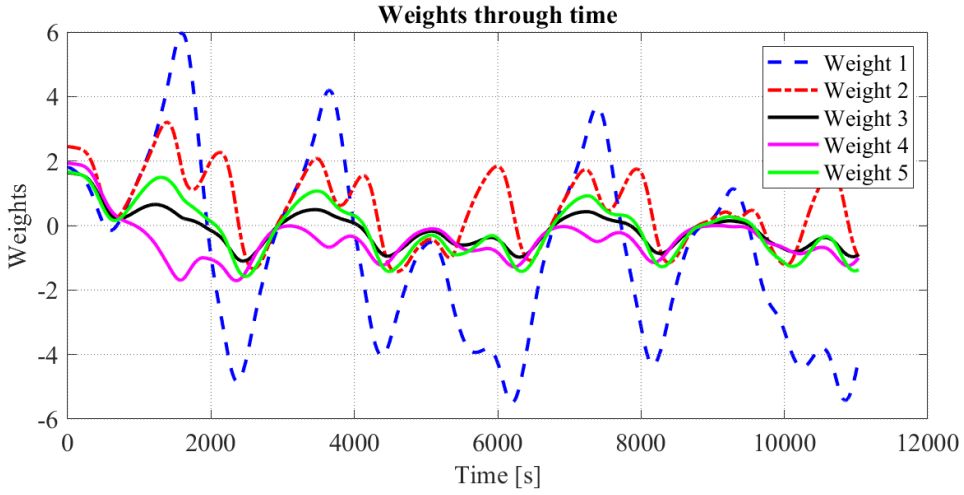

FIGURE 5.5. Weights of the AANN hidden layer during experiment

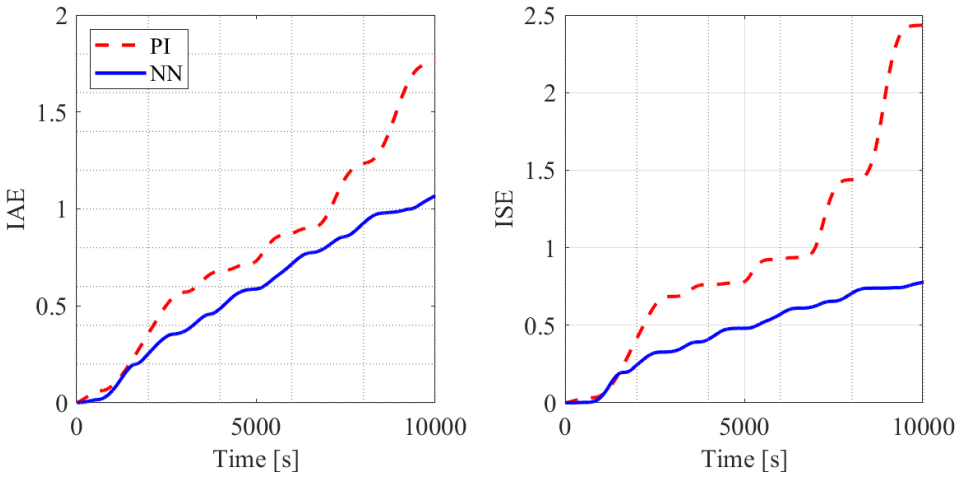

FIGURE 5.6. Comparison of IAE and ISE performance indices obtained with PI and AANN regulators.

IAE and ISE errors are shown in Figure 5.6. It is obvious that AANN gives much better results compared with the PI regulator. Because of the nonlinearities present in the scaled mock-up, the response performance is not satisfactory with the PI regulator. Contrary to AANN regulator, the PI regulator is not able to cancel effects of nonlinearities, so with AANN, the whole system is less sensitive to various conditions[4].

5.2 Summary

This chapter provides a detailed description and results from experimental tests obtained on scaled mock-up with Double Skin Façade. The proposed strategy with AANN tries to reduce the difference in the heat flow of walls and DSF of the scaled mock-up by adding an extra heat flow in DSF corridor. AANN is introduced in Chapter 3, simulated in Chapter 4 and used in Chapter 5 in laboratory experiments with the scaled-mock-up. Experiments were successful even though the mathematical model of the scaled mock-up was not known, time delays were present, parameter uncertainties were great, and disturbances were present. The configuration of AANN[5] is rather simple as it does not require complicated weight initialization procedure or any preliminary off-line training phase.

ANN learns on-line in real time and ensures the needed performance of the closed-loop system. However, for the full functionality of AANN, some time is needed to

[4] humidity, airflow, heat infiltration etc.
[5] one input layer, hidden layer etc.

automatically adjust the initial weights (initialization phase). At the beginning or when sudden large disturbance amplitudes occur the AANN regulation is not appropriate, the control signal is not able to decrease $T_{ir} - T_{if}$. These situations prevent AANN from being used in many applications[6]. However, for our application AANN is to be recommended because we do not expect large disturbance amplitudes and even if they occur there is no harm because AANN will recover relatively soon and regulate the process accordingly.

Experiments illustrate the capability of the proposed control strategy. The temperature responses to periodic external disturbance are shown. AANN performs well, and the weights of the hidden parameters are bounded as well as the control input. Weights and the error are bounded all the time. AANN can cope well with disturbance influence. It should be noted that the disturbance frequency of 0.5 mHz is appropriate for a slow process that we have (scaled mock-up). In experiments, both regulators (PI and AANN), were embedded on the same PC and Raspberry PI platform running real-time operating system. These experiments involve a closed-loop of particular complexity. Instead of comparison of closed-loop signals, the comparison of IAE and ISE performance indices is used to choose a better option between PI and AANN regulators. It was shown that AANN gives better results than the PI regulator.

[6]robotic control systems, path following systems, image processing etc.

Chapter 6

Conclusion and Future Work

In this final chapter, the main achievements and conclusions are summarized, and the remaining future work is addressed.

6.1 Conclusions

The dissertation deals with the design of an appropriate temperature regulator that can handle a nonlinear thermal process which is time-variant and for which internal and external variables cause an unpredictable change of its dynamics. Conventional temperature regulators are not able to deal with such a process because the mathematical model does not exist which could explain all possible working conditions. So, the natural choice was to choose those temperature regulators that do not need the mathematical model (neural network or fuzzy type). The time variation that is present in our thermal process led us toward the use of the adaptive neural network. After a thorough overview of the literature it was concluded that an adaptive neural network was not used for temperature regulation in building with DSF systems. It should be stressed here that using a neural network or fuzzy type of regulators without their adaptive behaviour will not give us the required performance. Also, there is no reference dealing with the elimination of heat flow differences in buildings with DSF.

The dissertation begins by providing a mathematical description of thermal behaviours in DSF systems where challenges above are addressed. The mathematical model is linearised and brought to standard form enabling heat flow calculation of the building with DSF (scaled mock-up). The linearized mathematical model can not represent system dynamics in all working regimes and all possible conditions (internal and external).

Nonlinearities that are common in this setting also change over time which makes solving the temperature regulation problem difficult. Nevertheless, the linearized model can be explored only for getting approximate qualitative temperature responses of the building to external temperature disturbances. From differences of the temperature responses ($T_{ir} - T_{if}$), the behaviour of the heat flow can be estimated. The heat flow represents the main information about the quality of the DSF system operation.

In order to apply adaptive artificial neural network (AANN) the passivity of the process (scaled mock-up) was investigated. From the passivity characteristic of the process the asymptotic stability was proven in Chapter 2. Asymptotic stability of the thermal process enables the use of the AANN regulator. The research resulted in the following accomplishments and original scientific contributions:

- A novel method for automatic control of corridor double skin façade systems is proposed and tested. This method can equalize the interior temperature, with the purpose of increasing user comfort and is simple enough to be used by non-experts.
- AANN is proven to perform better than conventional PI regulator for heat control in DSF corridor. Comparative analysis of non-controlled corridor double skin façade systems and automatically controlled double skin façade systems is performed. Controlled versus non-controlled heat flow in DSF shows advantages of the controlled solution.

Current regulation systems for heat conditioning in civil engineering cannot reach the equal distribution of temperatures in the same thermal zone. This problem is more intensive when the difference between desired and external temperatures is large. It is possible to reach one air temperature in the same closed space with double skin façade, if control engineering methods are applied.

The adaptive solution through Adaptive Artificial Neural Network (AANN) is based on Lyapunov-like tuning of weights in the hidden layer of AANN. This method is a well-known technique used in robotics. However, here the adaptive artificial neural network is applied for compensation of the critical heat loss of Double Skin Façade (DSF). Initial states, that are used in the weighting update mechanism, are dependent on characteristics of the thermal process in the DSF. Because of that, certain conditions must be satisfied while defining the initial states. These conditions are determined by using parameters of the linear model of the thermal process and Lyapunov function (see Chapter 3). If the walls and DSF are very thick, the time delay of the thermal transient

process is significant and should be compensated in order to improve the adaptive property (weighting update mechanism) of the AANN. The idea for this method has been found in [96] where a similar approach is used to compensate time-delay in telerobotic systems.

With persistent excitation, we will get desired performances even though parameters are varying in time and amplitude. The persistent excitation in this case is the external temperature variance which is periodical in time[1]. This fact enables the use of the AANN in buildings and scale mock-up as well. Scaling effects exist, and similarity between real buildings and scaled version of the same building (scaled mock-up) is not preserved. However, because the AANN regulator learns and adapts to the behaviour of the process, it will regulate and give desired performances for any time variant process. Experiments with the scaled mock-up show its capability of learning and adaptation, and we could conclude that it will also be the case in experiments in real buildings. Because real buildings have larger time constants, AANN could be even more effective in these applications.

6.2 Results of Simulations and Experiments

Simulation and experimental results are presented. These results showed that AANN should be recommended for use in buildings with DSF. A linear mathematical model was used in simulations to get some quantitative analysis of the open-loop and closed-loop system. Test 1 and Test 2 were performed to investigate the accuracy of the HAMBASE model while simulating the thermal process which is analysed in the thesis. Since both tests gave non-satisfactory results, an improved mathematical model was used in Test 3 to Test 5, where three different systems[2] and their responses to temperature disturbance of the square shape were given. The simulation results justify the use of AANN, but also indicate that the linear model is not appropriate to simulate the thermal transient process. AANN doesn't require any mathematical model, so there was no need to come up with the nonlinear model. Experiments on the scaled mock-up with PI and AANN are performed in Test 6 and Test 7. While the PI regulator gave the same response to the square shaped temperature disturbance in all periods of the square signal, the AANN is tuning the weights of the hidden layer all the time. This results in output responses that vary with the changing period of the square input signal. The control signal of the

[1] daily variation of temperatures with period of 24 hours
[2] open-loop, closed-loop with P, and closed-loop with AANN

AANN is more complex as it follows all three states[3] of the transient thermal process in the scaled mock-up, and not just the internal thermal difference ($T_{ir} - T_{if}$) like the control signal of the PI regulator. Experiments on the scaled mock-up with DSF enabled us to test the performance and capability of the AANN regulator. It was shown that the AANN is able to learn the dynamics of the process, tune the weights, adapt to external temperature disturbances, ensure the stability of the closed-loop system and regulate the process by bringing $T_{ir} - T_{if}$ to zero faster that would be the case in open-loop. Due to the fact that experiments were performed with the scaled mock-up the value of tuned coefficients in the hidden layer of the AANN is valid only for the used scaled mock-up. For other processes, such as scaled mock-up with different dimensions or the real building, the values of these coefficients will be different. Luckily, the adaptive capability of the AANN enables the AANN to tune the coefficients of any process, so we claim that the proposed AANN should be recommended. The AANN was never used for such purposes in any buildings. We didn't find any reference that describes the use of AANN in temperature regulation of buildings with DSF. However, the details are not inspected due to differences[4] in dynamics of a full scale building.

6.3 Future Work

In the future, experiments with a full-scale building should be performed to confirm AANN capability to give desired performances. Due to the lack of financial support, the proposed method was theoretically analysed, simulated and tested in the laboratory on a scaled mock-up[5]. Further work should cover experiments with a full-scale building where significant disturbances, such as solar radiation, could be tested. This future work could potentially be very financially demanding and time consuming, however it could have very real commercial potential if the methods correlate to the desired results. In [27] and [26] tests with full-scale buildings were described.

Following the achievements and findings in this dissertation, future work may also include the application of the proposed approach to a variety of buildings with integrated HVAC. Future development should explore multi-input multi-output (MIMO) control methods. These methods could use actuators consisting of heaters and fans which are not optimized. Also, other actuators could be added such as electro-mechanical shaft openings, adjustable sun blinds etc.

[3] $T_{ir} - T_{if}$,$(T_{ir} - T_{if})'$ and $T_c - T_{if}$

[4] process time constants, values of time delay, amplitudes of process states etc.

[5] scaled segment of the building with the DSF

Bibliography

[1] Gulin, M., Vašak, M., Baotić, M., "Estimation of the global solar irradiance on titled surfaces", in Proceedings of the 17th International Conference on Electrical Drives and Power Electronics, EDPE 2013, Dubrovnik, Croatia, October 2013.

[2] Martinčević, A., Starčić, A., Vašak, M., "Parameter estimation for low-order models of complex buildings", in Inovative Smart Grid Technologies Conference Europe (ISGT-Europe), 2014 IEE PES, Istanbul, Turkey, October 2014.

[3] Vašak, M., Starčić, A., Martinčević, A., "Model predictive control of heating and cooling in family house", in MIPRO, 2011 Proceedings of the 34th International Convention, Opatija, Croatia, May 2011, str. 739-743.

[4] Vašak, M., Martinčević, A., "Optimal control of a family house heating system", in MIPRO, 2013 Proceedings of the 36th International Convention, Opatija, Croatia, May 2013, str. 907-912.

[5] Starčić, A., Martinčević, A., Vašak, M., "Sensor applications symposium (SAS), 2015 IEEE", in MIPRO, 2013 Proceedings of the 36th International Convention, Zadar, Croatia, June 2015.

[6] Đula Nađ, "Guidance and control of autonomous underwater agents with acoustically aided navigation", Doktorski rad, Faculty of electrical engineering and computing, Zagreb, 2017.

[7] Mišković, N., "Primjena vlastitih oscilacija u vođenju i upravljanju plovilima", Doktorski rad, Fakultet Elektrotehnike i Računarstva Sveučilišta u Zagrebu, Zagreb, 2010.

[8] Misković, N., Đula Nađ, Vukić, Z., "Full-scale identification by use of self-oscillations for overactuated marine surface vehicles", International Journal of Adaptive Control and Signal Processing, Vol. 31, August 2016, str. 674-692.

[9] Kuljača, O., Horvat, K., Borović, B., "Design of Adaptive Neural Network Controller for Thermal Power System Frequency Control", Automatika, Vol. 52, No. 4, 2011, str. 319-328.

[10] Kuljaca, O., Lewis, F., Horvat, K., Inteligent control of industrial and power systems: Adaptive Neural Network and Fuzzy Systems. LAMBERT Academic Publishing, 2012.

[11] Horvat, K., Kuljača, O., Šoić, I., "Adaptive Neural Network Controller for Thermogenerator Angular Velocity Stabilization System", Brodogradnja, Vol. 64, No. 2, 2013, str. 1-13.

[12] Vitruvius, "Civil Buildings", in De Architectura, Vitruvius, (ur.). Naples: Antic Roman Empire, 15 BC.

[13] Zelig, "Brief guide to pompeii", pompei Ercolano Boscoreale Oplontis Stabia. 2011.

[14] Straube, J., Finch, G., "Ventilated Wall Claddings: Review, Field Performance, and Hygrothermal Modeling", University of Waterloo, Building Engineering Group Report for Building Science Press, Tech. Rep., 2009.

[15] Salonvarra, M., Karagiozis, A. N., Miller, M. P. W., "Air Cavities Behind Claddings—What Have We Learned", in Thermal Performance of Exterior Envelopes of Whole Buildings X International Conference, Florida, U.S.A., 2007.

[16] Raffnsøe, L. M., "Thermal Performance of Air Flow Windows", Master's thesis, Technical University of Denmark, Department of Civil Engineering, Kongens Lyngby, 2007.

[17] Labudović, B., Priručnik za ventilaciju i klimatizaciju. Zagreb, Croatia: Energetika Marketing, 2003.

[18] Fu, T. S., "Double Skin Façades as Mass Dampers", in 2013 American Control Conference (ACC), Washington, DC, USA, June 2013.

[19] Ding, W., Hasemi, Y., Yamada, T., "Smoke Control using a Double-skin Facade", in Proceedings of the Eighth International Symposium on Fire Safety Science, Beijing, China, September 2005, str. 1327-1337.

[20] Seppänen, B. O., William J. Fisk, P., Mendell, M. J., "Ventilation Rates and Health", ASHRAE Journa, Vol. 44, August 2002, str. 56-58.

[21] Meier, S., Lommel, A., Kegel, B., "Ventilation for Buildings: Design Criteria for the Indoor Environment - A New Initiative", in Proceedings of Healthy Buildings 2000, Vol. 2, Espoo, Finland, August 2000.

[22] VEZA, M. P. P. I., "O razvrstavanju, minimalnim uvjetima i kategorizaciji ugostiteljskih objekata", dostupno na: http://www.zakon.hr/ 1995.

[23] Minister, D. P., The Building Regulation 2000, Ventilation. NBS, RIBA Enterprises Ltd, 2006.

[24] GRADITELJSTVA, M. Z. O. P. U. I., "TehniČki propis o sustavima ventilacije, djelomiČne klimatizacije i klimatizacije zgrada", dostupno na: http://www.zakon.hr/ 2004.

[25] HSE, General Ventilation in the Workplace, Guidance for employers. HSE Books, 2000.

[26] Poirazis, H., Double Skin Façades for Office Buildings, Literature Review. Lund, Sweden: Lund University, Lund Institute of Technology, 2004.

[27] Brunoro, S., Rinaldi, A., "Double layer glass façade in the refurbishment and architectural renewal of existing buildings in Italy ", in World Renewable Energy Congress 2011, Low-Energy Architecture, Vol. 8, Linköping, Sweden, May 2011, str. 1898-1905.

[28] "Wood fibre insulation: Masonry wall applications", dostupno na: http://www.greenspec.co.uk 2017.

[29] "Icf panels", dostupno na: https://icfpanels.com/ 2017.

[30] Fuchs, H. U., The Dynamics of Heat: A Unified Approach to Theromdynamics and Heat Transfer. New York: Springer, 2010.

[31] Boake, T. M., B.Arch., M.Arch., "Understanding the General Principles of the Double Skin Façade System", dostupno na: http://www.academia.edu School of Architecture, University of Waterloo. November 2003.

[32] Magali, B., Elisabeth, G., "Bibliography study of control strategies in buildings equipped With Ventilated Double-skin Facades ", Université Catholique de Louvain UCL, Tech. Rep., July 2003.

[33] Boake, T. M., "Architecture, waterloo architecture cambridge", 2009.

[34] Samson, "Technology in architecture", dostupno na: https: //technologyinarchitecture.com/ 2017.

[35] Herzog, T., Krinppner, R., Lang, W., Facade Construction Manual. Basel Boston Berlin: Birkhäuser Verlag AG, 2004.

[36] Haase, M., Wong, F., Amato, A., "Double–Skin Facades for Hong Kong", Surveying and Built Environment, Vol. 18, December 2007, str. 17-32.

[37] Golnaraghi, F., Kuo, B. C., Automatic Control System. USA: John Wiley and Sons, Inc., 2010.

[38] Kratz, A. P., Konzo, S., "Temperature drop in ducts for forced - air heating systems", The Engineering Experiment Station, University of Illinois, Tech. Rep., May 1944.

[39] Hauer, A., Kempener, R., Simbolotti, G., Tosato, G., "Thermal", IEA-ETSAP and IRENA©, Tech. Rep., Januar 2013.

[40] Gevorkian, P., Solar Power in Building Design, The Engineer's Complete Design Resource. Mc Graw Hill, 2008.

[41] Stec, W. J., "Symbiosis of Double Skin Façade and indoor climate installation", Doktorski rad, Technische Universiteit Delft, Delft, Nederland, 2006.

[42] McQuiston, F. C., Parker, J. D., Spitler, J. D., Heating, Ventilating, and Air Conditioning, Analysis and Design, ser. 2. Hoboken,NJ,USA: John Wiley Sons Inc, 2005.

[43] Donjerković, P., Osnove i regulacija sustava grijanja ventilacije i klimatizacije. Zagreb: ALFA, 1996.

[44] Co., D. E. M., "Ventilation fundamentals", dostupno na: http://grainger.com/ dayton Grainger. 2005.

[45] Pletcher, R. H., Tannehill, J. C., Anderson, D., Computational Fluid Mechanics and Heat Transfer. USA: Taylor and Francis Inc., 2011.

[46] Pavković, B., Zanki, V., Handbook for Energy Certification in Buildings, UNDP, Zagreb Croatia, 2010.

[47] McBee, B. K., "Computational Approaches to Improving Room Heating and Cooling for Energy Efficiency in Buildings", Doktorski rad, Faculty of the Virginia Polytechnic Institute and State University, Blacksburg, Virginia, 2011.

[48] of Commerce, U. D., "Bureau of standards, journal of research", research papers Nos. 259 to 328. 1931.

[49] deWit, H. M., Part I Theory: Heat Air and Moisture model for Building And Systems Evaluation, Technische Universiteit Eindhoven, Eindhoven, Nederland, 2009, dostupno na: http://www.hambase.org

[50] van Schijndel, A. W. M., "Integrated Heat Air and Moisture Modeling and Simulation", Doktorski rad, Technische Universiteit Eindhoven, Eindhoven, Nederland, 2007.

[51] Shu, L., He, G., Zhang, S., Bai, Q., "Thermal Characteristics and Energy Performance of Double Skin Façade System in the Hot Summer and Cold Winter Zone", in Proceedings of ASIM 2012, Shanghai, China, 2012.

[52] "How moisture moves through a home", dostupno na: https://energy.gov/energysaver/energy-saver jan 2011.

[53] Moon, J. W., Lee, J. H., Yoon, Y., Kim., S., "Determining optimum control of double skin envelope for indoor thermal environment based on artificial neural network", Energy and Buildings, Vol. 6, No. ISSN 1996-1073, August 2013, str. 4223-4245.

[54] Moon, J. W., Chin, K., Kim, S., "Optimum application of thermal factors to artificial neural network models for improvement of control performance in double skin-enveloped buildings", Energies, Vol. 69, No. ISSN 0378-7788, 2014, str. 175-183.

[55] Kim, D.-W., Park, C.-S., "Integrated Control Strategies For Double Skin Systems", in Proceedings of Building Simulation 2011:12th Conference of International Building Performance Simulation Association, Sydney, Australia, November 2011, str. 601-608.

[56] Henninger, R. H., Witte, M. J., "EnergyPlus Testing with ANSI/ASHRAE Standard 140-2001 (BESTEST) ", Ernest Orlando Lawrence Berkeley National Laboratory, Berkeley, California, Tech. Rep., June 2004.

[57] Lin, S., Tee, B. T., Tan, C. F., "Indoor Airflow Simulation inside Lecture Room: A CFD Approach", Vol. 88, No. 1, 2015, str. 012008, dostupno na: http://stacks.iop.org/

[58] Niu, J., Tung, C., Wan, J., Cheng, J., "CFD simulation of interflat air flow for the study of the spread of aerosol transmitted infectious diseases", in Proceedings of Ninth International IBPSA Conference, Montreal, Canada, August 2005, str. 853-858.

[59] Woloszyn, M., Rode, C., "Tools for performance simulation of heat, air and moisture conditions of whole buildings", Building Simulation, Vol. 1, No. 1, 2008, str. 5-24.

[60] Dickson, A., "Modelling Double-Skin Facades", Master's thesis, Department of Mechanical Engineering University of Strathclyde, Glasgow UK, 2003.

[61] Anđelković, A. S., Cvjetković, T. B., Đaković, D. D., Stojanović, I. H., "The Development of Simple Calculation Model for Energy Performance of Double Skin Facades", Thermal Science, Vol. 16, 2012, str. 251-267.

[62] Xianfeng, Z., Junping, F., Xiaoqing, Y., "A simplified mathematical model of heat transfer process in double skin façade", in 2011 International Conference on Computer Distributed Control and Intelligent Environmental Monitoring, Changsha, Hunan, China, February 2011, str. 389-393.

[63] Kämpf, J. H., Robinson, D., "A simplified thermal model to support analysis of urban resource flows", Energy and Buildings, Vol. 39, No. 4, April 2007, str. 445–453.

[64] Martin de Wit, WAVO - A model for the simulation of the thermal and hygric performance of building and systems, Technische Universiteit Eindhoven, Eindhoven, Nederland, 2009, dostupno na: http://www.hambase.org

[65] de Wit, M., Driessen, H., van der Velden, R., ELAN, a computer model for building energy design, theory and validation, Bouwstenen, No 1. Eindhoven: Technische Universiteit Eindhoven, 1987.

[66] de Wit, M. H., "Aproximate Solutions to Boundary Layer Problems in Linear Kinetic Theory", Doktorski rad, Technische Universiteit Eindhoven, Eindhoven, Nederland, 1975.

[67] M. H. deWit, Part II Input and Output: Heat Air and Moisture model for Building And Systems Evaluation, Technische Universiteit Eindhoven, Eindhoven, Nederland, 2009, dostupno na: http://www.hambase.org

[68] Lewis, F. L., Liu, K., Yesildirek, A., "Modelling and simulation of HAM processes", Acta Technica Napocensis: Civil Engineering Architecture, Vol. 55, No. 3, December 2012, str. 205-212.

[69] Brayton, E. R., Aydogan, A., "ANSI/ASHRAE Standard 140-2001 (BESTEST)", dostupno na: https://www.ashrae.org/ American Society of Heating, Refrigerating and Air-Conditioning Engineers, Inc. 2004.

[70] de Wit, M., HAMBASE Heat Air and Moisture model for Building and Systems Evaluation. Eindhoven, Netherlands: Eindhoven University Press, 2008.

[71] Frank, M. J., "Warmte-koudeopslag na de oplevering BIJLAGENBOEK", Technische Universiteit Eindhoven, Building Services, Tech. Rep., February 2010.

[72] Maile, T., Bazjanac, V., O, J., Donnell, Garr, M., "A software tool to compare measured and simulated building energy performance data", in Proceedings of Twelfth International IBPSA Conference, Sydney, Australia, November 2011.

[73] Kalyanova, O., Jensen, R. L., Heiselberg, P., "Measurement of Air Flow Rate in a Naturally Ventilated Double Skin Facade", in Proceedings of Roomvent 2007, Helsinki, Finland, 2007.

[74] Carlos, J. S., Corvacho, H., Silva, P. D., Castro-Gomes, J., "Real climate experimental study of two double window systems with preheating of ventilation air", Energy and Buildings, Vol. 42, 2010, str. 928–934.

[75] Navvab, M., "Full Scale Testing and Computer Simulation of a Double Skin Façade Building", in Ninth International IBPSA Conference, Montréal, Canada, August 2005.

[76] Park, C.-S., "Occupant Responsive Optimal Control Of Smart Façade Systems", Doktorski rad, Georgia Institute of Technology, Georgia, 2003.

[77] Brayton, E. R., Aydogan, A., "Code of practice for use of glass in buildings - aisglass.com", dostupno na: http://www.aisglass.com/ AIS Glass Solutions Ltd. 2005.

[78] Sauer, T. J., Meek, D. W., Ochsner, T. E., Harris, A. R., Horton, R., "Errors in heat flux measurement by flux plates of contrasting design and thermal conductivity", Vadose Zone Journal, No. 2, 2003, str. 580–588.

[79] Holmberg, D. G., Womeldorf, C. A., "Performance and Modeling of Heat Flux Sensors in Different Environments", in Proceedings of the ASME, Nashville, TN, November 1999.

[80] Borggaard, J., Burns, J. A., Surana, A., Zietsman, L., "Control, Estimation and Optimization of Energy Efficient Buildings", in Proceedings of American Control Conference, ACC '09., Rio de Janeiro, Brazil, 2009.

[81] Eškinja, Z., Ružić, S., Kuljača, O., "Modelling heat loss through multi storey double skin corridor façade as preliminaries for an energy efficient control strategy", Gradevinar, Journal of the Croatian Association of Civil Engineers, Vol. 70, December 2018, str. 931-942.

[82] Bai, H., Arcak, M., Wen, J., Cooperative Control Design, A Systematic,Passivity-Based Approach. Springer, 2011.

[83] Mukherjee, S., Mishra, S., Wen, J. T., "Building Temperature Control : A Passivity-Based Approach", in 51st IEEE Conference on Decision and Control, Maui, Hawaii, USA, December 2012, str. 6902–6907.

[84] Moore, K. L., Vincent, T. L., Lashhab, F., Liu, C., "Dynamic Consensus Networks with Application to the Analysis of Building Thermal Processes", 2011, str. 3078–3083.

[85] Nakić, A., Pavčević, M. O., Mathematica 3 - Introduction to Graph Theory. Element, 2009.

[86] Øyvind Alvsvåg, "HVAC-systems Modeling, simulation and control of HVAC-systems", Master's thesis, Norwegian University of Science and Technology, Department of Engineering Cybernetics, Trondheim, 2011.

[87] HU, J., Karava., P., "Modeling and predictive control strategies in buildings with mixed-mode cooling", July 2012, str. 3577-3587.

[88] Gosselin, J., Chen, Q., "A dual airflow window for indoor air quality improvement and energy conservation in buildings", HVAC and R Research, Vol. 14, No. 3, 2008, str. 359-372.

[89] Wei, J., Zhao, J., , Chen, "Optimal design for a dual-airflow window for different climate regions in china", Energy and Buildings, Vol. 16, No. 6, 2010, str. 785-798.

[90] Linden, P. F., "The fluid mechanics of natural ventilation", Annual Review of Fluid Mechanics, Vol. 31, Jan. 1999, str. 201-238.

[91] Azzo, J. J., Houpis, C. H., Feedback Control System Analysis and Synthesis. Mc Graw Hill Book Company Inc., 1960.

[92] Vukić, Z., Kuljača, Lj., Automatic Control - linear system analysis. Zagreb: Kigen, 2005.

[93] de Wit, M. H., Zonneveldt, L., "Learning control of thermal systems", in Control of Complex Systems, Åström, K., Albertos, P., Blanke, M., Isidori, A., Schaufelberger, W., Sanz, R., (ur.). London, GB: Springer-Verlag, 2001, str. 317-337.

[94] "", in Artificial Neural Networks - Application, Hui, C. L. P., (ur.). InTech, 2011.

[95] Rai, R., "Introduction of softcomputing approach in slope stability", dostupno na: http://www.iitbhu.ac.in/ 2013.

[96] Lewis, F. L., Campos, J., Selmic, R., Nuro-Fuzzy Control Of Industrial Systems With Actuator Nonlinearities. Philadelphia, PA, USA: Society for Industrial and Applied Mathematics, 2002.

[97] Wan, E. A., "Control systems: Classical, neural, and fuzzy", oregon Graduate Institute. 1998.

[98] Lewis, F. L., Jagannathan, S., Yeşildirek, A., Neural Network Control of Robot Manipulators and Nonlinear Systems. Taylor and Francis Inc., 1999.

[99] Abdi, H., "Linear algebra for neural networks", in Encyclopedia of the Social and Behavioral Sciences, Smelter, N., Baltes, P., (ur.). London: Elsevier Science, 2001.

[100] Lewis, F. L., Optimal Control: Optimal control of Discrete-time Systems. John Wiley and Sons Inc., 1986.

[101] Lewis, F. L., Liu, K., Yesildirek, A., "Neural Net Robot Controller with Guaranteed Tracking Performance", IEEE Transactions on Neural Networks, Vol. 6, No. 3, May 1995, str. 703-715.

[102] Lewis, F. L., Yesildirek, A., Liu, K., "Multilayer neural net robot controller with guaranteed tracking performance", IEEE Transactions on Neural Networks, Vol. 7, No. 2, March 1996, str. 388-399.

[103] Narendra, K. S., Annaswamy, A. M., "A New Adaptive Law for Robust Adaption Without Persistent Excitation", IEEE Transactions on Automatic Control, Vol. 32, No. ISSN:0018-9286, Feb 1987, str. 134-145.

[104] Ioannou, P. A., Pitsillides, A., Modeling and Control of Complex Systems. CRC Press, 2008.

[105] Ahire, J. B., "Artificial neural networks: Some misconceptions", dostupno na: https://dzone.com/ 2018.

[106] Vukic, Z., "Sinteza adaptivnog sistema vođenja transportnih brodova", Doktorski rad, Elektrotehnicki Fakultet Sveučilišta u Zagrebu, Zagreb, 1989.

[107] Barron, A., "Universal approximation bounds for superpositions of a sigmoidal function", IEEE Trans. Info. Theory, Vol. 39, No. 3, 1993, str. 930-945.

[108] Narendra, K., "Adaptive Control Using Neural Networks", in Neural Networks for Control, Miller, W. T., Sutton, R. S., Werbos, P. J., (ur.). Cambridge: MIT Press, 1991, str. 115-142.

[109] Chen, T., "A Methodology for Thermal Analysis and Predictive Control of Building Envelope Heating Systems", Doktorski rad, Concordia University,, Montreal, Quebec, Canada, 1997.

[110] Meyer, C. D., Matrix Analysis and Applied Linear Algebra Book and Solutions Manual. Philadelphia, USA: SIAM, 2004.

[111] Petersen, K. B., Pedersen, M. S., "The matrix cookbook", dostupno na: http://www2.imm.dtu.dk/pubdb/p.php?3274 Version 20121115. nov 2012.

[112] Hahn, B., Valentine, D. T., Essentila MATLAB For Engineers and Scientists. Elsevier Butterworth Heinemann, 2007.

[113] Xie, C., Hazzard, E., Nourian, S., A Green Building Model Kit for Engineering Design, The Concord Consortium,, Concord, MA 01742, USA, 2012, dostupno na: http://concord.org/

[114] Parr, E. A., Programmable Controllers An engineer's guide. Oxford: Newnes, 2003.

[115] Sharma, N., Gobbert, M. K., "A comparative evaluation of Matlab, Octave, FreeMat, and Scilab for research and teaching", Department of Mathematics and Statistics, University of Maryland, Baltimore County, Tech. Rep., July 2010.

[116] Verchuren, P., Doorewaard, H., Designing a research project. Eleven International Publishing, 1999.

[117] Ingle, V. K., Proakis, J. G., Digital Signal Processing Using MATLAB. CENGAGE Learning, 2012.

[118] MathWorks, Dynamic System Simulation for MATLAB, Writing S-Functions, The MathWorks, Inc., Natick, MA 01760-2098, USA, 1998, dostupno na: http://www.mathworks.com

[119] Štefan Bucz, Kozáková, A., "PID controller design for specified performance", in Introduction to PID Controllers - Theory, Tuning and Application to Frontier Areas, Panda, R. C., (ur.). Rijeka, Croatia: InTech, 2012, str. 3-30.

[120] O'Dwyer, A., Handbook of PI and PID Controller Tuning Rules. London: Imperial College Press, 2009.

[121] Smuts, J. F., Process Control for Practitioners. OptiControls, 2011.

Abbreviations

AMSL	**A**bove **M**ean **S**ea **L**evel
AANN	**A**daptive **A**rtificial **N**eural **N**etwork
ANN	**A**rtificial **N**eural **N**etwork
ANSI	**A**merican **N**ational **S**tandards **I**nstitute
API	**A**pplication **P**rogramming **I**nterface
ASHRAE	**A**merican **S**ociety of **H**eating, **R**efrigerating and **A**ir-Conditioning **E**ngineers
BESTest	**B**uilding **E**nergy **S**imulation **Test**
BMS	**B**uilding **M**anagement **S**ystem
CSA	**C**anadian **S**tandard **A**ssociation
DSF	**D**ouble **S**kin **F**açade
FRC	**F**enestration **R**ating **C**ouncil
HIL	**H**ardware **I**n the **L**oop
HVAC	**H**eating **V**entilation and **A**ir **C**onditioning
IAE	**I**ntegral **A**bsolute **E**rror
IAQ	**I**ndoor **A**ir **Q**uality
ISO	**I**nternational **S**tandard **O**rganisation
IP	**I**nternet **P**rotocol
ISE	**I**ntegral **S**quare **E**rror
LTI	**L**inear **T**ime-**I**nvariant
MIMO	**M**ulti **I**nput **M**ulti **O**utput
NFRC	**N**ational **F**enestration **R**ating **C**ouncil
NN	**N**eural **N**etwork
PDE	**P**artial **D**ifferential **E**quation
PE	**P**ersistent **E**xcitation

PHI	**P**assive **H**ouse **I**nstitute
SISO	**S**ingle **I**nput **S**ingle **O**utput
TCP	**T**ransmission, **C**ontrol **P**rotocol
TES	**T**hermal **E**nergy **S**torage
UTES	**U**nderground **T**hermal **E**nergy **S**torage
UUB	**U**niformly **U**ltimately **B**ounded

Symbols

A	surface area	m^2
ach	air change rate in zone	h^{-1}
C_p	specific heat capacity of air	$\frac{J}{kgK}$
C_a	heat storage coefficient (capacitance) of indoor air $= \rho_a c_p Vol$	$\frac{J}{K}$
c	specific heat	$\frac{J}{kgK}$
R_r	thermal resistance by radiation	$\frac{K}{W}$
R_{cv}	thermal resistance by convection	$\frac{K}{W}$
R_{flow}	thermal resistance by airflow through the fenestration	$\frac{K}{W}$
h_r	surface heat transfer coefficient for radiation	$\frac{W}{m^2K}$
h_{cv}	surface heat transfer coefficient for convection	$\frac{W}{m^2K}$
h_e	total external surface coefficient	$\frac{W}{m^2K}$
Q_m	the air mass flow	$\frac{kg}{m^3}$
T_a	indoor air temperature when air is perfectly mixed	$^\circ C$
T_b	air temperature of zone b	$^\circ C$
T_x	'resultant' indoor wall temperature	$^\circ C$
T_y	'resultant' outdoor temperature for wall/envelope	$^\circ C$
T_e	outdoor air temperature	$^\circ C$
T_{d2c}	the temperature of air inserted into the corridor	$^\circ C$
T_{if}	the temperature of interior air directly behind the glazed surface of the DSF	$^\circ C$
T_{ir}	the temperature of interior air in front of the right wall, close to the centre of the wall	$^\circ C$
T_c	the temperature of the DSF corridor	$^\circ C$
L_{xa}	coupling coefficient (=C$_a$ach/3600)	$\frac{W}{K}$

$\mathbf{W}$	neural network weight matrix	
L	Lyapunov function	
e	error	
e_a	admittance error	
e_t	transmittance error	
$f(\mathbf{x})$	nonlinear function of vector $\mathbf{x}$	
$\hat{f}$	nonlinear function estimate	
$\tilde{f}$	error of nonlinear function estimation	
$\mathbf{x}$	vector of state variable	
VA	corridor ventilation rate	$\frac{m^3}{m^2 s}$
$\dot{\mathbf{W}}$	First derivation of neural network weight matrix	
$\ddot{\mathbf{W}}$	Second derivation of neural network weight matrix	
λ_{max}	Maximum singular value of matrix	
λ_{min}	Minimum singular value of matrix	
ς	activation function used in neural network	
$\phi(x)$	activation function when last hidden layer weights are fixed values V^T	
k_{t1}	transmittance coefficient 1	
k_{t2}	transmittance coefficient 2	
k_{t3}	transmittance coefficient 3	
k_{a1}	admittance coefficient 1	
k_{a2}	admittance coefficient 2	
k_{a3}	admittance coefficient 3	
ε	emissivity of the surface	
ρ_a	density of the air	$1.2\frac{kg}{m^3}$
ρ	density	$\frac{kg}{m^3}$
Φ_{out}	output heat rate - loss	W
Φ_{rez}	'resultant' heat rate of the system	W
Φ_{xy}	heat transfer rate from T_x node to T_y node	W
Φ_{ab}	heat transfer rate from T_a node to T_b node	W
Φ_{fin}	heat transfer rate from T_a node to Tc node	W
Φ_{fout}	heat transfer rate from T_c node to T_e node	W
Φ_{d2c}	heat transfer rate of the air mass directed to the corridor	W

Φ_r	heat transfer rate of the radiant input	W
U	total thermal transmittance	$\frac{W}{m^2K}$

List of Figures

List of Tables

Biography

Zdravko Eškinja has completed his Master degree at Faculty of Electrical Engineering and Computing, University of Zagreb in 2006. Same year Zdravko has been employed as a young researcher in Brodarski Institute Ltd, Zagreb, Croatia, in Control Engineering Department, where he gained practical experience in various projects involving measuring, data acquisition and processing. His scientific work started in a field of underwater systems as extension to his Master thesis ”Location of Autonomous Underwater Vehicles by Sonar Image Processing". In period from 2013 till 2015 he participated in Visiting Research Program of Center of Maritime Research and Experimentation, La Spezia, Italy. Meanwhile, due to the requirements of his employer, the scientific field changed to energy efficiency in buildings and industry. After additional education and series of certificates he was involved in dozen capital infrastructure projects with high level of complexity. He has taken opportunity in 2017 to work again in underwater systems at small R&D company "Marine Robotics and Systems". Most of his work was presented through national and international publications. More than ten papers where published in conferences. Also, he is first author of three journal papers in highly ranked scientific journals on different fields of automation control.

List of Published Papers

Journal Articles

1. Eškinja, Z., Ružić, S., Kuljača, O., “Modelling heat loss through Double Skin Façade as preliminaries for an energy efficient control strategy”, Građevinar, Vol. X, No. Y (ili Issue Y), October 20189., str. A-B.

2. Eškinja, Z., Horvat, K., Bakarić, V., Kuljača, O., “ Review of Turbine Governing System Tests performed on Hydro-Power Plants in Croatia”, International Journal of Contemporary ENERGY, Vol. 3, No. 1, February 2017, str. 51-56.

3. Eškinja, Z., Đula, N., Đapić, V., “Multiple Autonomous Systems in Underwater Mine Countermeasures Mission Using Information Fusion as Navigation Aid”, Brodogradnja : časopis brodogradnje i brodograđevne industrije, Vol. 64, No. 2, 2013.

4. Eškinja, Z., Mišković, I., Andročec, V., “ Wavemaker design for harbors and ships physical model testing”, Brodogradnja : časopis brodogradnje i brodograđevne industrije, Vol. 59, No. 2, 2008., str. 131-135.

Conference papers

1. Eškinja, Z., Miljanić, L., Kuljača, O., “Modelling Thermal Transients in Controlled Double Skin Façade Building by using Renowned Energy Simulation Engines”, MIPRO 2018, Opatija, 2018, str. 1060-1064.

2. Eškinja, Z., Mišković, I., Horvat, K., Bojić, D., Šikić, D., Stojsavljević, M. " Registrator prijelaznih pojava u sustavu turbinske regulacije ", Energetika 2012, Beograd, 2012, str. 209-213.

3. Stipanov, M., Eškinja, Z., Skelin, D. "MAREA – Maritime Environment Monitoring System", PROCEEDINGS ELMAR-2007, Croatian Society Electronics in Marine, 2010, str. 329-332.

4. Mišković, I., Eškinja, Z., Horvat, K. "Wavemaker Control System for Irregular Developed Sea Waves Generation", Proceedings of 16th Mediterranean Conference on Control and Automation, 2008.

5. Eškinja, Z., Fabeković, Z., Vukić Z. " Localization of Autonomous Underwater Vehicles by Sonar Image Processing ", PROCEEDINGS ELMAR-2007, Croatian Society Electronics in Marine, 007, str. 103-106.

6. Fabeković, Z., Eškinja, Z., Vukić Z. " Micro ROV Simulator", PROCEEDINGS ELMAR-2007, Croatian Society Electronics in Marine, 2007, str. 97-101.

Životopis

Zdravko Eškinja je diplomirao na Fakultetu Elektrotehnike i Računarstva na Sveučilištu u zagrebu 2006. godine. Iste godine se zapošljava kao mlađi istraživač u Brodarskom institutu u Zagrebu, u odijel za upravljanje procesima, gdje je kroz niz projekata stekao razna iskustva u mjerenju, prikupljanju i obradi podataka. Njegov znanstveni rad je počeo podvodnih sustava kao nastavak na diplomski rad pod nazivom " Obrada sonarskog signala za potrebe lokalizacije bespilotne ronilice ". U razdoblju od 2013 do 2015 sudjelovao je u programu "Visiting Research Program" razvojno istraživačkog centra "Center of Maritime Research and Experimentation" u gradu La Spezia, u Italiji. U međuvremenu, zbog potreba poslodavca područje znanstvenog rada je usmjereno u eneregetsku efikasnost u zgradama. Nakon dodatnog osposobljavanja i niza certifikata, sudjelovao je u desetak kapitalnih infrastrukturnih projekata visoke složenosti. 2017. godine se zapošljava u malu razvojno-istraživačku kompaniju "MArin Robotics and Systems" gdje ponovno ima priliku raditi na podvodnim sustavima. Većina njegovog rada je objavljena u domaćim i internacionalnim publikacijama. Više od deset radova je objavljeno na konferencijama. Također, bio je prvi autor u tri članka visoko rangiranih znanstvenih časopisa u tri različite grane automatskog upravljanja.